Fabrication and Characterization of an Artificial Mucus Layer for Mammalian-Microbial Co-Culturing Applications

by

Andy Jia Bo Huang

Submitted in partial fulfilment of the requirements
for the degree of Master of Applied Science

at

Dalhousie University
Halifax, Nova Scotia
July 2021

TABLE OF CONTENTS

LIST OF TABLES

LIST OF FIGURES

ABSTRACT

The human mucus layer plays a vital role in maintaining health by acting as a selectively diffusive barrier to opportunistic pathogens and foreign particles that enter the body. In areas such as the respiratory and gastrointestinal tract, the mucus hydrogel lining provides a unique microenvironment inhabited by both commensal and pathogenic bacteria, where the bacteria use mucin, the glycoprotein that makes up the mucus hydrogel network, as an attachment site. To model the host-microbe interactions, *in vitro*, in both health and disease, it is crucial to provide a proper microenvironment that can support the growth of both mammalian and microbial cells in a controlled manner. Recent advances in modelling host-microbe interactions include compartmentalized microfluidic devices or transwell co-cultures. However, these techniques lack sufficient control of the mucus microenvironment and require highly specialized skills to fabricate and operate, and therefore are difficult for the average life science laboratory to adopt.

In this study, we aim to address these concerns by fabricating an artificial mucus layer using a simple ionic gelation technique with calcium chloride to generate an alginate-mucin (ALG-MUC) semi-interpenetrating polymer network hydrogel to be incorporated into a polyethylene glycol-dextran (PEG-DEX) aqueous two-phase system (ATPS) co-culture platform. We demonstrated the utility of ALG-MUC hydrogels using two sets of mammalian-microbial co-cultures. First, we used a human bronchial epithelial cell line, 16-HBE, co-cultured with a common airway pathogen, *Pseudomonas aeruginosa*. The second was a colorectal adenocarcinoma cell line, Caco-2, co-cultured with a gut pathogen, *Shigella flexneri*. Additionally, we characterized the viscosity and diffusivity of the ALG-MUC hydrogels.

The findings showed that the ALG-MUC hydrogels were compatible with a PEG-DEX ATPS by reducing PEG-mediated cytotoxicity when cells were overlaid with a hydrogel layer. It was also found that diffusion of biomolecules (IgG and LL-37) was more affected by hydrogel composition (presence of mucin) rather than differences in viscosity. Moreover, the concentration of mucin as well as ATPS formulation affected the spatial distribution and antibiotic resistance of bacteria within this multiphase co-culture system.

The ALG-MUC hydrogel was shown to have similar diffusive characteristics to natural mucus as well as support the simultaneous culture of pathogenic bacteria with mammalian cells, *in vitro*. With the ability to readily form a mucus-like hydrogel directly on top of mammalian cells, we provide a controlled co-culture platform that has the potential for assessing host-pathogen interaction and antibiotic testing in a realistic microenvironment. Future studies will further characterize the bacterial colony formation within the hydrogel layer and explore different ATPS formulation with modified ALG-MUC compositions to model complex bacterial infections at the mucosal interface.

LIST OF ABBREVIATIONS USED

3D	3-Dimensional
ALG	Alginate
AMP	Antimicrobial Peptide
ASL	Airway Surface Liquid
ATPS	Aqueous Two-Phase System
CD	Crohn's Disease
CF	Cystic Fibrosis
CFTR	Cystic Fibrosis Transmembrane Conductance Regulator
CFU	Colony Forming Unit
COPD	Chronic Obstructive Pulmonary Disease
DAPI	4',6-diamidino-2-phenylindole
D_{eff}	Effective Diffusion Coefficient
DEX	Dextran
DMEM	Dulbecco's Modified Eagle Medium
DMSO	Dimethyl Sulfoxide
DSS	Dextran Sulfate Sodium
D-T	Distance-Time
ECM	Extracellular Matrix
ELISA	Enzyme-Linked Immunosorbent Assay
FBS	Fetal Bovine Serum
FITC	Fluorescein Isothiocyanate

G	α-L-Guluronate
GC	Growth Control
GDL	D-(+)-Gluconic Acid δ-Lactone
GFP	Green Fluorescent Protein
GI	Gastrointestinal
IBD	Inflammatory Bowel Disease
IL	Interleukin
IPN	Interpenetrating Polymer Network
kDa	Kilodalton
LB	Luria Broth
M	β-D-Mannuronate
MDa	Megadalton
MIC	Minimum Inhibitory Concentration
mM	Milimolar
MTT	3-(4,5-Dimethylthiazol-2-yl)-2,5-Diphenyl-2H-Tetrazolium Bromide
MUC	Mucin
NF-κB	Nuclear Factor Kappa-Light-Chain-Enhancer of Activated B Cells
OD$_{600}$	Optical Density at 600 nm wavelength
PBS	Phosphate-Buffered Saline
PCL	Periciliary Layer
PDMS	Polydimethylsiloxane
PEG	Polyethylene Glycol
PMN	Polymorphonuclear

PTS	Proline-Threonine-Serine
RFP	Red Fluorescent Protein
RGD	Arginine-Glycine-Aspartic Acid
ROS	Reactive Oxygen Species
RPMI	Roswell Park Memorial Institute
RT	Room Temperature
SC	Sterility Control
SD	Standard Deviation
SP-SDS	Single Plate-Serial Dilution Spotting
TCPS	Tissue Culture Polystyrene
TSB	Tryptic Soy Broth
UC	Ulcerative Colitis
UV	Ultraviolet
v/v	Volume per Volume
w/v	Weight per Volume
x g	Times Gravity

ACKNOWLEDGMENTS

First and foremost, I would like to express my sincere gratitude for my supervisor, Dr. Brendan Leung. Not only has Dr. Leung provided me with this research opportunity, but also countless opportunities to develop my leadership skills and develop as a person. The lessons that you have taught me will be carried with me for the remainder of my career. Next, I would like to thank the rest of my committee members, Dr. John Frampton and Dr. Andrew Stadnyk for the continuous support and guidance throughout this degree. Thank you for all the insightful comments and questions during committee meetings.

I would also like to acknowledge past and present lab members for discussion and feedback during lab meetings as well as always challenging me with questions and conversation in the lab. Your contribution to this project, whether big or small, did not go unnoticed.

Lastly, I would like to thank all of those who helped me in completing this project. Dr. Catherine Whitman and Dr. Alicia Oickle for helping with the lyophilization of my alginate samples. Dr. Zhenyu Cheng and Karla Valenzuela for providing the bacterial strains used and teaching me the necessary techniques to work with them. As well as my colleagues Anas Tahir for helping with the modification of the MATLAB code used, and Jonathan Tjong and Nicholas Dawe for their help in my final experiments.

CHAPTER 1.   INTRODUCTION

1.1   Thesis Overview

This thesis contains 6 chapters describing the novel work that has been carried out to fabricate an artificial mucus hydrogel for the purposes of modelling host-microbe interaction at the mucosal interface. Chapter 1 provides a thorough review of the current host-microbe interaction models as well as the role of the human mucus layer in both health and disease. Chapter 2 outlines the main research aims and objectives of this project. This is followed by the methods and materials used to carry out this work in Chapter 3. Chapter 4 describes the key findings of the research that has been conducted. Chapter 5 will discuss the impact of this research project and its relevance to the current literature, as well as some of the limitations. Finally, Chapter 6 summarizes the key findings and conclusions made throughout this project followed by considerations for future work.

1.2   Current Models for Host-Microbe Interaction

The human mucus layer is a niche microenvironment where complex interactions between pathogenic and commensal bacteria as well as host cells take place. Alterations in the bacterial composition or dysregulation in mucus homeostasis can result in chronic infection and inflammation in diseases such as inflammatory bowel diseases (IBD) and cystic fibrosis (CF).[1,2] A representative host-microbe interaction model is essential for gaining a better understanding of the complex interactions and potential new drug therapies. To accurately model the complexities of host-microbe interaction at the human mucosal interface, researchers must consider an appropriate mucosal microenvironment and controlled bacterial abundance and composition

within the model. The current gold standard for modeling host-microbe interaction remains to be the use of animal models, predominantly with the use of mice,[3] with an emergence of *in vitro* mammalian-microbial co-culture models in recent years. Considering the variation in microbial composition between individuals,[4] *in vivo* studies utilize gnotobiotic (or germ-free) animals, which allows for the inoculation of a specified bacterial composition.[5-7] Over the years, *in vivo* studies have been instrumental in uncovering the role of the human microbiota in IBDs and chronic respiratory infections caused by CF.[8-11] However, due to differences in pathophysiology between animal and humans, *in vivo* findings do not always translate into clinical findings.[12,13]

1.2.1 In Vivo

With the use of gnotobiotic animals, IBD can be induced using various methods including genetic modification,[14] chemical induction,[15] and adaptive transfer.[16] One of the earlier models of IBD is interleukin-10 (IL-10) knockout mice. IL-10 plays an important role in the anti-inflammatory response, and by generating IL-10 deficient mice with targeted deletion, mouse models develop spontaneous inflammation of the colon.[14,17] One study using IL-10 deficient mice demonstrated the inoculation of *Akkermansia muciniphila*, an otherwise non-pathogenic bacteria, promoted intestinal inflammation, suggesting that *A. muciniphila* is a potential pathobiont of the gut.[18] The chemical induction of colitis in mice can be carried out by oral administration of dextran sulfate sodium (DSS) through drinking water, which is a well-established method for studying colitis in mice.[15] The uptake of DSS and distribution within animal tissue demonstrate its capability of penetrating the mucosal barrier. DSS has been found to accumulate in macrophages leading to lowered phagocytic ability, resulting in increased bacterial load and inflammation.[15,19] Another study utilizing the DSS colitis model demonstrated

a shift in microbiota species between colitis induced mice and control mice.[20] More recently, adaptive transfer models have gained more attention, where naïve T cells from healthy mice are transferred into syngeneic (immunologically compatible) immunodeficient mice.[21,22] This model has demonstrated inflammation of the small intestine 6-12 weeks after the T cell transfer.[21]

Despite the advances in modelling IBD *in vivo*, there are several differences between the human and mouse GI tract. First, the distribution of goblet cells (mucus-producing) in humans are highly abundant from the cecum to the rectum. Compared to mice, where goblet cells are more abundant in the proximal colon with a lowered abundance towards the distal colon and rectum.[12] Second is the location of antimicrobial peptide (AMP) secreting cells. Paneth cells are a specialized secretory cell found within the GI epithelium, that secrete AMP products to maintain homeostasis of the microbiota.[23] In humans, Paneth cells are found throughout the intestinal tract with highest abundance in the small intestinal crypts.[24] In comparison, Paneth cells are uniquely localized in the cecum in mice.[12] These differences in specialized cell distribution between animals and humans can affect how the microbiota within the GI tract are distributed in animal models regardless of bacterial composition that is introduced.

Using mice to model CF has shown both success and failure in mimicking the human lung CF phenotype. CF in humans typically results in thickened airway mucus leading to reduced mucociliary clearance and chronic infection.[25-27] Animal models in CF studies involve genetic modification of the cystic fibrosis conductance regulator (CFTR) gene, which is responsible for regulating ion transport into the mucus layer to maintain homeostasis of the airway surface liquid (ASL), also known as the periciliary layer (PCL).[28] Murine models have been shown to generate altered mucociliary clearance, but ciliary beating frequencies were not different from the normal mice.[10,29] It has been hypothesized that an alternative chloride

conductance regulator in the mouse airway epithelial cells secrete chloride ions into the ASL resulting in less severe airway pathology.[30,31] Although mouse models have demonstrated some impairment of the mucociliary clearance, CFTR knockout mice do not develop spontaneous infection of the lung, which has been thought to be the result of the clean conditions the mice are kept.[32] Other studies have found CF mouse models to show no difference in ASL levels, which are known to harbor antimicrobials that efficiently kill opportunistic pathogens, thereby preventing spontaneous infection from occurring in these models.[33] As a result, CF studies utilizing the mouse model frequently challenge the animals with pathogenic bacteria.[34,35] However, new techniques involving the use of *P. aeruginosa* embedded agarose beads for bacterial inoculation has been shown to better resemble CF patient infection in mice.[36]

To broaden the range of animal models, pigs and ferrets have been explored as potential alternatives to the mouse CF model. Stoltz et al. (2010) reported the use of a pig model which was able to generate spontaneous disease progression and infection of the airway like that of CF patients.[37] Like pigs, ferrets have also demonstrated spontaneous lung infection and impaired mucociliary transport.[11] The limitations of using large animal studies are that they require more space and resources, leading to increased cost of pre-clinical studies. Other studies reported life threatening complications with both pigs and ferrets, that required surgical intervention, making it even more difficult for widespread implementation.[37,38]

1.2.2   In Vitro

Given these challenges with animal models, there has been an increasing interest in developing a representative *in vitro* host-microbe interaction model. Some of the established models include the use of compartmentalized systems for mammalian microbial co-culture

including microfluidic devices and transwell co-culture.[39-42] The use of microfluidic devices and transwells are similar in that both techniques involve compartmentalization using a semi-permeable membrane to separate endothelial and epithelial cell growth (in microfluidic devices), or compartmentalization of the mammalian cell and bacterial cell populations (in transwell co-culture). Jalili-Firoozhinezad et al. (2019) have demonstrated the use of a gut-on-a-chip, where differentiated, mucus producing epithelial cells were grown in the upper channel of the microfluidic device with endothelial cells in the lower compartment and isolated bacteria were introduced into the system by flow through the upper channel.[39] An airway model has also been developed using microfluidics to mimic the fungal and bacterial interactions in the bronchial microenvironment.[43]

In contrast, transwell co-culture techniques allow for the simultaneous growth of mammalian cells and bacterial cells within the same compartment (transwell insert), while providing the additional fresh media through the receiver well.[41,44,45] The two different cell populations can also be grown in either compartment, separated by the semi-permeable membrane, which can be used to assess chemical communication between the host and microbial cells as well as immune cell migration.[40] Although the use of both microfluidic devices and transwell co-culture have been shown to effectively maintain mammalian-microbial interaction over several days, there are some clear limitations. Both techniques, while allowing for mucus production, can be limited by the amount of mucus that is produced, where differentiated cell mucus production has been shown to produce thin layers of mucus over long periods of time.[39,40,46] Microfluidic device fabrication tends to require highly trained personnel and specialized equipment, thus limiting its adoption and use in the general life science laboratory.[42] Transwell co-culture techniques, while commercially available and convenient, do not allow for

controlled bacterial growth and can be limited to chemical communication without physical interaction between the two cell populations.

In addition, another co-culture method which has been less explored is the use of a liquid-liquid scaffolding for bacterial deposition onto mammalian cells, known as aqueous two-phase system (ATPS) co-culture.[47] An ATPS is a biphasic system that can be formed by dissolving two immiscible polymers in solution that generates a lower and upper phase and can be used to manipulate the distribution of cells by physical separation. The application of ATPS in mammalian-microbial co-culture involves resuspension of a bacterial population in the lower phase, where a single droplet of the bacteria-rich lower phase can be deposited directly onto a mammalian monolayer, grown in the upper phase. For instance, Dwidar et al. (2013) demonstrated the deposition of *Escherichia coli* onto a mammalian monolayer using a polyethylene glycol-dextran (PEG-DEX) ATPS, where the lower DEX-phase was used to confine bacteria to a localized region on top of a mammalian monolayer grown in the upper PEG-phase.[47] The use of an ATPS co-culture allows for efficient bacterial deposition to localized regions of the culture vessel; however, the limits of the ATPS stability over time has not yet been explored. Additionally, this system lacks the mucus hydrogel layer to provide the niche microenvironment for bacterial interaction.

1.3   Role of Mucus in the Human Body

The human mucus layer is known to play a crucial role in maintaining health by acting as a protective barrier for the underlying epithelial cells.[48] In areas such as the respiratory and GI tract, the mucus hydrogel lining provides a unique microenvironment inhabited predominantly by commensal bacteria, which is collectively known as the microbiota. By harboring commensal

bacteria within the mucus layer, added protection is provided by bacterial competition between the commensal bacteria and any opportunistic pathogens that may enter the body.[45,49] Additionally, the mucus layer is also known to harbor a range of secreted antimicrobial biomolecules, such as AMPs and immunoglobulins (Ig).[50,51]

The mucus layer is a selectively diffusive barrier that allows for oxygen and nutrient diffusion to the underlying epithelial cells while preventing harmful pathogens and foreign particles from coming in direct contact with the mucosal tissue by size exclusion (or steric hinderance) and interaction filtering of smaller molecules.[52-54] In the GI tract, specifically in the colon, the mucus layer is organized in a bi-layer structure, where the inner layer (closer to the epithelium) is a sterile, dense layer. The outer layer (closer to the intestinal lumen) is less dense, which allows commensal bacteria to diffuse in and reside.[55-57] Harboring commensal bacteria in the mucus layer provides a mutually beneficial relationship between the microbiota and the host. Mucus is constantly secreted into the lumen of the gut by goblet cells and can be used by the bacteria as a carbon source as well as attachment sites.[58,59] In return, commensal bacteria groups such as *Firmicutes* and *Bacteroides* aid in nutrient breakdown of otherwise indigestible polysaccharides for the host.[60] Additionally, commensal bacteria compete with incoming pathogens for space by secreting bacteriocins as a direct mechanism to kill pathogens.[49,61]

In the airway, the mucus layer function is conserved; however, the mechanism of protection differs based on the mucus layer arrangement and physiology.[62] Here, the mucus hydrogel layer is much thinner (~50 μm) than in the GI tract (123 – 830 μm), and rests on top of the ASL that allows for ciliary motion of the upper airway epithelial cells.[63,64] The ciliary motion thus propels the upper mucus layer out of the airway, which may have entrapped pathogens and inhaled foreign particles.[65] Furthermore, the mucus is constantly being replenished by secretory

goblet and Club cells to maintain the mucociliary escalator.[66] Like the GI mucus, the role of commensal bacteria in the airway has also been demonstrated to provide host protection against bacterial pathogens. A probiotic species, *Bifidobacterium longum*, was shown to protect host lungs from *Klebsiella pneumoniae* by inducing increased reactive oxygen species (ROS) production in alveolar macrophages to reduce the bacterial load of pathogenic *K. pneumoniae*.[67] Other studies demonstrate and characterize the bacteriocin production and activity of *Bifidobacterium* and *Lactobacillus* species.[68,69] However, bacterial strains such as *Pseudomonas aeruginosa* have demonstrated resistance to bacteriocins, which can lead to chronic infection of the lungs.[70]

Additionally, in both the airway and intestinal mucosal surface, epithelial cells secrete IgA and AMPs, such as alpha-defensin and LL-37, that become incorporated into the mucus hydrogel as part of the innate defense provided by the mucus.[50,71] These biomolecules are typically retained in the mucus layer through electrostatic and physical interactions with the negatively charged mucin glycoproteins that make up the mucus hydrogel network.[50] Although not as commonly found in GI mucus as IgA, IgG has also been reported to be found in patient airway mucus secretions, which plays a major role in host defense in the distal airway and adaptive immunity.[72,73]

1.4   Composition and Structure of Mucins and their Contribution to Mucus Function

The mucus layer is a viscoelastic biological hydrogel, secreted by goblet cells, that is known to have non-Newtonian rheological properties.[74] Hydrogels can be defined as water swollen crosslinked polymer networks, where the mucus hydrogel network consists of crosslinked (covalent and non-covalent) glycoproteins, called mucins, along with lipids, salts,

and other proteins involved in host defense.[75] The core peptide of a mucin monomer generally consists of repeated PTS domains (proline-threonine-serine) that become highly glycosylated, giving mucin a brush-like structure, with cysteine-rich terminals that allow for disulfide crosslinking between monomers (Figure 1).[75]
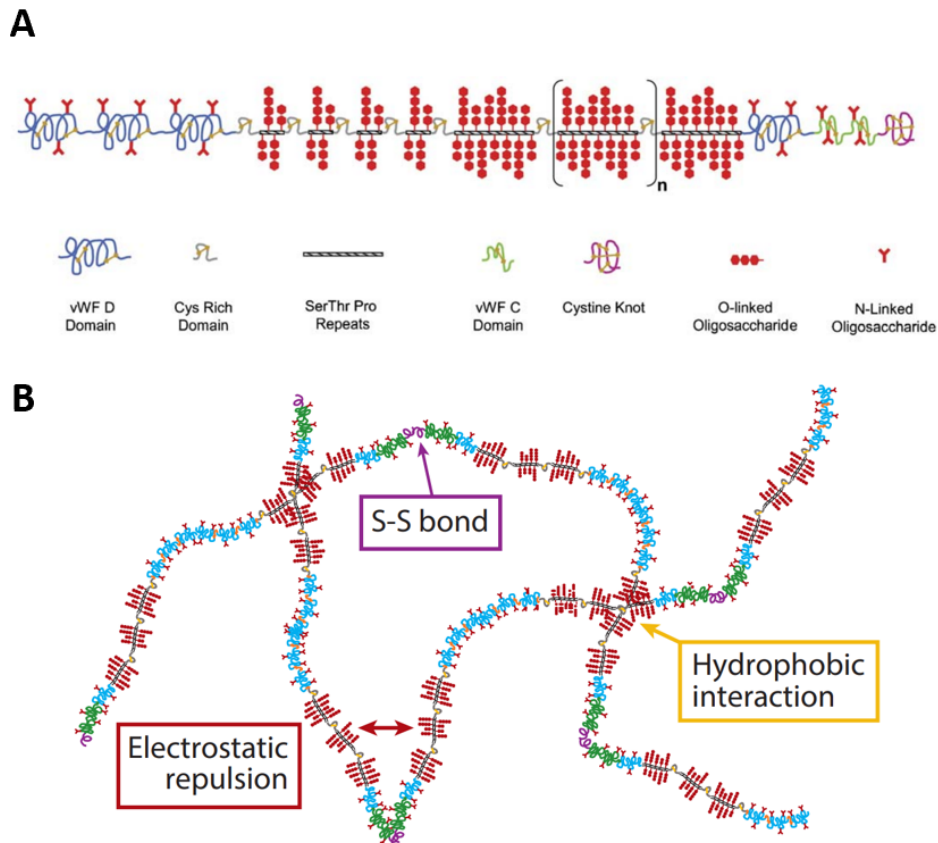
Figure 1: Illustration of mucin monomer structure and glycoprotein components. (A) Schematic of a mucin monomer with the core glycosylated region and flanked regions with low glycosylation (Adapted from Bansil & Turner, 2006).[75] **(B)** Schematic of mucin network formed through various covalent and non-covalent interactions (Adapted from Wagner et al., 2018).[76]

In humans, the mucus hydrogel mainly consists of the gel-forming mucins secreted into the extracellular space.[77] After the translation of mucin peptides, post-translational glycosylation takes place and mucins are then tightly packed into secretion granules within epithelial and

goblet cells.[78] Once cells are signaled to degranulate and release mucin into the extracellular environment, the mucin electrolyte content becomes diluted leading to swelling and the formation of a mucus hydrogel.[79]

The size and structure of mucin have a direct impact on the physical properties of mucus. Mucin monomers are known to have a broad range in molecular weight, ranging from 250 kDa to 2 MDa, where the bulk of the mucin mass is derived from the O-linked oligosaccharide side chains.[80] The combination of long interconnected mucin chains, physical entanglement, and ionic interaction between the carbohydrate sidechains all contribute to the viscoelastic properties of mucus in that it is more viscous at low shear rates and less viscous at higher shear rates.[74] The viscoelasticity of mucus can be altered based on the ionic composition. Chen et al. (2010) demonstrated that increased bicarbonate concentrations in mucus reduces the viscosity by chelating calcium ions and thus reducing the ionic interaction between mucin chains.[81] This illustrates the importance of maintaining homeostasis within the mucus through ion channel regulators at the mucosal interface for healthy barrier function of the mucus layer.

Maintaining the microbiota is another important function of the mucus layer. The carbohydrate sidechains of mucin peptides carry negatively charged sulfate and sialic acid groups.[82] These negative charges allow mucus to interact with positively charged secreted AMPs, such as alpha-defensins and LL-37.[71] Additionally, secreted IgA and IgG are retained in the mucus layer through interaction of similar oligosaccharide structures as the mucin.[50] Upon secretion of IgA, they are known to be covalently bound to glycosylated secretory components.[83] Studies have demonstrated the localization of AMPs and Ig within the mucus layer to prevent commensal bacteria from over proliferation.[50,71,84]

1.5 Mucus Dysregulation and Associated Pathologies

Knowing the importance of the role mucus plays in maintaining human health, it is not surprising that its dysregulation leads to complications and disease progression. Mucus dysregulation in the airway typically leads to chronic infection of the lungs due to excessive accumulation of mucus that is unable to be cleared via ciliary motion.[85] Inflammatory bowel disease has been thought to be caused by dysbiosis due to prolonged mucus dysregulation in the GI tract, although the direct cause remains unclear.[7,86]

Associated pathologies of mucus dysregulation in the airway can either be caused by mucus hypersecretion or thickened mucus due to dysfunctional ion channels in the epithelia.[87] Mucus hypersecretion is most commonly known to occur in chronic obstructive pulmonary diseases (COPD), typically occurring in individuals who smoke or are exposed to high levels of air pollutants.[88,89] Inhaled particulate (i.e. cigarette smoke or air pollutants) will trigger epithelial cells to secrete neutrophil chemoattractant that concentrate at the airway lumen.[90] It has been shown that patients with COPD have increased neutrophil accumulation in the airway epithelium, which stimulates degranulation of mucin producing cells with neutrophil elastase.[90] Cystic fibrosis, on the other hand, has been well studied and stems from mutations in the CFTR gene that is responsible for chloride ion homeostasis in the lung. Without a functional CFTR channel, mucus becomes dehydrated resulting in loss of the ASL layer and the inability to clear mucus out of the airway.[91] This thickened mucus provides a microenvironment for opportunistic bacteria to replicate and persist, with a common opportunistic pathogen being *P. aeruginosa*, which are notorious for their persistence and antibiotic resistance once colonized in the thickened airway mucus.[92] *P. aeruginosa* in a mucoid state are known to secrete alginate, which allow for

the bacteria to better resist administered antibiotics as well as avoidance from the host immune response.[92,93]

Diseases in the GI tract includes IBDs, such as Crohn's disease (CD) and Ulcerative Colitis (UC), which can be defined as chronic inflammation and ulceration of the mucosa. Generally, it is thought to be a shift in the abundance of commensal bacteria to larger proportions of pathogenic bacteria.[94] In contrast, other studies suggest disruption in the mucus layer leads to extended exposure to commensal bacteria, which normally does not cause inflammation.[7,18] There has also been evidence produced that suggest some patients have genetic predispositions to IBDs which result in altered O-glycosylation of mucins, in turn causing poor barrier function of the mucus layer.[95,96] To investigate the role of microbial species in IBDs, multiple studies have been carried out involving the inoculation of mouse models with patient derived commensal and pathogenic bacterial species.[7,97,98] However, Tamboli et al. (2004) emphasize the importance of distinguishing between the fecal flora (typically what is used in animal studies) and the mucosal flora, suggesting that the use of fecal flora may not be a full representation of intestinal microbiota.[99]

Moreover, other species of bacteria have developed different mechanisms of bypassing the mucus layer under healthy conditions, such as *Helicobacter pylori* and *Shigella flexneri*. *H. pylori* can change the pH of the mucus microenvironment to reduce the viscosity allowing the bacteria to pass through the mucus layer in the stomach.[100] Species such as *S. flexneri* produce mucolytic enzymes that breakdown the mucin chains where mucin is used as a nutrient source as they pass through the dense mucus layer of the colon to infect underlying cells.[101]

1.6 Applications and Biocompatibilities of Aqueous Two-Phase Systems

The formation of an ATPS can be achieved by mixing either two immiscible polymers, a polymer and a salt, or ionic liquids and alcohols in a solvent such as water at specific concentrations, which eventually separate into two distinct phases.[102] This separation phenomenon is based on the incompatibility of the two solutes chosen, where the hydrophobic or hydrophilic properties determine the separation.[103] However, this is not always the case, where specific concentrations of polymer or salt are required for phase separation to occur. By generating a plot of concentrations of polymer 1 and polymer 2 or salt, a binodal curve can be used to determine the concentrations needed for phase separation where concentration ratios above and to the right of the curve will phase separate, whereas concentrations below and to the left of the curve will form a common phase (Figure 2).[102]
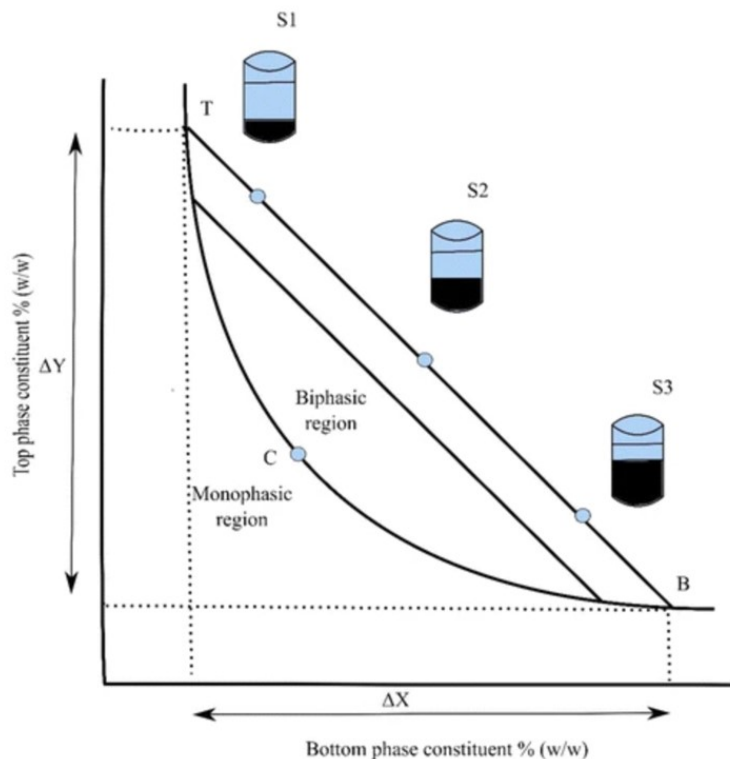
Figure 2: Schematic example of an aqueous two-phase system binodal curve. Concentrations at or above the binodal curve will form an aqueous two-phase system (T, C, or B), with tie-lines (T-B), which indicate formulations of the same phase composition and varying mass ratios of the top and bottom phase. Figure adapted from Iqbal et al. (2016).[102]

13

In the past, ATPS has been predominantly used for partitioning and isolation of biomolecules as a more economical purification technique. When using a polymer-polymer ATPS such as PEG and DEX, generally hydrophobic molecules will partition into the upper PEG-rich phase while hydrophilic molecules partition into the lower DEX-rich phase.[104,105] The use of both a PEG-DEX and PEG-phosphate ATPS are both widely used tools for protein isolation and purification with yield recoveries ranging from 89% to 95%.[106,107] In addition to differentiating and partitioning proteins based on hydrophobicity, Kim et al. (2015) demonstrated the ability of a PEG-DEX ATPS to isolate extracellular vesicles for molecular characterization of biological fluids.[108]

In recent years, researchers have expanded the use of ATPS in novel applications such as cell partitioning and micropatterning for studying interactions of different cell populations as well as optimization of immune assays such as enzyme-linked immunosorbent assay (ELISA).[109-111] While the applications mentioned are important for advancing the ATPS technology, the use of ATPS in mammalian-microbial interaction has potential and has been largely unexplored. One study has demonstrated the use of a PEG-DEX ATPS in mammalian-microbial co-culture by depositing bacteria-rich DEX phase directly on top of mammalian cells grown in a PEG-phase.[47] Additionally, Yaguchi et al. (2012) demonstrated the ability to study bacterial interaction between species using ATPS.[112] These cell population interaction studies allow for the physical contact between cells as well as chemical communication by free diffusion of proteins through the ATPS interface.[47,112,113] However, one of the major limitations of a PEG-DEX ATPS in mammalian-microbial co-culture is that PEG is cytotoxic towards mammalian cells in a molecular weight dependent manner.[114] The mechanism of PEG-mediated cell death is

primarily due to its ability to interrupt cellular membranes as well as generation of reactive

oxygen species (ROS).[114]

1.7 Biomedical Applications of Alginate Hydrogels

Alginate is a naturally occurring polymer that can be isolated from brown seaweed and

has numerous uses within the biomedical field. Applications include cell encapsulation, drug

delivery, wound healing, and fabrication of synthetic biomaterials.[115-117] These applications all

involve the formation of alginate hydrogels through crosslinking with divalent cations, such as

Ca^{2+}. Alginate can be described as linear co-polymers containing blocks of (1, 4)-linked β-D-

mannuronate (M) and α-L-guluronate (G) residues. The composition of both the G and M

residues dictate the crosslinking density between monomers, where it is only the G residues that

are thought to form ionic crosslinks between alginate monomers.[118] Characteristics that make

alginate such a desirable material for biomedical applications are its ease of use and

biocompatibility both *in vivo* and *in vitro*.

Alginate molecules are known to be inherently non-cell adhesive, where cell

encapsulation or tissue engineering applications typically require alginate modification or

combining with cell adhesive molecules to form hybrid hydrogels.[115,119,120] A popular method of

alginate modification involves the covalent attachment of arginine-glycine-aspartic acid (RGD)

ligands, which have demonstrated significantly increased cell adherence to alginate substrates.[115]

These modified alginate hydrogels have been shown to allow for cell encapsulation and

differentiation for tissue regeneration and transplantation applications.[121,122] Alternatively, other

studies have used a blended hydrogel network involving alginate and gelatin or collagen, which

are natural components of the extracellular matrix (ECM) within the human body.[119,120]

Similarly, these studies also demonstrate the successful adherence of mammalian cells that can be differentiated and were studied for up to 30 days.[120] Interestingly, alginate hydrogels have also been used to study *P. aeruginosa* biofilm formation by encapsulation, which was found to form bacterial aggregates similar to those found in CF patient mucus.[123] This finding is not surprising considering the alginate production of *P. aeruginosa* during chronic infection of the lung.[93]

Other biomedical applications of alginate include drug delivery and fabrication of wound dressings. Small molecular weight drugs have been ionically linked to alginate hydrogel beads that have shown slowed and controlled release of anti-inflammatory drug, flurbiprofen, which was controlled by crosslinking density.[116] Anticancer drugs such as Doxorubicin and Methotrexate were previously shown to be covalently linked to alginate hydrogel backbones and incorporated within the pores of the hydrogel, respectively. This allowed for a combination treatment method that could enable fast release of Methotrexate and slowed release of the Doxorubicin through hydrolysis of the linker molecule.[124] In the fabrication of alginate wound dressings, alginate hydrogels are first formed through ionic crosslinking, like the mentioned applications; however, they are further processed by freeze drying to form porous sheets. These freeze-dried sheets can be applied to wounds to absorb any fluids and maintain the moisture of the site and minimize the risk of bacterial infection.[125] Furthermore, these alginate dressings can be functionalized with bioactive factors that increase the healing process by promoting cell proliferation.[117,126]

Although uncommon, two studies involving the mixture of alginate and mucin to fabricate mucus-like hydrogels have been identified, where alginate is used as the gel-forming network considering the loss of gelation ability in reconstituted purified mucin. For example,

Pacheco et al. (2019) generated an alginate-mucin hydrogel by crosslinking with calcium carbonate ($CaCO_3$) and D-(+)-gluconic acid δ-lactone (GDL), allowing the immobilization of mucin within a crosslinked alginate hydrogel.[127] The intended application of this hydrogel was for the assessment of drug diffusion, where conventional methods tend to neglect the thick mucus layer that orally administered drugs face when ingested.[127] In contrast, Taylor et al. (2005) simply mixed alginate and mucin solutions to allow for alginate-mucin and mucin-mucin interaction to be used as a substrate for studying *P. aeruginosa* growth in a mucus-like microenvironment.[128] Both formulations were reported to have viscoelastic properties similar to native mucus and are promising hydrogel formulations to address a simple modifiable mucus hydrogel for various applications.

CHAPTER 2.   THESIS AIMS

2.1 Overview

The overall goal of this thesis is to address the need for a simple, yet robust *in vitro* mammalian-microbial co-culture platform for studying host-microbe interaction. By designing and fabricating an artificial mucus hydrogel for a PEG-DEX ATPS mammalian-microbial co-culture using common laboratory chemicals and equipment, this model can be easily accessible and utilized in the typically equipped life science laboratory for disease modelling and antibiotic resistance testing. Although some work has been done to recapitulate the mucus microenvironment by cell differentiation, this process is time consuming and is limited by the low levels of mucus secretion. The investigation of alternative mucus microenvironments for host-microbe interaction remains largely unexplored.

The principal aims of this study are to: (1) Explore alginate hydrogel formulations to fabricate a mucus-like hydrogel that can be readily formed on top of mammalian cells and is compatible with a PEG-DEX ATPS co-culture system. (2) Characterize and understand the relationships between the physical properties and the biological functions of an alginate-mucin hydrogel in an ATPS co-culture system. (3) Establish a mammalian-microbial co-culture using a PEG-DEX ATPS for bacterial deposition on top of an artificial mucus hydrogel.

2.2 Aim 1: Identification of Hydrogel Formulations Suitable for ATPS Mammalian-Microbial Co-Culture

Objective: To identify a hydrogel formulation that can be readily formed directly on top of mammalian cells and characterize its compatibility with ATPS mammalian-microbial co-culture

based on specific design criteria including: gelation time, cytocompatibility, mammalian cell adherence, selective diffusivity, and the stability of ATPS formation (Table 1).

Hypothesis 1: With a hydrogel overlaying the mammalian monolayer, the PEG-mediated cytotoxicity will be reduced and allow for a stable ATPS formation directly on top of the hydrogel surface.

Rationale: The ease of use of alginate hydrogels as well as its cytocompatibility and non-cell adherent characteristics are all desired properties of an artificial mucus for the application of direct addition on top of a mammalian monolayer. To mimic the natural biochemical characteristics of mucus within an alginate hydrogel, alginate-mucin (ALG-MUC) semi-interpenetrating polymer network (semi-IPN) can be fabricated, where mucin is immobilized within the crosslinked alginate network. The simple ionic crosslinking of alginate also allows for the ability to easily tune the physical characteristics of the ALG-MUC semi-IPN by modifying the crosslinking density. Additionally, PEG used in current ATPS formulations is known to be cytotoxic towards mammalian cells; therefore, a mucus layer can function as a barrier to mitigate direct contact of PEG with the underlying mammalian cells.

Table 1: List of artificial mucus hydrogel design parameters.

Design Criteria	Design Input	Design Rationale
Gelation time	*The time of hydrogel gelation should take no longer than 1 hour.*	*Media is removed during the gelation process, which can result in significant cell death.*
Cytocompatibility	*Hydrogels overlaid onto mammalian cells shall not cause significant cell death compared to when no hydrogel is present.*	*Natural mucus is non-harmful toward host cells.*
Mammalian cell adherence	*Hydrogels shall be non-cell adherent in that mammalian monolayer remains intact after removal of hydrogel layer.*	*Cell adherent hydrogels may result in cell migration into the network, which is not representative of natural mucus epithelium cell behavior.*
Selective diffusivity	*Hydrogel overlay shall provide mammalian cells protection from PEG-mediated cytotoxicity in that cell viability does not significantly differ from cells grown in normal cell culture media.*	*PEG is cytotoxic towards mammalian cells; therefore, hydrogel must mitigate PEG diffusion while allowing for nutrient and oxygen diffusion for cell survival.*
Stable ATPS formation	*Hydrogel surface shall remain flat after gelation to allow for stable DEX droplet formation upon ATPS deposition.*	*Upon deposition of the DEX-phase droplet, a flat hydrogel surface is required to avoid movement of the DEX droplet.*

2.3   Aim 2: Characterization of Alginate-Mucin Hydrogel Viscosity and Diffusivity

Objective: To measure the viscosity of the artificial mucus hydrogels, assess the diffusivity of DEX and relevant biomolecules (IgG, LL-37) through the hydrogels, and compare the observed physical characteristics to the biological functions observed in objective 3.

Hypothesis 2: Increasing the mucin content within the alginate-based hydrogel will increase hydrogel viscosity and reduce the diffusivity of biomolecules and deposited bacteria compared to alginate hydrogels without mucin.

Rationale: The physical characteristics, such as viscosity and diffusivity, of mucus can affect how the mucus layer functions. The rate at which molecules and bacteria travel through mucus can be altered based on the composition, where low viscosity materials will allow for increased diffusion and vice versa. Therefore, it is important to have the ability to control the physical properties of the artificial mucus hydrogel. Mucins are also known to carry overall negative charges, which can impact the diffusion of charged molecules through electrostatic interactions.

2.4   Aim 3: Establishment of a Mammalian-Microbial Co-Culture using a PEG-DEX ATPS Containing an Artificial Mucus Layer

Objective: To demonstrate the spatial distribution of bacterial species within the ATPS co-culture with an artificial mucus hydrogel layer and assess the effect of mucin on bacterial growth as well as the effects of antibiotics on bacterial growth within the artificial mucus hydrogels.

Hypothesis 3a: Alginate-based hydrogels containing mucin will provide a microenvironment for increased bacterial growth and bacterial persistence after antibiotic treatment.

Hypothesis 3b: Alginate-based hydrogel containing mucin will provide an improved barrier function to pathogenic bacteria to reduce the level cell death of the underlying mammalian cells compared to alginate hydrogel without mucin.

Rationale: The human mucus layer provides a spatially complex microenvironment for polymicrobial growth and host-microbe interaction. Host cell death and inflammatory response are often dependent on the barrier function of the mucus layer and proximity of the microbes to the mucus-epithelium interface. Therefore, it is important to assess the spatial distribution of bacterial species within the system to understand the barrier functions of the artificial mucus in this *in vitro* model (Figure 3). Moreover, bacterial antibiotic resistance within the mucus

environment is a common occurrence in chronic infection; thus, it is important to assess the

effects of antibiotics on bacterial proliferation within this *in vitro* co-culture system.
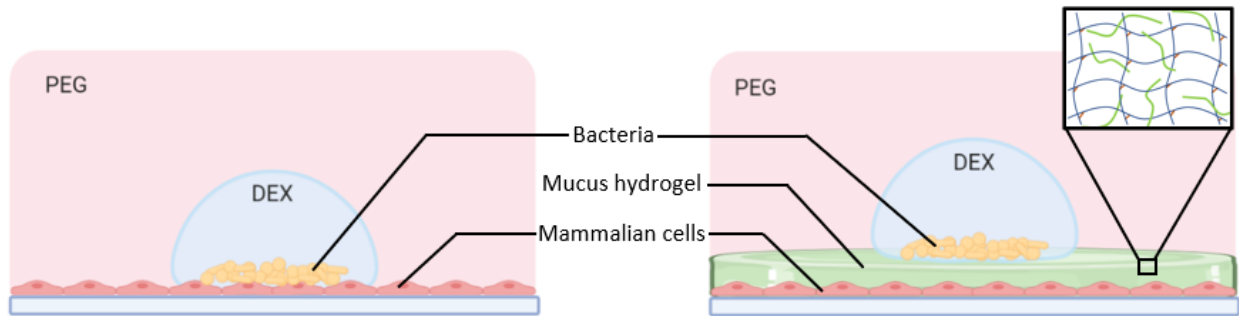
Figure 3: Illustration of a PEG-DEX ATPS mammalian-microbial cell co-culture with and without an artificial mucus hydrogel layer. Mammalian-microbial co-culture, where bacteria cells are grown directly on top of a mammalian monolayer (left) or on top of an incorporated artificial mucus hydrogel layer (right) with bacteria confined within a DEX-phase droplet.

CHAPTER 3. MATERIALS AND METHODS

3.1 Preparation of Aqueous Two-Phase System Formulations

Aqueous two-phase system (ATPS) formulations were prepared using polyethylene glycol (PEG, 35 kDa, Sigma-Aldrich) and dextran (DEX, 500 kDa, Pharmacosmos). The two formulations used consisted of 5% PEG/5% DEX (5% ATPS) and 10% PEG/10% DEX (10% ATPS) (w/v), where PEG and DEX were dissolved in either RPMI medium (Gibco) or Dulbecco's Modified Eagle Medium (DMEM, 1x, Gibco) containing 1% (v/v) fetal bovine serum (FBS, Thermo Fisher Scientific) and 1% (v/v) antibiotic-antimycotic (anti-anti, 100x, Gibco) (F1 and F2, Table 2). Anti-anti was only used for PEG-mediated cytotoxicity assays when bacteria was not being introduced into the cell culture (F3 and F4, Table 2). To make the ATPS, PEG and DEX were dissolved in cell culture medium (RPMI or DMEM) by mixing overnight on a rocking platform shaker (VWR) followed by addition of 1% (v/v) FBS and 1% (v/v) Anti-Anti, then sterilized by suction filtration (0.22 μm). Filter sterilized ATPS were centrifuged for 90 minutes at 3000 x g to obtain phase separation of the PEG-phase (upper) and DEX-phase (lower). The two phases were then aliquoted into separate Falcon tubes and stored at 4 °C.

Table 2: List of ATPS formulations used within this study.

	Weight and Volumes for 40 ml			
	PEG (g)	DEX (g)	FBS (ml)	Anti-Anti (ml)
F1	2	2	0.4	0.4
F2	4	4	0.4	0.4
F3	2	2	0.4	-
F4	4	4	0.4	-

3.2   Mammalian Cell Culture

Cell lines used in this study include a human bronchial epithelial cell line, 16-HBE (kindly provided by Dr. Elizabeth Cowley, Dalhousie University), and a colorectal adenocarcinoma cell line, Caco-2 (kindly provided by Dr. Andrew Stadnyk, Dalhousie University). 16-HBE cells were grown and maintained in DMEM/F-12 media (10% FBS, 1% anti-anti), a 1:1 ratio mixture of DMEM (Gibco) and Ham's F-12 Nutrient Mixture (Gibco), at 37 °C, 5% CO_2. Caco-2 cells were grown and maintained in DMEM (10% FBS, 1% Anti-Anti) at 37 °C, 5% CO_2. During experiments, cells were seeded into 24-well plates at a cell density of ~4000 cells/well (for Caco-2) and ~8000 cells/well (for 16-HBE) then grown for 24 hours followed by a media change to low FBS containing RPMI (1% FBS, 1% Anti-Anti) or DMEM (1% FBS, 1% Anti-Anti) for 16-HBE and Caco-2, respectively. Mammalian cell stocks were stored and maintained in the appropriate culture media containing 5% dimethyl sulfoxide (DMSO, Sigma-Aldrich) at ~1 million cells/ml in cryotubes at -196 °C, in liquid nitrogen.

3.3   Bacterial Strains and Culture

Bacterial strains used include *Pseudomonas aeruginosa* PA14 and *Shigella flexneri* M90T (gifted by Dr. Zhenyu Cheng, Dalhousie University). *P. aeruginosa* cultures were grown in LB broth (Sigma-Aldrich) supplemented with 250 µg/ml carbenicillin disodium salt (Sigma-Aldrich) and incubated at 37 °C with shaking at 200 rpm. All cultures were grown from single colonies after streaking LB agar (1.5 %, w/v, Sigma-Aldrich) plates (250 µg/ml carbenicillin) from frozen stocks. *P. aeruginosa* stocks were stored in 1 ml LB broth containing 25% (v/v) glycerol and 250 µg/ml carbenicillin at -80 °C.

S. flexneri cultures were grown in tryptic soy broth (TSB, Fisher Scientific) supplemented with 100 µg/ml ampicillin (Sigma Aldrich) and incubated at 37 °C with shaking at 200 rpm. All cultures were grown from single, red-pigmented colonies after streaking TSB Congo red (200 µg/ml, Sigma-Aldrich) agar (1.5 %, w/v) plates (100 µg/ml ampicillin) from frozen stocks. *S. flexneri* stocks were stored in 1 ml TSB containing 25% (v/v) glycerol and 100 µg/ml carbenicillin at -80 °C.

3.4   Preparation of Alginate and Alginate-Mucin Interpenetrating Polymer Network Hydrogels

To find the appropriate alginate gelation technique for ATPS co-culture, three different crosslinking methods were explored using either: (1) 100 mM $CaCl_2$, (2) $CaCO_3$, or (3) low concentration $CaCl_2$ (4.5 mM – 6 mM). Alginate stock solutions were made by mixing alginic acid sodium salt (low viscosity, MP Biomedicals) in distilled water for a 2% (w/v) solution that was mixed slowly using a magnetic stir rod overnight and filtered sterilized (0.45 µm). Filtered alginate solutions were then frozen in 50 ml Falcon tubes (15 ml per tube, frozen on side) at -20 °C and lyophilized (FreezeZone 2.5 Liter Benchtop Freeze Dryer, LABCONCO) for 24 hours. Prior to use, the lyophilized alginate was placed into a petri dish and UV sterilized (254 nm wavelength) for 1 hour, then reconstituted in PBS. Unused lyophilized alginate was stored at -20 °C and used within 2 weeks after reconstitution.

To crosslink alginate hydrogels with 100 mM $CaCl_2$, 300 µl of a 1% (w/v) alginate solution was added to a 24-well plate. Crosslinking solutions were made by dissolving calcium chloride ($CaCl_2$, Sigma-Adrich) in water at 100 mM and filter sterilized (0.22 µm). Crosslinking

solution was then deposited (300 µl) on top of the 1% alginate in a dropwise manner to crosslink the alginate solution, where excess $CaCl_2$ solution was removed using a pipette.

Slow alginate hydrogel crosslinking was carried out using calcium carbonate ($CaCO_3$, Sigma-Aldrich) and D-(+)-gluconic acid δ-lactone (GDL, Sigma-Aldrich) at a 1:2 ($CaCO_3$:GDL) molar ratio to maintain a neutral pH. First, an alginate solution was mixed with a $CaCO_3$ suspension in PBS and vortexed for 1 minute. GDL solution (in PBS) was then added and vortexed for 1 minute, where the alginate:$CaCO_3$:GDL mixture was transferred into a 24-well plate and incubated at 37 °C for 30 minutes for gelation. All solutions were added at volumes for final concentrations of 1% (w/v) alginate and 60 mM:120 mM $CaCO_3$:GDL.

Alternatively, alginate hydrogels were crosslinked using $CaCl_2$ at low concentrations (4.5 mM – 6 mM) to form partially crosslinked, soft alginate hydrogels. The low concentration $CaCl_2$ solutions were made in DMEM by mixing aliquots of a filter sterilized (0.22 µm), 100 mg/ml $CaCl_2$ stock solution (in distilled water) at different volumes to generate $CaCl_2$ concentrations of either 9 mM, 9.5 mM, 10 mM, 11 mM, or 12 mM. All crosslinker solution were made fresh prior to crosslinking. To fabricate the partially crosslinked alginate hydrogels, 2% (w/v) alginate solutions were mixed with the $CaCl_2$ crosslinker solution (in DMEM, 9 mM, 9.5 mM, 10 mM, 11 mM, or 12 mM), where alginate and $CaCl_2$ volumes were mixed at a 1:1 ratio for final concentrations of 1% (w/v) alginate and $CaCl_2$ concentrations of 4.5 mM, 4.75 mM, 5 mM, 5.5 mM, or 6 mM. Alginate:$CaCl_2$ mixtures were immediately transferred to a 24-well plate and incubated for 1 hour at 37 °C for gelation.

Alginate-mucin (ALG-MUC) semi-interpenetrating polymer networks (semi-IPN) hydrogels were prepared using low $CaCl_2$ concentrations as described above. Four different ALG-MUC semi-IPN hydrogels were tested: 1% alginate with 0.1% mucin (1%

ALG/0.1%MUC), 1% alginate with 0.5% mucin (1% ALG/0.5% MUC), 1% alginate with 1%

mucin (1% ALG/1% MUC), and 1% alginate with 1.5% mucin (1% ALG/1.5% MUC). A 3%

(w/v) alginate solution was mixed with a 10% (w/v) solution of Mucin Type II (Sigma-Aldrich),

where mucin was sterilized by spreading dry mucin on a petri dish and covered with 95% ethanol

to be incubated at 70 °C for 24 hours, followed by reconstituting the sterilized mucin in PBS.

The alginate and mucin solutions were mixed in a microcentrifuge tube or Falcon tube at

volumes that would generate the desired final concentrations, where an amount of PBS was

added to make up half of the total volume. The remaining half of the total volume was DMEM

containing 9 mM, 9.5 mM, 10 mM, 11 mM, or 12 mM $CaCl_2$, where the ALG-MUC hydrogel

mixture was mixed carefully using a pipette to prevent air bubble formation (See Table 3 for

example volumes). Immediately after mixing the hydrogel mixtures, they were then deposited

into 24-well plates either into an empty well (for hydrogel stability testing, Tilt Test) or directly

onto a monolayer within a 24-well plate, where plates were incubated at 37 °C for one hour.

Table 3: Alginate and alginate-mucin semi-IPN hydrogel component volumes (µl) for a 900 µl hydrogel.

	Hydrogel Formulation				
	1% ALG	1% ALG/ 0.1% MUC	1% ALG/ 0.5% MUC	1% ALG/ 1% MUC	1% ALG/ 1.5% MUC
3% alginate sol.	300	300	300	300	300
PBS	150	141	105	60	15
10% mucin sol.	0	9	45	90	135
$CaCl_2$ (in DMEM)	450	450	450	450	450
Total vol.	**900**	**900**	**900**	**900**	**900**

To test the stability of the hydrogel (at various crosslinking concentrations: 4.5 mM, 4.75

mM, 5 mM, 5.5 mM, and 6 mM) after one hour of gelation, a modified inverted tube test[129] ("tilt

test") was carried out using a 24-well plate. The 24-well plates, containing 500 µl of hydrogel

per well, were tilted at an ~80 ° angle for 10 seconds and imaged using a digital camera to observe the stability of the hydrogels.

3.5   Assessing the Roles of Hydrogels in PEG-Mediated Cytotoxicity Mitigation

To demonstrate the cytotoxic effects of PEG-phase media on 16-HBE cells, cells were seeded into wells of a 24-well plate at 40% confluency (~8000 cells/well) and incubated for 24 hours. Culture media was then changed to low FBS media (RPMI, 1% FBS, 1% anti-anti) and incubated for 24 hours. Media was then removed from each well and cells were washed once with PBS followed by the addition of a 5% (F1) and 10% (F2) PEG-phase solution and incubated for 96 hours. A Live/Dead Assay (Thermo Fisher Scientific) and Hoechst stain (Hoechst 33342, Thermo Fisher Scientific) were performed to assess cell viability at 48-, 72-, and 96-hour time points. Calcein AM and Ethidium homodimer-1 working concentrations were both at 4×10^{-4} mM, while Hoechst was used at 5 μg/ml (8.1×10^{-3} mM), all diluted in PBS.

To assess the ability of alginate-based hydrogels in mitigating PEG-mediated cytotoxicity, 16-HBE cells were seeded into 24-well plates as mentioned above and incubated in PEG-phase solutions (5% and 10%) with 300 μl of hydrogel overlaid on top of the monolayer. Cells were washed once with PBS followed by the addition of 1% ALG or ALG-MUC (1% ALG/0.5% MUC or 1% ALG/1% MUC) hydrogels. PEG-phase (F1 or F2) or RPMI media (1% FBS and 1% Anti-Anti) was added on top of the hydrogels and incubated at 37 °C, 5% CO_2 for 48 hours. After the incubation period, media and hydrogels were removed from the wells by suction and Live/Dead Assay and Hoechst stain were performed to assess cell viability.

After Live/Dead staining, fluorescent microscopy was performed where 5 images were taken per well using DAPI (nuclei), GFP (live cells), and RFP (dead cells) channels. Each image

was analyzed using Celleste Image Analysis Software to count the number of nuclei and dead cells. Cell viability was calculated by using equation 1.

$$Cell\ Viability\ (\%) = \frac{Total\ \#\ of\ cells - Dead\ cells}{Total\ \#\ of\ cells}\ x\ 100 \tag{1}$$

3.6 Determination of Hydrogel Viscosities using a Falling Ball Viscometer Method

Mucin-Alginate hydrogels were formulated as described above, making a total volume of 6 ml of hydrogel in 15 ml centrifuge tubes. Hydrogel density was measured each time by weighing 0.5 ml of the hydrogel sample on a scale. The 6 ml hydrogel samples were transferred into shortened 15 ml centrifuge tubes (cut at the 7 ml mark) for viscosity measure using a falling ball viscometer method.

To measure the hydrogel viscosity, 4 mm (diameter) chrome steel ball bearings (Bearings Canada) were dropped into the tubes containing either a 1% ALG, 1% ALG/0.5% MUC, or 1% ALG/1% MUC hydrogel sample. First, 2 balls were dropped into the tubes consecutively and recorded using a digital camera at 60 frames per second. A third ball was dropped into the hydrogel sample either 1 hour or 3 hours after the initial two drops. Recorded videos were analyzed using Tracker software to generate distance-time (D-T) graphs of the vertical distance travelled by the dropped balls. The terminal velocities of each ball were determined by performing a linear regression (line-of-best-fit) at the linear portion of each D-T curve on Prism GraphPad to determine the slope of the first drop in each hydrogel sample. The viscosity of each hydrogel was then calculated using equation 2 below, derived from Stoke's Law, where η is the viscosity, r is the radius of the steel ball, g is gravity, ρ_b is the density of the steel ball, ρ_l is the density of the hydrogel, and v_t is the terminal velocities of the initial drops (Drop 1).

$$\eta = \frac{2r^2 g(\rho_b - \rho_l)}{9v_t} \tag{2}$$

3.7 Measurement of Diffusion Coefficient within Hydrogels by Fluorescent Imaging

Diffusion coefficients of fluorescein tagged DEX, IgG, and LL-37 were all assessed by fluorescent imaging over time. FITC-DEX (150 kDa, Sigma Aldrich) and 5-FAM-LL-37 (AnaSpec) were used at 50 μg/ml, while Anti-Human IgA-FITC (IgG-FITC, Sigma Aldrich) were diluted 1:30 in PBS (37 μg/ml). To assess diffusion through alginate and alginate-mucin semi-IPN hydrogels, straight channels within a polydimethylsiloxane (PDMS) chip were fabricated using a 3D printed mold, where channels were 0.5 mm (height) x 0.5 mm (width) x 10 mm (length) with 2 mm diameter biopsy punched holes (vertical) at both ends. PDMS chips were formed using a silicone elastomer kit (Sylgard) by mixing PDMS elastomer with curing agent at a 10:1 ratio (elastomer:curing agent) and poured into the 3D printed molds to be degassed in a vacuum chamber and cured at room temperature (RT) for 48 hours. PDMS chips were then incubated in PBS at 37 °C overnight prior to use to remove any air trapped within the chip, and plasma oxidized onto glass slides (Figure 4A). Hydrogel mixtures were then formed as mentioned above and injected into the straight channels using a wide bore pipette tip until hydrogel front reached the end of the channel and incubated at RT for 1 hour (Figure 4B). Custom pipette tips were 3D printed using an opaque resin with a straight edge and narrowing tip as reservoir holders that were inserted at both ends of the straight channels (Figure 4A). Prior to fluorescent imaging, reservoirs at each end of the straight channels were filled with half diluted DMEM (in PBS) using a 25-guage syringe and incubated at RT for 3 hours to allow the hydrogel to reach the swelling capacity. The diluted DMEM was then removed from the reservoir opposite

to the hydrogel injection site and filled with the fluorescent mixture (in half diluted DMEM) using a 25-gauge syringe needle. The diffusion device was then placed into a humidified chamber (single-well plate containing presoaked Kim wipes) and imaged for 6 hours at 4-minute intervals.

Diffusion profiles (2 mm, starting at the hydrogel-liquid interface) were generated using ImageJ for the first 30 frames (2 hours). Fluorescent values were normalized to the fluorescence of a channel only containing fluorescent solution, where a matrix of normalized data was used to calculate the effective diffusion coefficient using a custom MATLAB code from Hettiaratchi et al. (2018) to fit the data to a 1-dimensional diffusion function (equation 3), where *erfc* is the complementary error function, F is the fluorescence normalized to the initial timepoint, x is the distance from the reservoir-hydrogel interface (cm), t is elapsed time, and D_{eff} is the effective diffusion coefficient (cm^2/s).[130]

$$F(x,t) \propto erfc\left(\frac{x}{2\sqrt{D_{eff}t}}\right) \tag{3}$$
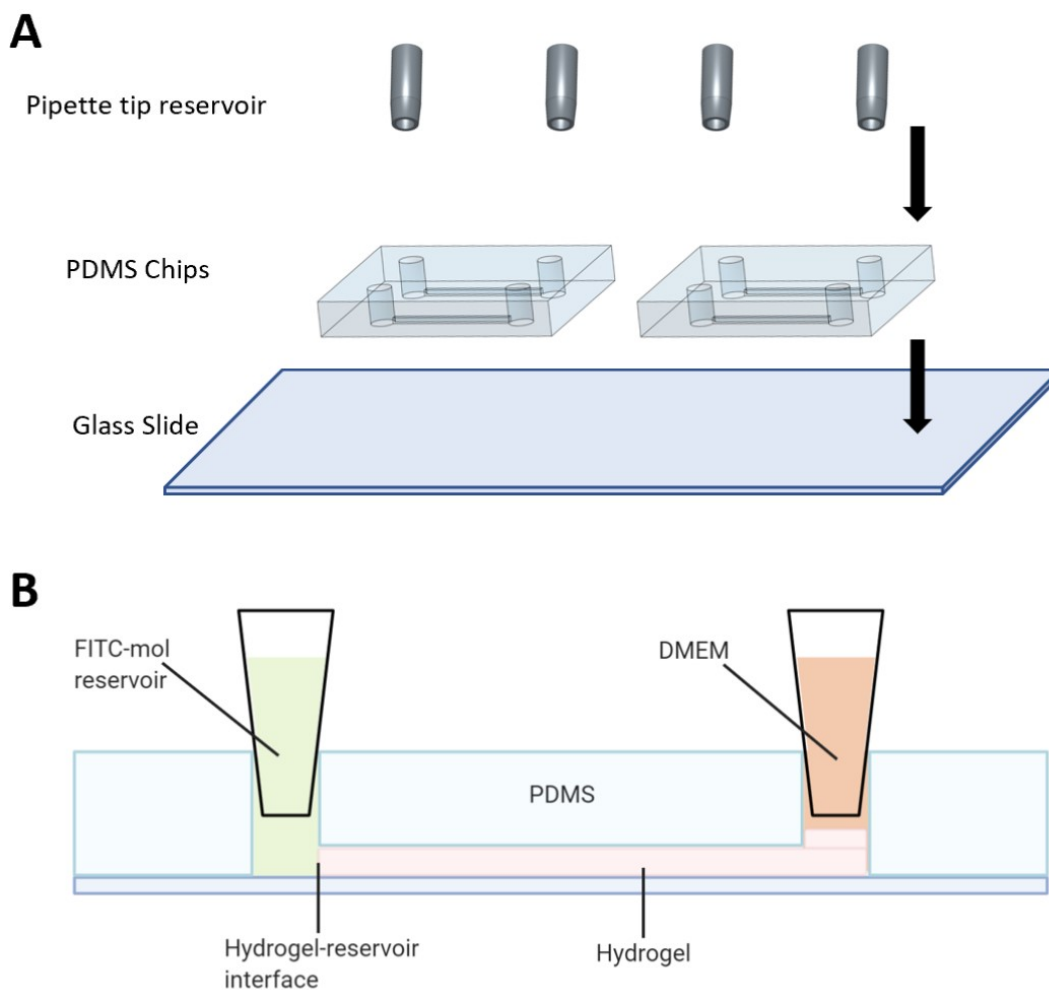
Figure 4: Schematic of PDMS diffusion device set-up. (A) PDMS straight channel chip assembly, where PDMS chips were covalently attached to a glass slide, followed by insertion of 3D-printed pipette tip reservoirs. **(B)** Side view of PDMS straight channel containing hydrogel and fluorescein tagged molecules reservoir.

3.8 PEG-DEX ATPS Contact Angle Measurement on Hydrogel Surfaces

The stability of an ATPS is dependent on the interfacial tension between the two phases, which is positively correlated with the contact angle formed by the DEX droplet on the surface in which it is in contact.[131] Therefore, to assess the stability of the ATPS on the different alginate-based hydrogel surfaces the contact angles of the DEX droplets were measured. To measure the contact angle of DEX droplets, custom well plates were fabricated by using a hand-held rotary tool (Dremel Micro) to carve out 4 wells from a 24-well plate. Wells were cut out to have a front

and back opening where glass cover slips were epoxied for a front and rear window with a plastic ledge at the front window to prevent meniscus formation (Figure 5). Alginate and alginate-mucin hydrogels were fabricated as mentioned above and deposited into the custom wells until the volume was level with the plastic ledge. After 1 hour of incubation at RT, an ATPS was formed on each hydrogel surface and tissue culture polystyrene (TCPS) with a 2 μl DEX droplet and imaged from a sideview using a Trinocular Stereo Zoom Microscope (3.5X – 180X, AmScope). Contact angles were then estimated using the angle tool on ImageJ, where two angles were measured per DEX droplet and averaged.

Additionally, the DEX droplet dispersion was assessed by imaging of a fluorescent DEX droplet on the different alginate-based hydrogels surfaces. To generate the fluorescent DEX-phase, 15 μl of a 1% (w/v) FITC-DEX (150 kDa) was added to 300 μl of either a 5% or 10% DEX-phase. Alginate-based hydrogels (1% ALG, 1% ALG/0.5% MUC, and 1% ALG/1% MUC) were formed in 24-well plates using 300 μl of hydrogel and 200 μl of PEG-phase deposited on top of the hydrogel. The fluorescent DEX was deposited (2 μl) into the PEG-phase using a liquid handling robot (Biomeck 4000, Beckman Coulter) and allowed to settle onto the hydrogel surface for 5 minutes.
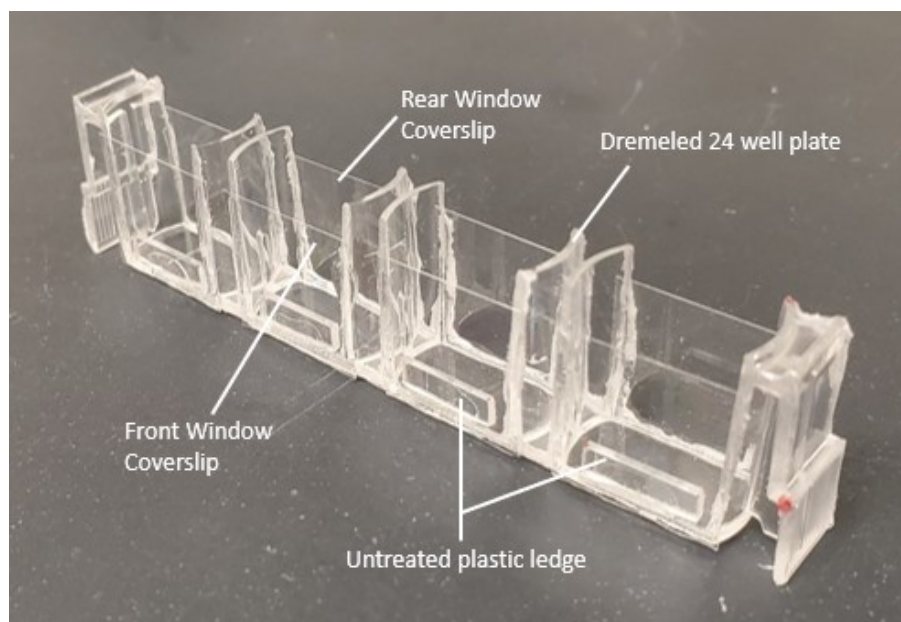
Figure 5: Custom 4-well plate used for sideview imaging of ATPS formulation on alginate-based hydrogels. Custom well plate cut using a Dremel, where coverslips were epoxied to form a side window with a plastic ledge to prevent meniscus formation after hydrogel deposition.

3.9 Determination of Minimum Inhibitory Concentration (MIC) of Ciprofloxacin for *P. aeruginosa* and *S. flexneri*

Minimum inhibitory concentrations (MIC) of ciprofloxacin for the two strains of bacteria used (*P. aeruginosa* and *S. flexneri*) were determined by performing a broth dilution technique adapted from Wiegand et al. (2008). First, each bacterial strain was grown in overnight cultures and serially diluted to be plated on agar plates to perform a colony forming unit (CFU) count to determine the correlation between measured optical density at 600 nm (OD$_{600}$) and CFU/ml.

Both *P. aeruginosa* and *S. flexneri* were grown in the appropriate broth for 18 hours. The overnight cultures were diluted by a factor of 10 in their respective broth and OD$_{600}$ was measured using Varioskan Lux plate reader (Thermo Fisher Scientific). The diluted cultures were further diluted seven times (1:10 dilutions). Dilutions of $10^{-5} - 10^{-7}$ were plated (100 µl) onto agar plates and spread using a sterile spreader. Plates were then incubated for 18-20 hours.

Only plates containing colony counts of 100 – 400 colonies per plate were used to calculate the CFU/ml associated with the measured OD_{600}.

To determine the MIC of ciprofloxacin for *P. aeruginosa* and *S. flexneri*, ciprofloxacin was added to 1 ml of bacterial culture broth (LB for *P. aeruginosa* and TSB for *S. flexneri*) in a microcentrifuge tube for a final concentration of 64 µg/ml. A 100 µl aliquot of the Ciprofloxacin containing broth was added to the first well of 2 rows in a 96-well plate, where the following 9 wells in each row contained 50 µl of the respective broth in each well. The antibiotic was then serially diluted by a factor of 1:2. The last two wells of each row were used as a growth control (GC) and sterility control (SC), where the GC well contained 50 µl of broth and the SC well contained 100 µl of broth. Bacteria overnight cultures were then adjusted to bacterial densities of 1 x 10^8 CFU/ml by determining the OD to adjust to using the ratio of OD to CFU/ml as described above. The adjusted bacteria culture was added (50 µl) to each antibiotic containing well and the GC well for a final bacterial density of 5 x 10^5 CFU/ml and antibiotic concentrations at half of the original concentration (Table 4). The 96-well plate was then incubated at 37 °C, 5% CO_2 for 16 hours. The next day, the MIC was determined by visually inspecting for bacterial growth (cloudiness), where the first clear well adjacent to a cloudy well was concluded to be the MIC.

Table 4: Antibiotic (Ciprofloxacin) dilutions carried out and 96-well plate layout with growth control (GC) and Sterility Control (SC).

	Well Number											
	1	2	3	4	5	6	7	8	9	10	11	12
Ciprofloxacin Concentration (µg/ml)	32	16	8	4	2	1	0.5	0.25	0.125	0.0625	GC	SC

3.10 Determination of Bacteria Abundance within the Liquid and Hydrogel Components of an ATPS Co-Culture through Colony Forming Unit Counting

Bacterial distribution within the co-culture system was determined by performing a colony forming unit (CFU) count by single plate-serial dilution spotting (SP-SDS) as described by Thomas et al. (2015).[132] Briefly, PEG-phase and hydrogels were removed using a pipette (wide bore for hydrogels, ~3 mm diameter) and transferred into separate microcentrifuge tubes. Samples were then diluted with 500 µl of PBS and vortexed for 30 seconds per tube. Tubes were then centrifuged at 16,000 x g for 10 minutes to pellet bacteria and resuspended in 200 µl (PEG-phase sample) or 300 µl (hydrogel sample) of PBS. Resuspended samples were then serial diluted in a 96-well plate (10^{-2} – 10^{-9}). Diluted samples were then spot plated (20 µl) accordingly in each section of the agar plates and airdried for 10 minutes to be incubated at 37 °C, 5% CO_2 for 16 hours. Colonies were counted the next day and CFU/ml was calculated using the equation (4), where N is the CFU/ml, C is the colony count, and D is the number of 1:10 dilutions.

$$N = \frac{C \ x \ 50}{10^{-D}} \qquad (4)$$

3.11 Establishment of Mammalian-Microbial Co-Culture

Two sets of mammalian-microbial co-cultures were carried out: 16-HBE cells with *P. aeruginosa* and Caco-2 cells with *S. flexneri*. First, each cell line was seeded into a 24-well plate at ~40% confluency and incubated for 24 hours at 37 °C, 5% CO_2. A media change was then performed, RPMI (1% FBS) for 16-HBE cells and DMEM (1% FBS) for Caco-2 cells, and incubated for 24 hours at 37 °C, 5% CO_2. Alginate and alginate-mucin hydrogels (300 µl) were deposited on top of the monolayers and incubated at 37 °C for 1 hour to allow for hydrogel

gelation. As hydrogels were incubating, *P. aeruginosa* and *S. flexneri* overnight cultures were resuspended in DEX-phase at a bacterial density of ~3 x 10^8 CFU/ml. PEG-phase (200 µl) was then carefully pipetted into each well containing hydrogels followed by deposition of 0.5 µl of the bacteria-rich DEX-phase, with the respective mammalian cells, using a Biomek 4000 (Beckman Coulter) liquid handling robot. The 24-well plate was then imaged for 12 hours using an automated microscope (Evos FL Auto 2, Invitrogen) with an onstage incubator at 37 °C, 5% CO_2 with 80% humidity.

Co-culture experiments involving the use of antibiotic were initially set up as mentioned above but incubated for 7 hours to establish bacterial communities within the DEX droplet. After the 7-hour incubation, the PEG-phase was carefully removed using a pipette, and 200 µl of PEG-phase supplemented with 0.125 µg/ml Ciprofloxacin (Sigma-Aldrich) was added slowly to avoid disrupting the bacterial communities formed on top of the hydrogels. The antibiotic treated co-cultures were then incubated for another 12 hours under the same conditions. Live/Dead and Hoechst staining was carried out after both antibiotic treatment and non-antibiotic treatment experiments.

3.12 Statistical Analysis

All statistical analysis was performed on Graphpad Prism (Version 7.0), where mean values were reported with standard deviation (SD) as error bars (mean ± SD). At least 3 independent experiments were carried out prior to any statistical analysis. Statistical significance for all cell viability tests were determined using multiple t-test. Statistical significance of viscosity values and contact angles was determined by performing a one-way and two-way

analysis of variance (ANOVA), respectively. A two-way ANOVA was also carried out for effective diffusion coefficient and bacterial abundance data.

CHAPTER 4.   RESULTS

4.1   Comparison of Alginate Hydrogel Crosslinking Methods

To fabricate a hydrogel as an artificial mucus layer for this *in vitro* system, alginate was selected as the main component of the hydrogel network for its cytocompatibility, non-cell adherent characteristics, and ease of use. The first method of alginate crosslinking tested was using conventional $CaCl_2$ concentrations of 100 mM. This method allowed for instant alginate gelation as the $CaCl_2$ solution was deposited on top of the alginate in a dropwise manner. The resulting hydrogels were found to form uneven surfaces, which was an undesirable characteristic for ATPS formation. The uneven surface topology was identified after depositing a volume of DMEM media onto the hydrogel, where the thicker areas of hydrogel were covered by less media, and therefore observed as clear patches, and thinner areas of hydrogel were covered with more DMEM, observed as pink patches (Figure 6).
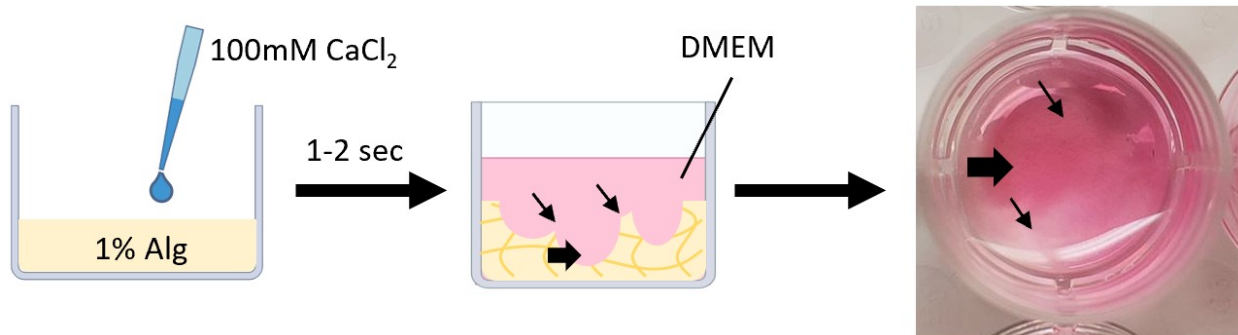
Figure 6: Illustration of fast gelling alginate using 100 mM CaCl₂. Alginate hydrogel (1%, w/v) formed through the addition of a 100 mM $CaCl_2$ solution in a drop-wise manner, demonstrating an uneven hydrogel surface formation within a 24-well, as indicated by the large (➡, thin hydrogel region) and small arrows (➜, thick hydrogel region).

Through the testing of the initial alginate crosslinking method, it was apparent that the rate at which the crosslinking reaction was occurring was an additional variable to consider. This

led to testing a slowed gelation method using $CaCO_3$ as the crosslinking agent. Because $CaCO_3$ is poorly soluble in water, a weak acid such as GDL is needed to dissociate Ca^{2+} from the CO_3^{2-} for crosslinking to occur. This method allowed for a slower rate of crosslinking, where the alginate:$CaCO_3$:GDL mixtures were vortexed in centrifuge tubes prior to depositing into a 24-well plate and incubated for 30 minutes for full gelation to occur (Figure 7A). When incubated in a PEG-phase solution, hydrogels were found to contract considerably over time. Additionally, the hydrogels formed using this technique were opaque as opposed to the transparent hydrogel formed when using $CaCl_2$ as the crosslinking agent (Figure 7B). Air bubble formation was also observed due vortexing of the hydrogel mixture prior to deposition.
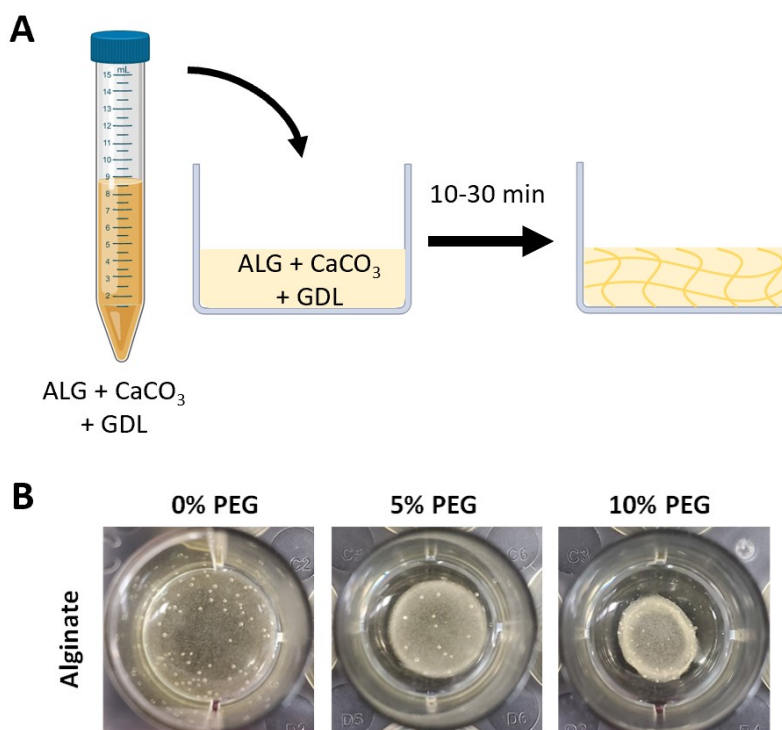
Figure 7: Slow gelling alginate hydrogels using CaCO₃ and GDL. (A) Illustration of 1% alginate hydrogel fabrication using $CaCO_3$ and GDL for controlled gelation. **(B)** Alginate hydrogel contraction after incubation in a 5% and 10% PEG-phase solution for 24 hours.

Another alternative method to using 100 mM $CaCl_2$ was to use lower concentrations of $CaCl_2$ to form more pliable, partially crosslinked hydrogels. This low $CaCl_2$ method was tested at concentrations ranging from 4.5 – 6 mM, where alginate solutions were mixed with the $CaCl_2$ crosslinking solution prior to depositing the hydrogel mixture into a 24-well plate. To test whether these low $CaCl_2$ concentrations could form intact alginate hydrogels, the 24-well plates were tilted to an ~80 ° angle to visually assess the stability, where the stability of the hydrogel was based on whether the hydrogels would shift after 10 seconds. This tilt test revealed that at the lower end of the $CaCl_2$ concentration range (4.5 mM, 4.75 mM, and 5 mM), hydrogels were more fluid-like, showing a shift within the well as the plate was tilted (Figure 8A, 0% mucin row). Hydrogels crosslinked using the higher $CaCl_2$ concentrations (5.5 mM and 6 mM) were more hydrogel-like with improved structural stability, where the hydrogel surface remained parallel to the bottom of the 24-well plate as it was tilted (Figure 8A, 0% mucin row).

Mucin was then added to the alginate mixtures prior to mixing with the $CaCl_2$ crosslinking solutions to form an alginate-mucin semi-IPN, where mucin monomers were immobilized within the crosslinked alginate network (Figure 8B). The lower crosslinked hydrogels (4.5 mM – 5 mM) with added mucin were observed to be less fluid-like, compared to alginate hydrogels without mucin. Additionally, it was found that the addition of mucin reduced the pH of the hydrogel environment, as indicated by the colour change of the Phenol Red (Figure 8A). Therefore, based on the stability and pH of these hydrogels, the 0.5% and 1% mucin containing alginate hydrogels were chosen for further experimentation, along with the 0% mucin alginate gel for comparison purposes (at 5.5 mM $CaCl_2$).
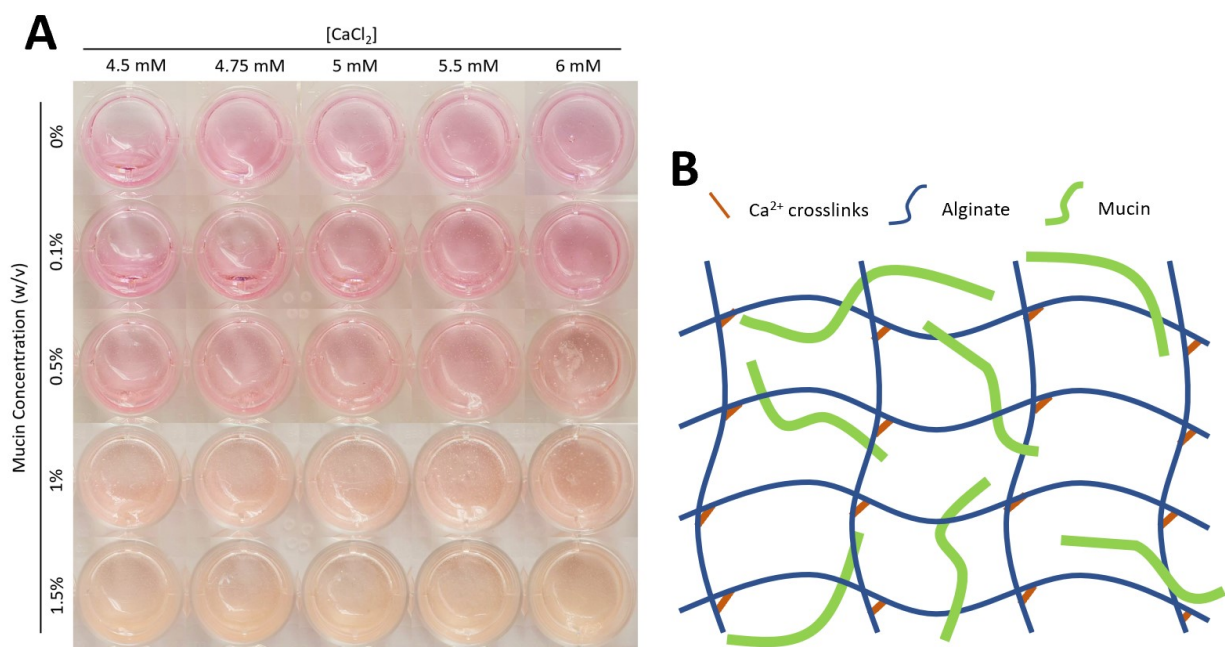
Figure 8: Qualitative assessment of alginate-based hydrogel structural integrity at various CaCl2 concentrations. (A) Alginate-based hydrogels crosslinked using low CaCl$_2$ concentrations in a 24-well plate tilted on an 80° angle. **(B)** Illustration of alginate-mucin semi-IPN with CaCl$_2$ crosslink bridges between alginate monomers.

When incubating the partially crosslinked alginate hydrogels in PEG-phase media, contraction was only observed in hydrogels containing mucin and not in the 1% ALG hydrogels (Figure 9). The degree of contraction was dependent on the concentration of PEG, where ALG-MUC hydrogel in the 10% PEG solution showed a higher level of contraction compared to those incubated in the 5% PEG-phase media. The concentration of mucin also played a role in this phenomenon, where the 1% ALG/1% MUC contracted more than the 1% ALG/0.5% MUC hydrogel in both the 5% and 10% PEG-phase solutions (Figure 9).
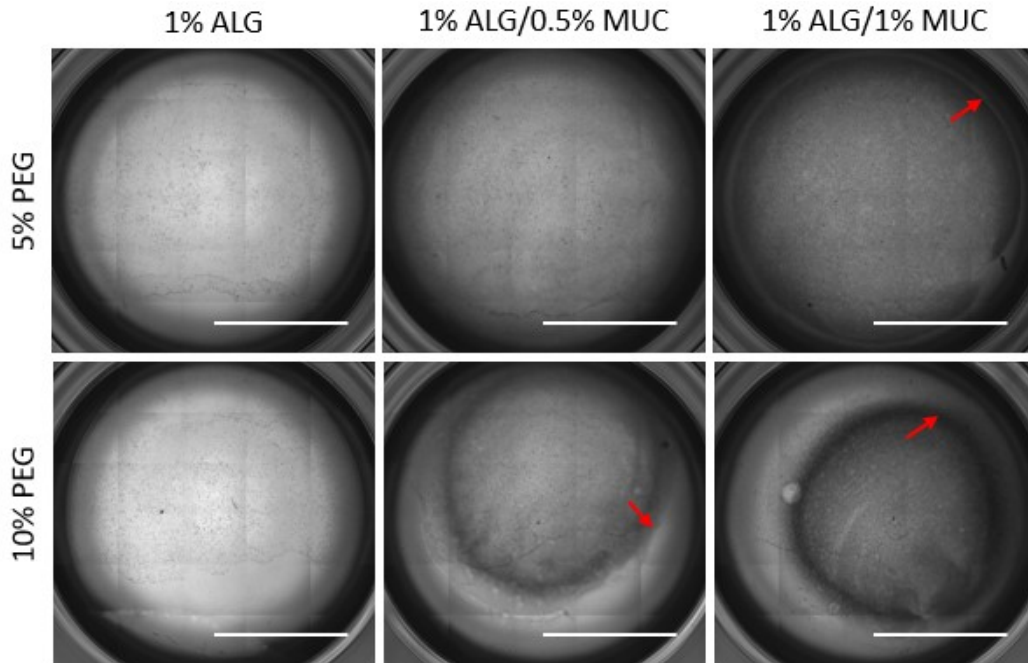
Figure 9: Alginate and alginate-mucin hydrogel contraction after incubation in PEG-phase solution for 24 hours. Stitched brightfield images of entire tissue culture wells (24-well plate) containing alginate-based hydrogels (1% ALG, 1% ALG/0.5% MUC, and 1% ALG/1% MUC), at 5.5 mM $CaCl_2$ concentrations, after 24 hours of incubation in a 5% and 10% PEG-phase solution, where red arrows indicate the outer edge of the contracted hydrogels (Scale bars = 5 mm).

4.2   Alginate and Alginate-Mucin Hydrogels Mitigate PEG-Mediated Cytotoxicity

A major problem with using a PEG-DEX ATPS for prolonged mammalian-microbial co-culture is that PEG is known to pose cytotoxic effects towards mammalian cells in a molecular weight dependent manner. Therefore, it is necessary for the artificial mucus hydrogel overlay to mitigate PEG from contacting the mammalian cells. Prior to testing the role of alginate-based hydrogels in PEG mitigation, we demonstrated that PEG is in fact cytotoxic towards mammalian cells in a concentration and time dependent manner. Both 5% and 10% PEG-phase solutions were used to incubate 16-HBE cells over a 96-hour period, where cell viability was significantly reduced after 48 hours (49.3 ± 14.2%) of incubation in a 10% PEG-phase and 72 hours (93.2 ± 1.0%) in a 5% PEG-phase solution compared to cells incubated in RPMI media (Figure 10).
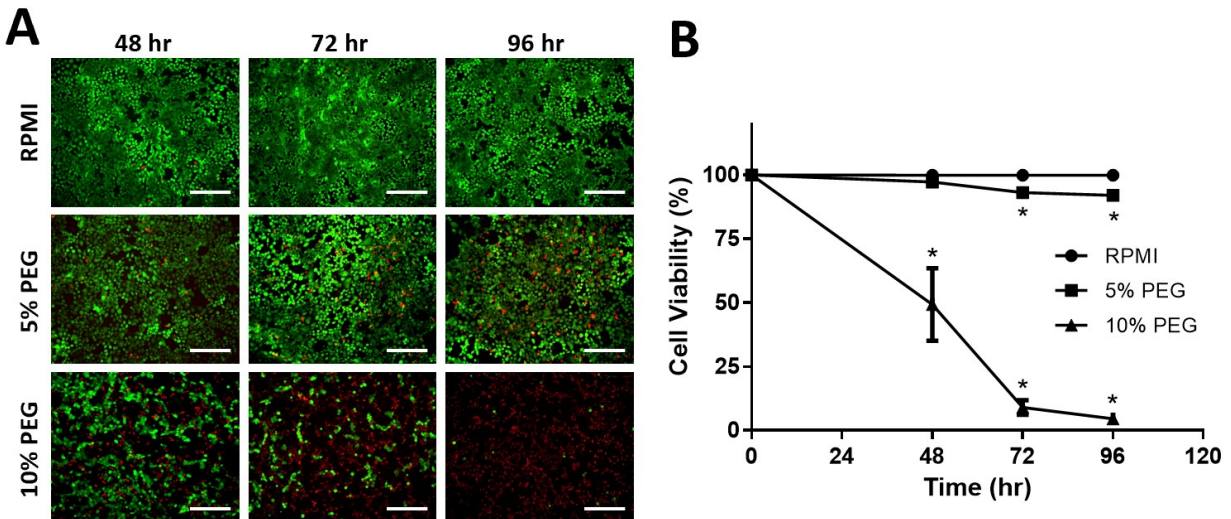
Figure 10: Cell viability of 16-HBE cells after 48, 72, and 96 hours of exposure to PEG-phase solution. (A) Fluorescent images of 16-HBE cells exposed to a 5% and 10% PEG-phase solution for up to 96 hours, after Live/Dead staining, where green cells are viable and red cells are non-viable (Scale bar = 500 μm). **(B)** Cell viability of 16-HBE cells over time, incubated in either 5% or 10% PEG-phase solution, where cells incubated in RPMI were used as a control (* indicates $p < 0.05$, n = 3).

To assess the role of the alginate-based hydrogels in mitigating PEG-mediated cytotoxicity, 300 μl of alginate-based hydrogel was deposited on top of 16-HBE cells grown in a 24-well plate prior to the addition of a 5% and 10% PEG-phase solution. With the addition of a hydrogel overlay on top of the mammalian monolayer, cell death was significantly reduced compared to cells without a hydrogel overlay, regardless of the hydrogel formulation (Figure 11A). When comparing between ATPS formulations, cell viability remained lower in the presence of 10% PEG-phase solution compared to the 5% PEG-phase solution, even with the incorporation of the hydrogel overlay (Figure 11).

A

1%ALG

Cell Viability (%)

*

*

5% PEG	-	+	-	-	+	-
10% PEG	-	-	+	-	-	+
Gel	-	-	-	+	+	+

1%ALG, 0.5%MUC

Cell Viability (%)

*

*

5% PEG	-	+	-	-	+	-
10% PEG	-	-	+	-	-	+
Gel	-	-	-	+	+	+

1%ALG, 1%MUC

Cell Viability (%)

*

*

5% PEG	-	+	-	-	+	-
10% PEG	-	-	+	-	-	+
Gel	-	-	-	+	+	+

B

No hydrogel	1% ALG	1% ALG/0.5% MUC	1% ALG/1% MUC

RPMI

5% PEG

10% PEG
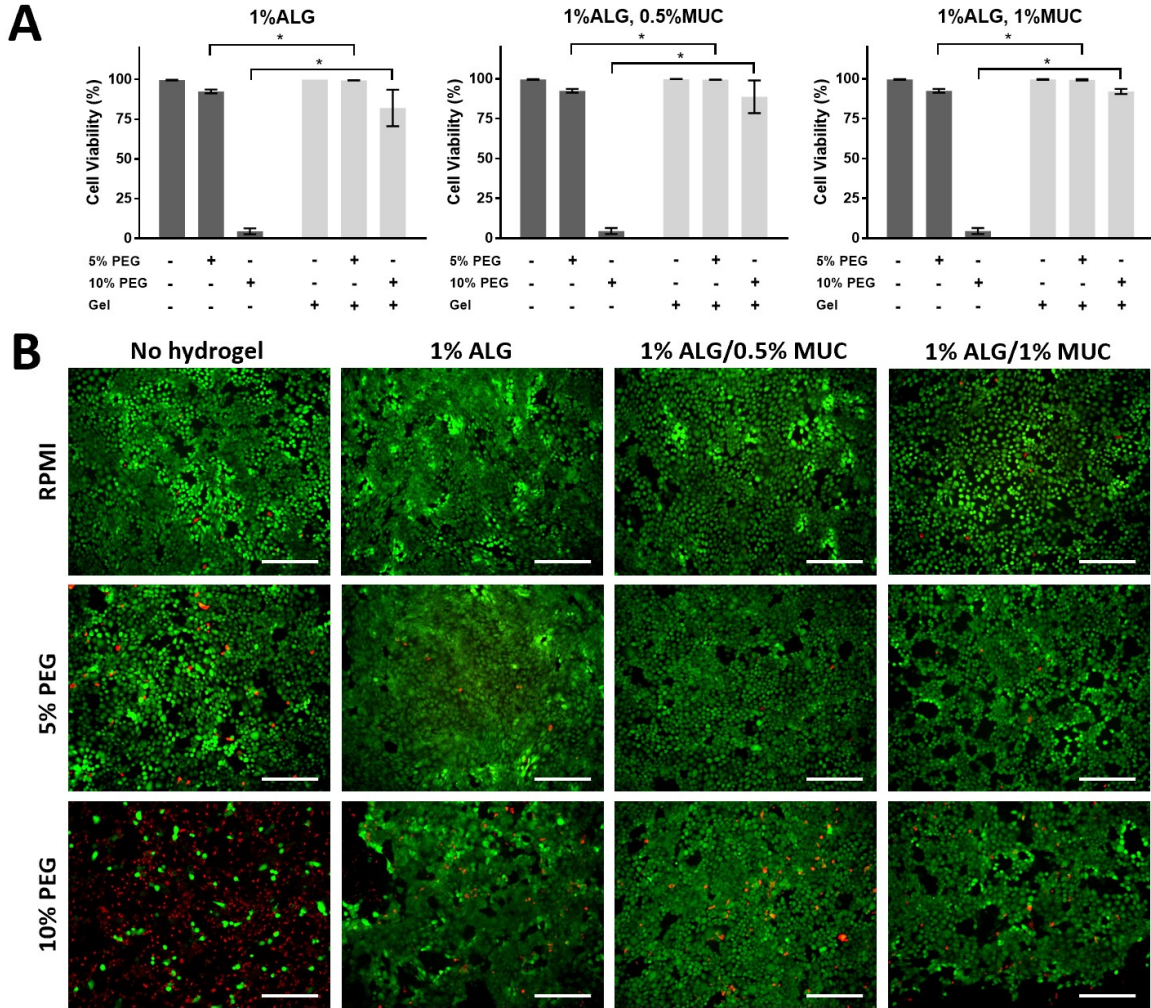
Figure 11: Mitigation of PEG-mediated cytotoxicity in 16-HBE cells through the addition of alginate-based hydrogel layers on top of cell monolayers. (A) Cell viability of 16-HBE cells with and without alginate-based hydrogel layers (1% ALG, 1% ALG/0.5% MUC, and 1% ALG/1% MUC) between monolayer and PEG-phase solution, where hydrogel layers were found to significantly reduce PEG-mediated cell death (* indicates $p < 0.05$, n = 3). **(B)** Fluorescent images of Live/Dead stained 16-HBE cells exposed to 5% and 10% PEG-phase solution with or without an alginate-based hydrogel (1% ALG, 1% ALG/0.5% MUC, and 1% ALG/1% MUC) overlay (scale bar = 500 μm).

4.3 Physical Characterization of Alginate and Alginate-Mucin semi-IPN Hydrogels

4.3.1 PEG-DEX ATPS stability on alginate-based hydrogels is improved with increasing mucin concentrations within the hydrogel

To further assess the compatibility of the ALG-MUC hydrogel with an ATPS co-culture, it is essential that a DEX droplet can be deposited within the PEG-phase on top of the hydrogel surface. First, to determine whether an ATPS could be formed on top of the hydrogels, a FITC-DEX formulation was used and imaged using fluorescent microscopy. DEX droplets deposited onto 1% ALG hydrogels were dispersed unevenly (or non-symmetrical) as opposed to a more circular formation on the ALG-MUC hydrogels (1% ALG/0.5% MUC and 1% ALG/1% MUC) (Figure 12B). The DEX droplets were found to remain on top of the hydrogel surface, which was determined by the difference in the focal plane of the y-axis compared to the DEX droplet at the bottom of the tissue culture polystyrene well (TCPS, with no hydrogel) (Figure 12B).

The stability of the ATPS was characterized by measuring the contact angles of each DEX droplet, where higher contact angles indicated higher ATPS stability. Sideview images of the DEX droplets were taken, where contact angles were measured using ImageJ. Contact angles were found to increase with increasing mucin concentrations within the alginate hydrogels (Figure 12A & C). A TCPS surface was used as the control for DEX droplet formation. Only the DEX droplets on the 1% ALG hydrogel surface produced significantly smaller contact angles (54.6 ± 2.7°, for 5% ATPS; 66.1 ± 5.4°, for 10% ATPS) than the droplet formed on TCPS surfaces (79.2 ± 7.9°, for 5% ATPS; 86.1 ± 1.5°, for 10% ATPS) (Figure 12C). Moreover, DEX droplet contact angles were significantly lower in the 5% ATPS (62.4 ± 2.7°, on a 1% ALG/0.5% MUC surface; 68.8 ± 4.8°, on a 1% ALG/1% MUC surface) compared to the 10% ATPS (77.4 ±

4.4°, on a 1% ALG/0.5% MUC surface; 82.63 ± 3.6°, on a 1% ALG/1% MUC surface) on the

ALG-MUC hydrogel surfaces, but not on the 1% ALG hydrogel surface (Figure 12C).
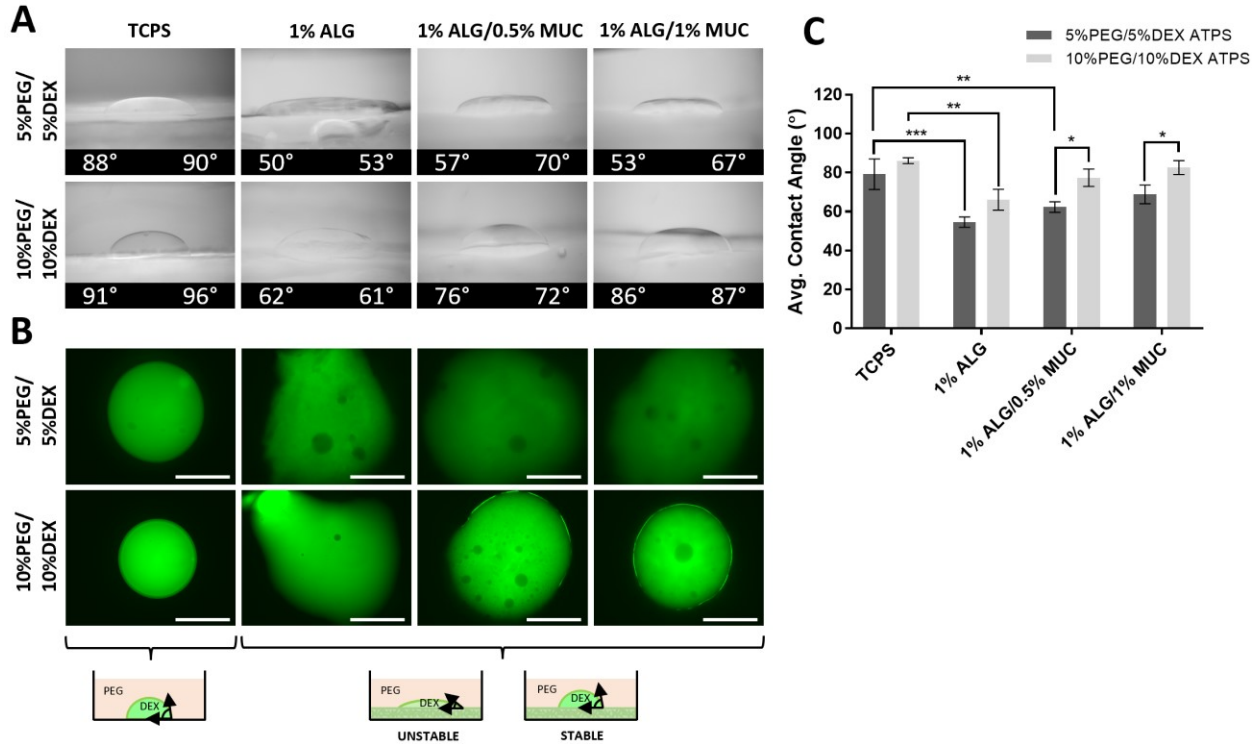
Figure 12: PEG-DEX ATPS formation on top of alginate-based hydrogel surfaces. (A) Side view images of DEX droplets formed on tissue culture polystyrene (TCPS), or alginate-based hydrogels surfaces (1% ALG, 1% ALG/0.5% MUC, 1% ALG/1% MUC) with left and right contact angle measurements. **(B)** Fluorescent images of FITC-DEX droplets formed within a PEG-DEX ATPS on top of TCPS, or alginate-based hydrogels (Scale bar = 1 mm). **(C)** Average contact angles of DEX droplets formed within a PEG-DEX ATPS on top of the different surfaces, where * indicates $p < 0.05$, ** indicates $p < 0.01$, and *** indicates $p < 0.001$ (n = 3).

4.3.2   Alginate-based hydrogel viscosity decreases with increasing mucin concentrations

The alginate-based hydrogels used in this study are partially crosslinked, which gave the hydrogel more pliability and lower levels of stiffness. Fabricating softer hydrogel allowed for the use of the falling ball viscometer methods to measure the apparent viscosity. The calculated viscosity values of the three different hydrogel formulations were found to decrease with

increasing mucin concentrations, where the 1% ALG/1% MUC hydrogel (7.3 ± 2.5 Pa-s) showed significantly reduced viscosity compared to the 1% ALG hydrogel (12.8 ± 3.9 Pa-s) (Figure 13).
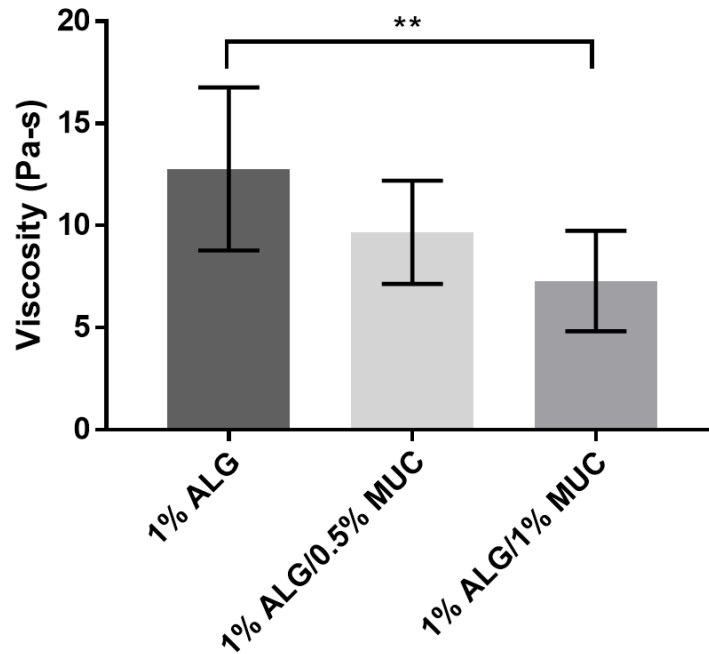
Figure 13: Apparent viscosity values of alginate-based hydrogels. Viscosity values calculated using equation 1 and terminal velocities derived from falling ball viscometer data, where ** indicates $p < 0.01$ ($n = 8$).

In this falling fall viscometer experiment, another interest was whether the hydrogels could recover the path that was carved into each sample by the steel balls. To test this, a second ball drop was performed (immediately after the initial drop) and a third delayed drop that was carried out either 1 hour or 3 hours after the second drop. It was found that the immediate subsequent drop (drop 2) was able to travel through the hydrogel volume with less resistance compared to the initial drop, resulting in increased slope in the D-T plot (Figure 14). For the 1-hour delayed drop, the D-T plots were more similar to the plots of drop 2, suggesting that the hydrogels did not recover from the initial disruption, after 1 hour (Figure 14, top). With a 3-hour

recovery time, the D-T plots showed a curve that was between the initial and the second drop in the 1% ALG and 1% ALG/0.5% MUC hydrogels, suggesting partial recovery of the path disruption. As for the 1% ALG/1% MUC hydrogel, the 3-hour delay seemed to allow for full recovery, where the D-T plot was overlapping with the initial drop (drop 1) (Figure 14, bottom).
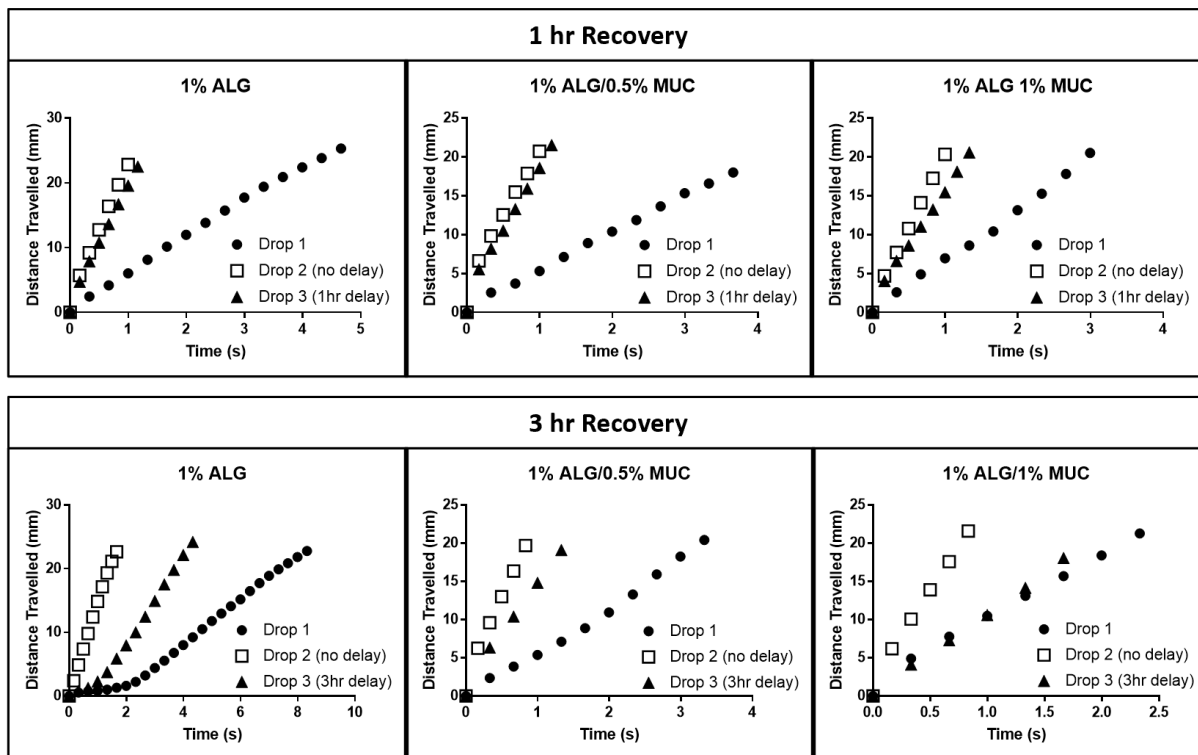
Figure 14: Distance-Time graphs of steel ball travel through alginate-based hydrogels with delayed drops. Delayed drops were performed either 1 hour or 3 hours after the initial two drops.

One concern with this falling ball viscometer method was whether the subsequent ball drops (drop 2 & 3) were following the same travel path through the hydrogel samples as the initial drop (drop 1). This was confirmed by plotting the X- and Y-coordinates of each ball travelling through the alginate-based hydrogel samples. It was found that all drops (1, 2, & 3)

followed very similar ball path trajectories between drops within each hydrogel sample (Figure 15).
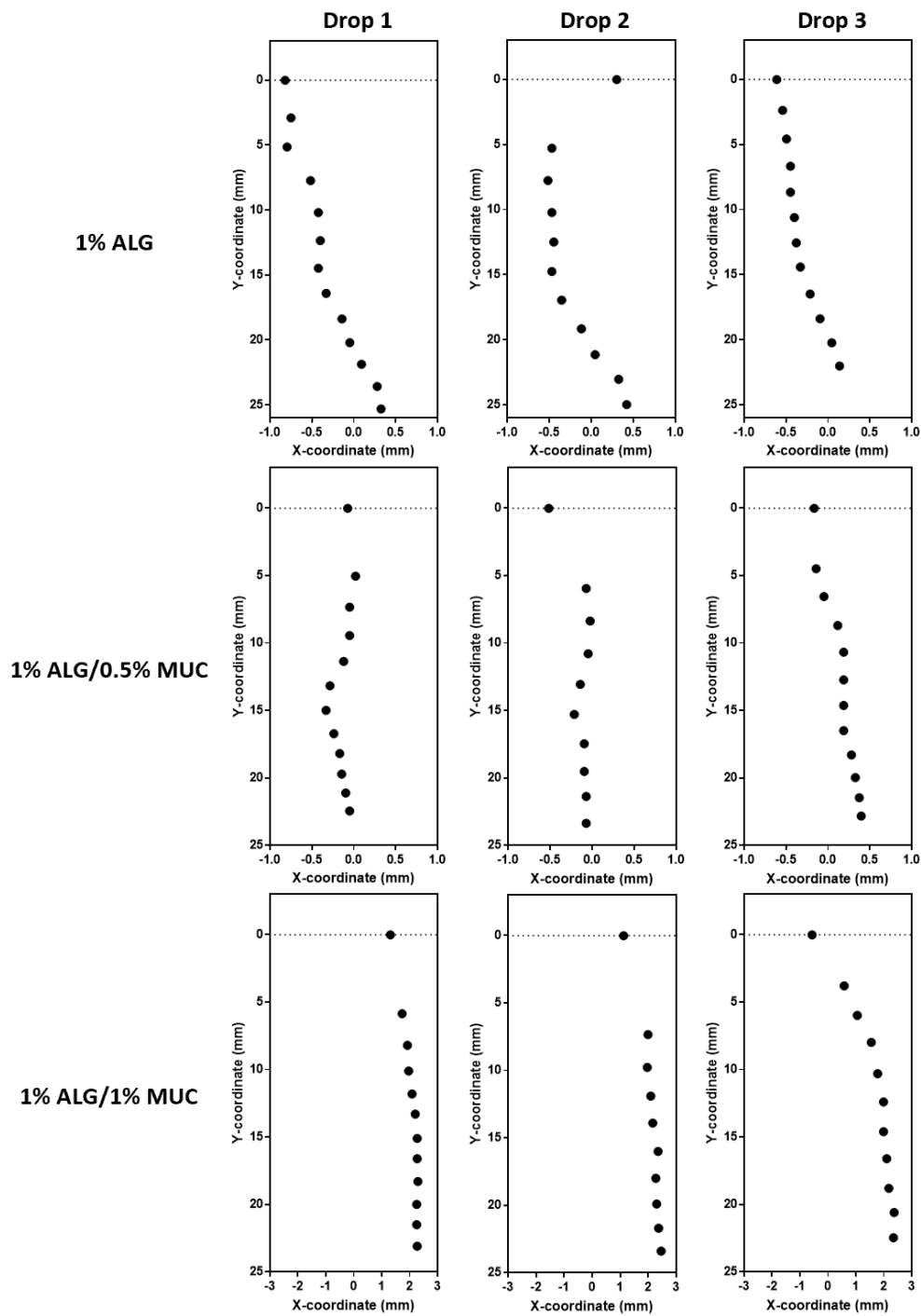
Figure 15: Steel ball trajectory through alginate-based hydrogels in falling ball viscometer experiments.

4.3.3 Presence of mucin within alginate-based hydrogels affects the diffusivity of charged biomolecules

The diffusivity of fluorescein labelled DEX, IgG, and LL-37 were assessed through fluorescent imaging by capturing the diffusion of each molecule through a straight channel containing the hydrogels every 4 minutes. The cross-sectional fluorescence intensity profiles (1 mm away from the liquid-hydrogel interface) were found to increase over time, showing a similar trend between all alginate-based hydrogels with FITC-DEX (Figure 16). FITC-IgG, however, was found to increase more between 60 minutes and 180 minutes in the 1% ALG hydrogel compared to the ALG-MUC hydrogels (1% ALG/0.5% MUC and 1% ALG/1% MUC) (Figure 16).
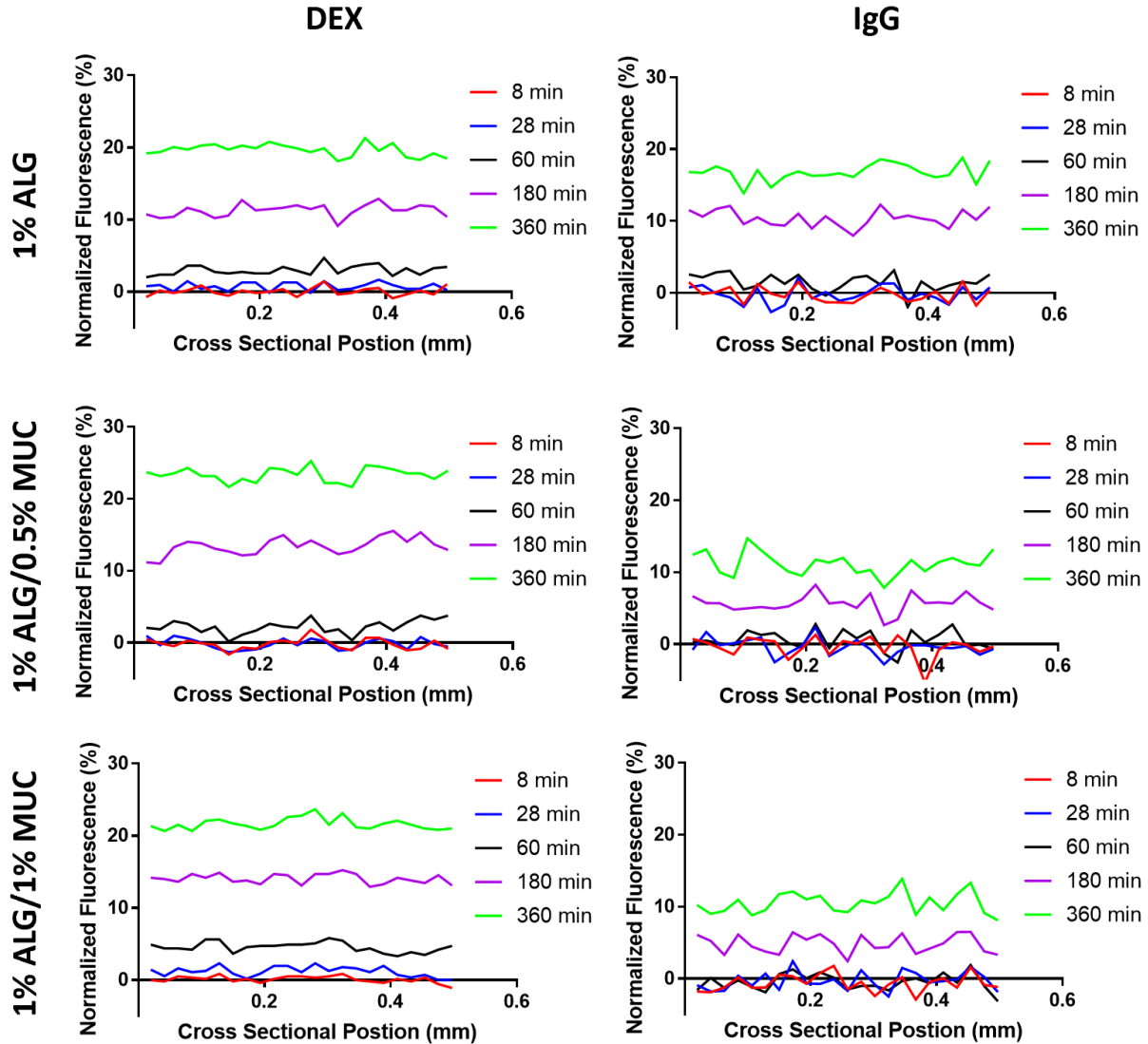
Figure 16: Change in fluorescein labelled DEX and IgG diffusion profiles through alginate-based hydrogels using PDMS straight channels over time. Normalized fluorescence diffusion profiles of DEX and IgG over a 6-hour period in alginate-based hydrogels.

Interestingly, the D_{eff} of DEX and IgG between the three hydrogels did not show any significant differences (Figure 17). The non-significant differences show higher D_{eff} of DEX in the 1% ALG/0.5% MUC hydrogel ($3.84 \times 10^{-4} \pm 2.02 \times 10^{-4}$ cm^2/s) compared to the 1% ALG ($2.31 \times 10^{-4} \pm 8.68 \times 10^{-5}$ cm^2/s) and 1% ALG/1% MUC ($2.26 \times 10^{-4} \pm 4.03 \times 10^{-5}$ cm^2/s) hydrogels. The D_{eff} of IgG, on the other hand, showed higher values in ALG-MUC hydrogels

$(1.68 \times 10^{-4} \pm 2.80 \times 10^{-5}$ cm^2/s, 1% ALG/0.5% MUC; $1.54 \times 10^{-4} \pm 6.32 \times 10^{-5}$ cm^2/s, 1%

ALG/1% MUC) than the 1% ALG hydrogel $(1.21 \times 10^{-4} \pm 1.13 \times 10^{-5}$ cm^2/s) (Figure 17).
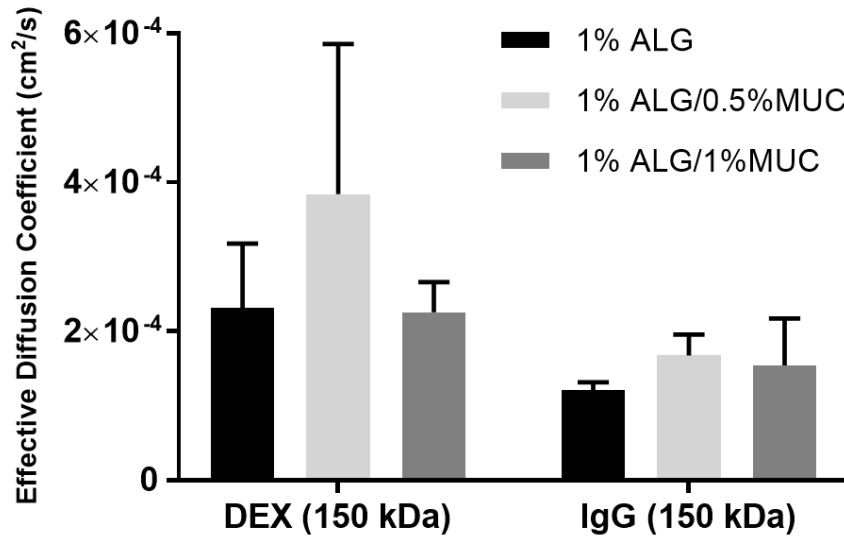
Figure 17: Effective diffusion coefficients (Deff) of DEX and IgG through alginate-based hydrogels. No significance (two-way ANOVA) was found between any D_{eff} values (n = 3).

With the diffusion of LL-37, D_{eff} was not calculated as a result of diminishing

fluorescence over time. Fluorescent cluster formation was also observed throughout the reservoir

solution over time. Additionally, fluorescent clusters were found to form within the hydrogels

containing mucin (1% ALG/0.5% MUC and 1% ALG/1% MUC), but not in the 1% ALG

hydrogels (Figure 18).
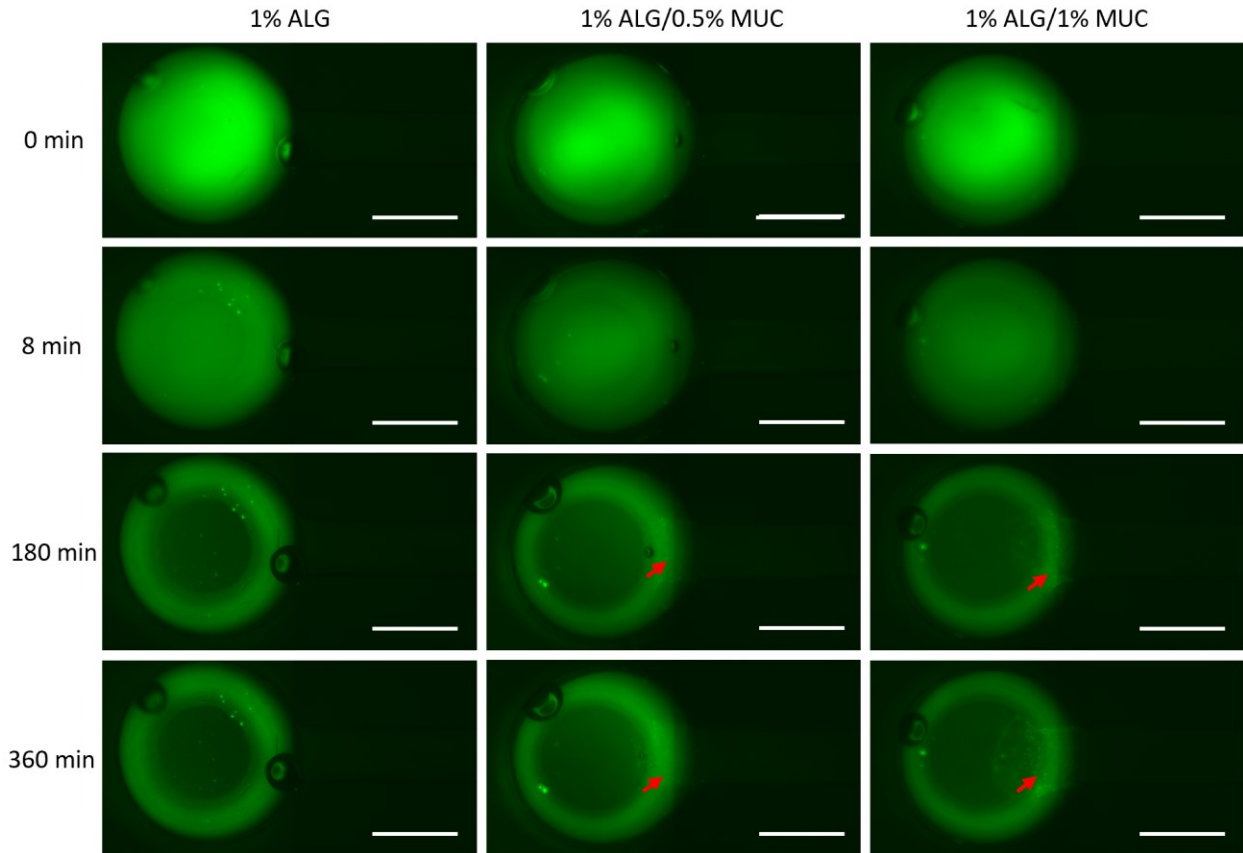
Figure 18: Diminishing fluorescence of carboxy fluorescein labelled LL-37 reservoirs over a 6-hour period. Red arrows indicate the development of fluorescent clusters within the mucin containing hydrogels (Scale bar = 1 mm).

4.4 Mammalian-Microbial Co-Culture

To establish the mammalian-microbial ATPS co-culture system containing artificial mucus, two pairs of co-cultures were carried out. 16-HBE was cultured with *P. aeruginosa* to model the host-pathogen interaction in the airway and Caco-2 was cultured with *S. flexneri* to model host-pathogen interaction in the colon. Here, we were interested in characterizing the bacterial distribution within our *in vitro* system as well as the effects of pathogenic bacterial presence on the mammalian cell viability, with and without the supplementation of antibiotics (Figure 19). For mammalian cell viability findings, no statistical analysis was performed due to the uncountable nuclei after the Live/Dead staining of mammalian cells after co-culturing with

bacteria. The following descriptions highlight both the significant and non-significant differences in mean bacterial abundance as well as crude differences in live to dead cell proportions.
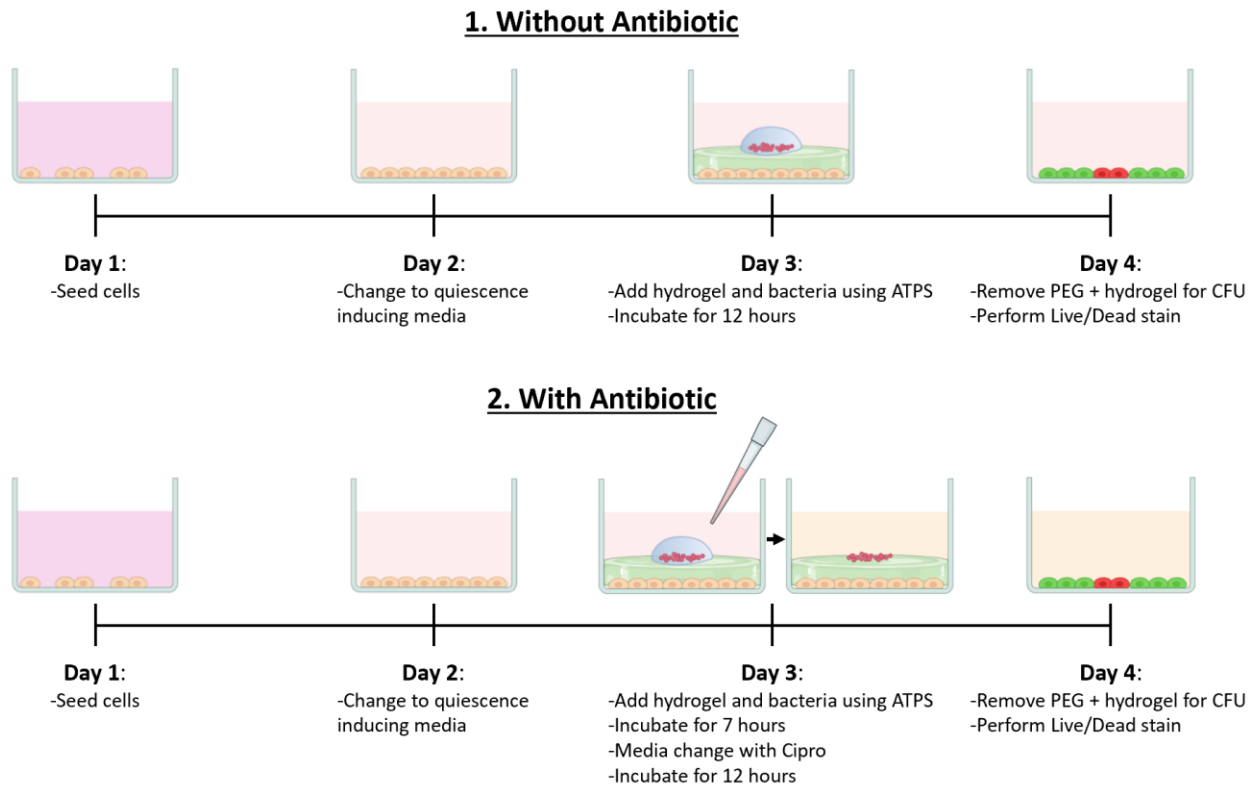
Figure 19: Schematic of mammalian-microbial co-culture experimental timelines with and without antibiotic treatment.

4.4.1 ATPS formulation and the presence of mucin affects where bacterial species preferentially grow within the ATPS mucosal co-culture model

To assess the bacterial distribution within an ATPS mammalian-microbial co-culture containing ALG-MUC hydrogels, the total abundance of bacteria escaping into the PEG-phase and total abundance of bacteria that entered the hydrogel were measured by performing CFU counts after 12 hours of incubation. For *P. aeruginosa* in the 5% ATPS, bacterial abundance was found to be over 7-fold higher in the 1% ALG hydrogel layer as opposed to the PEG-phase.

Wells containing ALG-MUC hydrogels (1% ALG/0.5% MUC and 1% ALG/1% MUC) showed the opposite trend, where *P. aeruginosa* abundance was almost 18- and 11-fold higher in the PEG-phases compared to the 1% ALG/0.5% MUC and 1% ALG/1% MUC hydrogel layers, respectively (Figure 20A). Co-cultures using a 10% ATPS showed a similar trend in bacterial abundance in the wells containing 1% ALG hydrogels, where CFU/ml was 3-fold higher in the hydrogel layer compared to the PEG-phase. With mucin present in the alginate-based hydrogels, the levels of *P. aeruginosa* were found to be roughly the same between the PEG-phase and hydrogel, in 10% ATPS (Figure 20B).

     S. flexneri, on the other hand, showed more consistent growth trends in terms of bacterial abundance between the 5% ATPS and the 10% ATPS. The total bacterial abundance within the hydrogel layer of the 5% ATPS co-cultures was approximately 2-fold higher than the abundance within the PEG-phase for all hydrogel formulations (1% ALG, 1% ALG/0.5% MUC, and 1% ALG/1% MUC). Generally, the overall abundance of *S. flexneri* within the co-cultures increased with increasing mucin concentrations (Figure 20C). A similar trend in *S. flexneri* abundance was observed in the 10% ATPS, where higher CFU/ml was observed in the hydrogel layers compared to the PEG-phase, but with more pronounced differences between the PEG-phase and the hydrogel layers (Figure 20D). These findings suggest that both the presence of mucin within the hydrogels as well as the ATPS formulation affects where bacteria preferentially grow within this *in vitro* co-culture system.
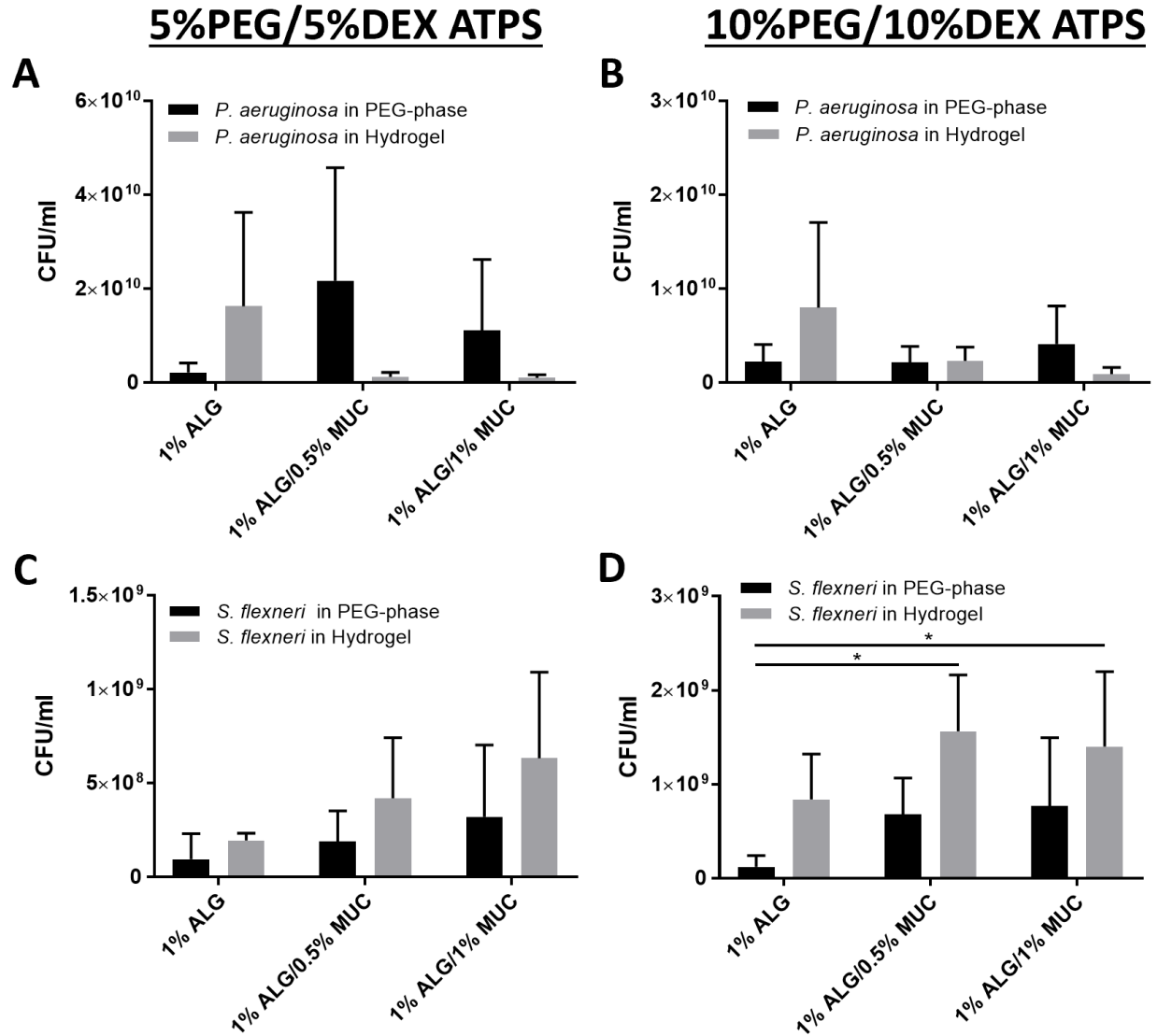
Figure 20: *P. aeruginosa* **and** *S. flexneri* **abundance (CFU/ml) within PEG-phase or hydrogel after 12 hours of co-culture incubation with 16-HBE and Caco-2, respectively.** CFU/ml values were calculated from *P. aeruginosa* grown in either a 5%PEG/5%DEX ATPS **(A)** or 10%PEG/10%DEX ATPS **(B)**, and *S. flexneri* in a 5%PEG/5%DEX ATPS **(C)** or 10%PEG/10%DEX ATPS **(D)**, where * indicates $p < 0.05$ (n = 4).

Table 5: *P. aeruginosa* (PA) and *S. flexneri* (SF) CFU/ml values within PEG-phase or hydrogel after 12 hours of co-culture incubation with 16-HBE and Caco-2, respectively.

		5%PEG/5%DEX ATPS			10%PEG/10%DEX ATPS		
		1% ALG	0.5% MUC	1% MUC	1% ALG	0.5% MUC	1% MUC
PA	PEG-phase	2.18×10^9	2.17×10^{10}	1.11×10^{10}	2.21×10^9	2.14×10^9	4.10×10^9
	Hydrogel	1.63×10^{10}	1.21×10^9	1.00×10^9	7.98×10^9	2.30×10^9	9.21×10^8
SF	PEG-phase	9.49×10^7	1.90×10^8	3.20×10^8	1.22×10^8	6.79×10^8	7.69×10^8
	Hydrogel	1.94×10^8	4.19×10^8	6.33×10^8	8.39×10^8	1.56×10^9	1.40×10^9

4.4.2 Ciprofloxacin reduces bacterial proliferation within the PEG-phase

The human mucus layer plays an important role in drug diffusion and the effectiveness of the drug on the bacteria within the mucus, which is often neglected when studying drug efficacy. Therefore, we were interested in exploring the effects of antibiotics on both *P. aeruginosa* and *S. flexneri* growth and distribution within the ATPS co-culture with artificial mucus hydrogels. The antibiotic used in this experiment was ciprofloxacin, an antibiotic that is known to disrupt bacterial DNA replication.[133] Ciprofloxacin was used at a minimum inhibitory concentration (MIC) which was determined to be 0.125 µg/ml for both *P. aeruginosa* and *S. flexneri*.

After 12 hours of incubation with ciprofloxacin supplemented PEG-phase, *P. aeruginosa* abundance was 4-fold higher in the 1% ALG hydrogel layer compared to the PEG-phase, in the 5% ATPS (Figure 21A). In comparison to no antibiotic treatment (Table 5), the CFU/ml was reduced from 2.18×10^9 CFU/ml (in the PEG-phase) and 1.63×10^{10} CFU/ml (in the hydrogel layer) to 1.2×10^6 CFU/ml and 5.57×10^6 CFU/ml (Table 6), respectively. In the 5% ATPS co-cultures containing ALG-MUC hydrogels, *P. aeruginosa* abundance was reduced such that the CFU/ml in the PEG-phase was roughly even with the abundance in the 1% ALG/0.5% MUC hydrogel layer. Whereas the 5% ATPS co-culture containing a 1% ALG/1% MUC hydrogel

layer showed approximately 1.7-fold higher abundance of *P. aeruginosa* in the PEG-phase compared to the hydrogel layer (Figure 21A). In the 10% ATPS co-cultures, *P. aeruginosa* abundance was higher in the hydrogel layer compared to the PEG-phase for all hydrogel formulations, where CFU/ml increased with increasing MUC concentrations (Figure 21B).

Ciprofloxacin treatment was shown to be much more effective against *S. flexneri*, where bacteria were almost fully eradicated within the PEG-phases, but not within 1% ALG/0.5% MUC and 1% ALG/1% MUC hydrogels for co-culture using both the 5% and 10% ATPS. In 5% and 10% ATPS co-cultures containing 1% ALG hydrogels, bacteria were eradicated in the PEG-phase and with 3 x 10^4 CFU/ml (5% ATPS) and 6.08 x 10^4 CFU/ml (10% ATPS) remaining in the hydrogel layer (Table 6 and Figure 21C & D). In the presence of mucin, *S. flexneri* could better resist the effects of the antibiotic treatment, where bacteria within the PEG-phase was reduced but not within the ALG-MUC hydrogel layers (Figure 21C & D). *S. flexneri* abundance was observed to increase with increasing mucin concentrations within the hydrogel layer, where CFU/ml were found to be 2.82 x 10^7 CFU/ml (5% ATPS) and 2.40 x 10^7 CFU/ml (10% ATPS), in the 1% ALG/0.5% MUC hydrogels, and 7.98 x 10^7 CFU/ml (5% ATPS) and 1.28 x 10^8 CFU/ml (10% ATPS), in the 1% ALG/1% MUC hydrogels (Table 6).
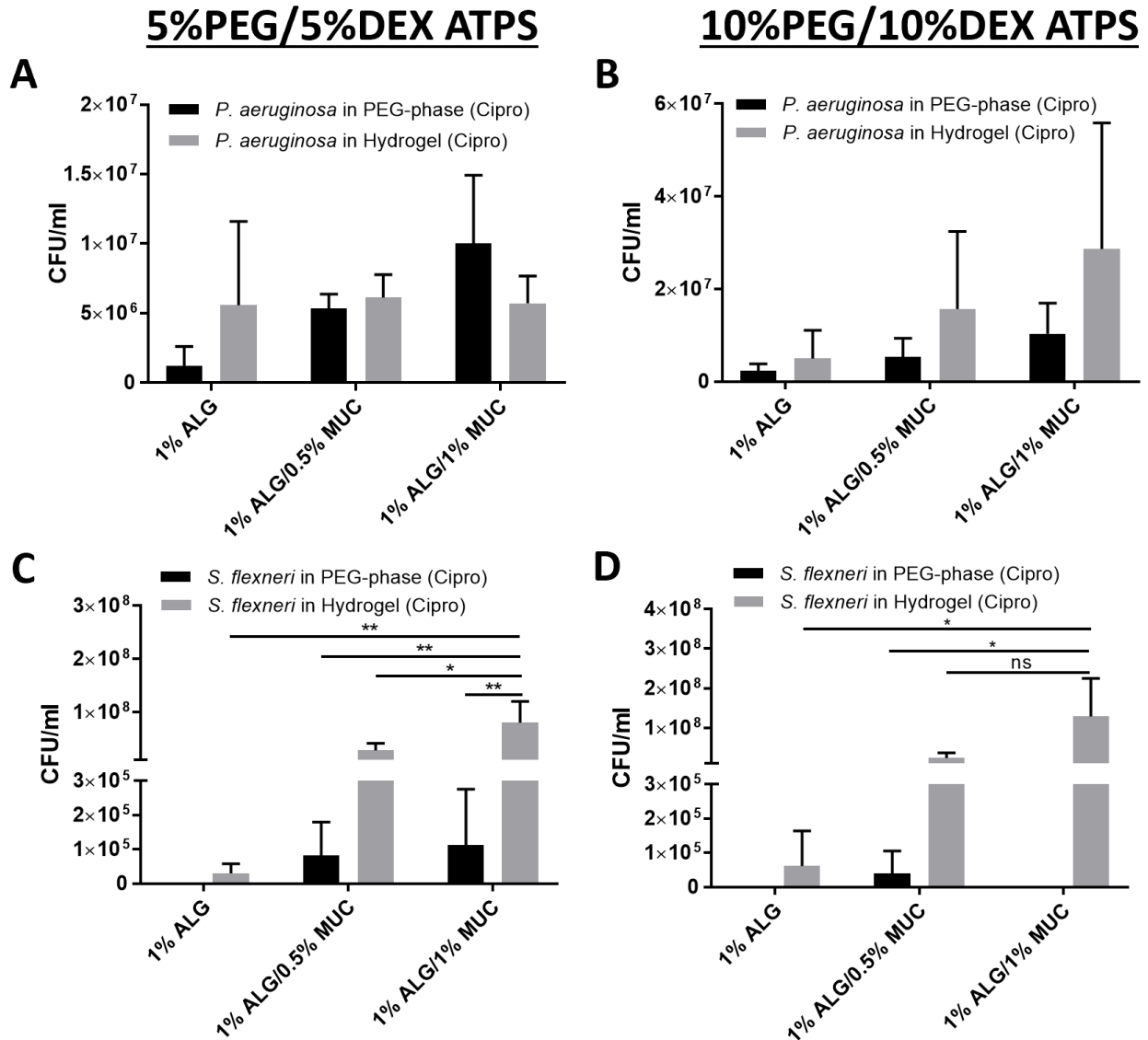
Figure 21: *P. aeruginosa* **and** *S. flexneri* **abundance (CFU/ml) within PEG-phase or hydrogel after 12 hours of co-culture incubation with 16-HBE and Caco-2, respectively, where PEG media was supplemented with ciprofloxacin (0.125 µg/ml).** CFU/ml values were calculated from *P. aeruginosa* grown in either a 5%PEG/5%DEX ATPS **(A)** or 10%PEG/10%DEX ATPS **(B)**, and *S. flexneri* in a 5%PEG/5%DEX ATPS **(C)** or 10%PEG/10%DEX ATPS **(D)**, where * indicates $p < 0.05$, ** indicates $p < 0.01$, and ns = non-significant (n = 3).

Table 6: *P. aeruginosa* (PA) and *S. flexneri* (SF) CFU/ml values within PEG-phase or hydrogel after 12 hours of co-culture (with 0.125 μg/ml) incubation with 16-HBE and Caco-2, respectively.

		5%PEG/5%DEX ATPS			10%PEG/10%DEX ATPS		
		1% ALG	0.5% MUC	1% MUC	1% ALG	0.5% MUC	1% MUC
PA	PEG-phase	1.20×10^6	5.33×10^6	1.00×10^7	2.32×10^6	5.33×10^6	1.03×10^7
	Hydrogel	5.57×10^6	6.13×10^6	5.70×10^6	4.97×10^6	1.57×10^7	2.87×10^7
SF	PEG-phase	0	8.17×10^4	1.12×10^5	0	4.02×10^4	0
	Hydrogel	3.00×10^4	2.82×10^7	7.98×10^7	6.08×10^4	2.40×10^7	1.28×10^8

4.4.3   Regional mammalian cell viability in co-culture

After the 12-hour incubation of each mammalian-microbial co-culture, the mammalian cell component was assessed by performing a Live/Dead assay, where all images were taken directly underneath the area of the DEX droplet (the area of highest bacterial density), adjacent to the DEX droplet, and exposed areas (not covered by hydrogel, only in 10% ATPS co-cultures). For both cell lines (16-HBE and Caco-2), two control wells were used where an ATPS was formed either with or without bacteria suspended in the deposited DEX droplet directly on top of the monolayer. In control wells with direct deposition of a bacteria-rich DEX droplet, both cell lines (16-HBE and Caco-2) displayed the highest level of cell death within the area of the DEX droplet. When 16-HBE cells were co-cultured with *P. aeruginosa*, the level of cell death was found to be negatively correlated with increasing mucin concentrations within the alginate-based hydrogels. Additionally, co-culture with 16-HBE and *P. aeruginosa* in a 5% ATPS showed an overall lower viability of 16-HBE cells compared to co-cultures using a 10% ATPS (Figure 22). Caco-2 cells, on the other hand, showed consistently high levels of cell viability when co-cultured with *S. flexneri* on top of all hydrogel formulations (Figure 22).
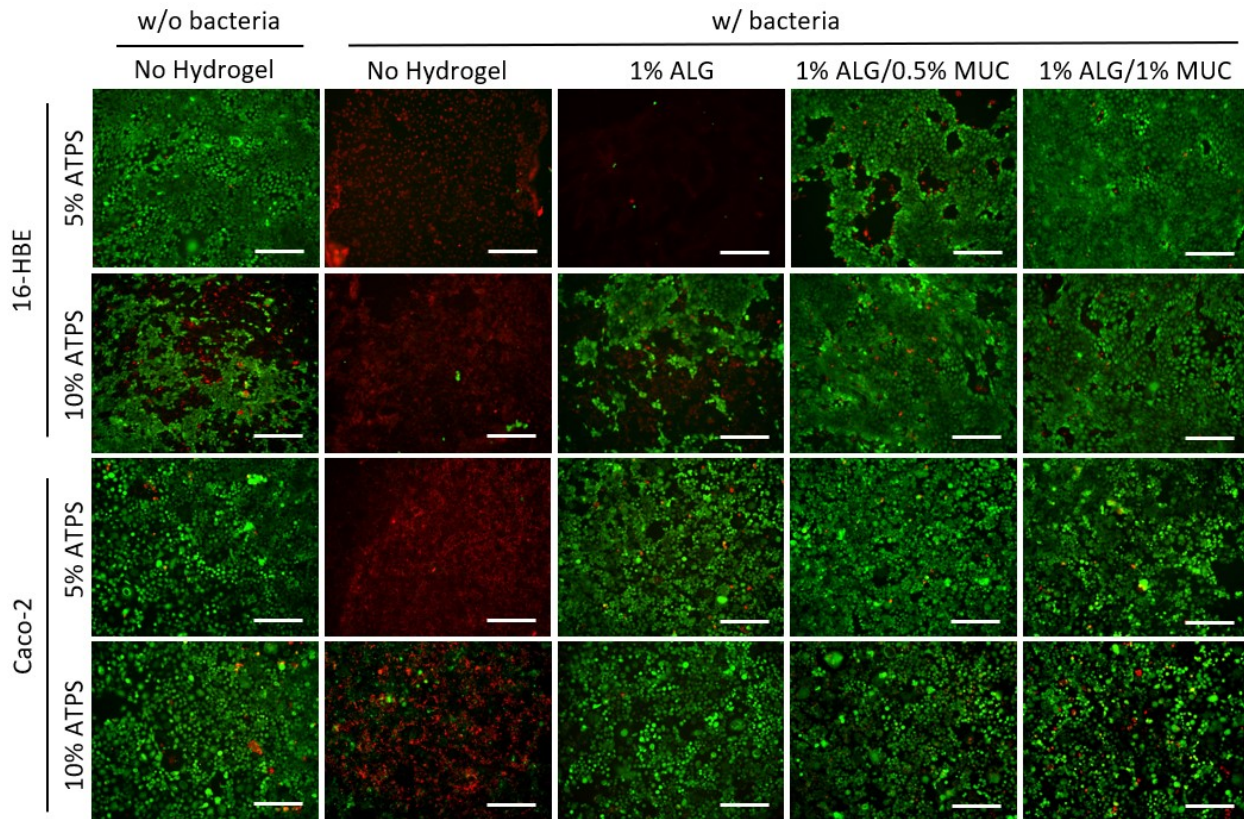
Figure 22: Live/Dead staining images of 16-HBE and Caco-2 monolayers after a 12-hour co-culture incubation with *P. aeruginosa* or *S. flexneri*, respectively, deposited with a PEG-DEX ATPS either with or without alginate-based hydrogels between monolayer and ATPS. Bacteria were deposited using a 5% PEG/5% DEX ATPS or 10% PEG/10% DEX ATPS onto monolayers with or without an alginate-based hydrogel overlay, where a DEX droplet without bacteria was deposited directly onto a monolayer as a control (Scale bars = 500 μm).

With the introduction of the ciprofloxacin supplemented PEG-phase, 16-HBE cells showed improved viability in co-cultures containing a 1% ALG hydrogel overlay (5% and 10% ATPS) (Figure 23). However, 16-HBE cells with an ALG-MUC hydrogel overlay were less viable than those cultured without ciprofloxacin supplementation (Figure 23). Similarly, this was observed for Caco-2 cells grown in a 5% ATPS but not the 10% ATPS, where Caco-2 cells showed similarly high levels of survival (Figure 23).
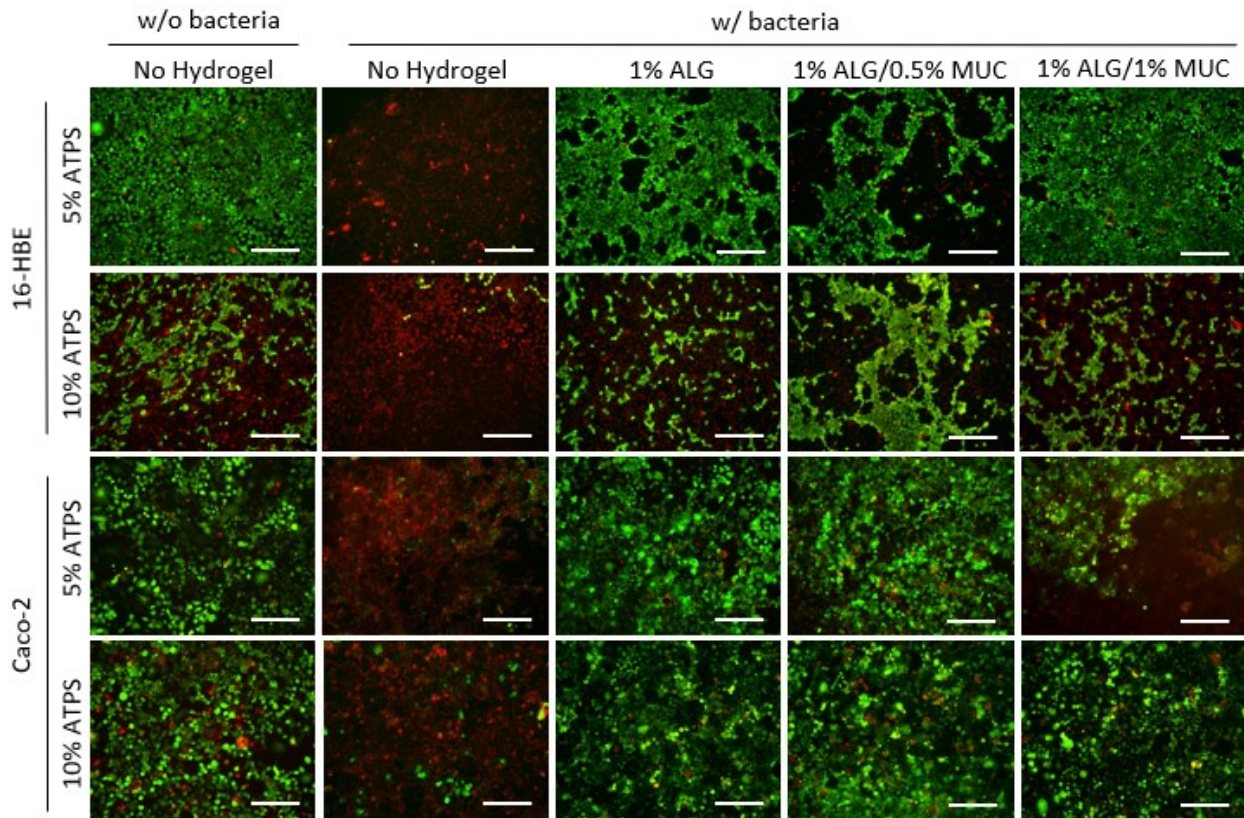
Figure 23: Live/Dead staining images of 16-HBE and Caco-2 monolayers after a 19-hour (cipro added at 7 hr) co-culture with *P. aeruginosa* or *S. flexneri*, respectively, either with or without an alginate-based hydrogel between monolayer and ATPS. Bacteria were deposited using a 5% PEG/5% DEX ATPS or 10% PEG/10% DEX ATPS onto monolayers with or without an alginate-based hydrogel overlay, where a DEX droplet without bacteria was deposited directly onto a monolayer as a control (Scale bars = 500 μm).

Considering the hydrogel contraction observed in the mucin containing hydrogels, Live/Dead images were taken at various regions within the co-culture wells using a 10% PEG-DEX ATPS. Mammalian cells directly underneath the contracted hydrogel, whether directly underneath the bacteria dense region or adjacent to it, were found to be predominantly viable (Figure 24, regions 1 & 2). Higher levels of cell death were observed in the exposed areas that were no longer covered by hydrogel (Figure 24, region 3).
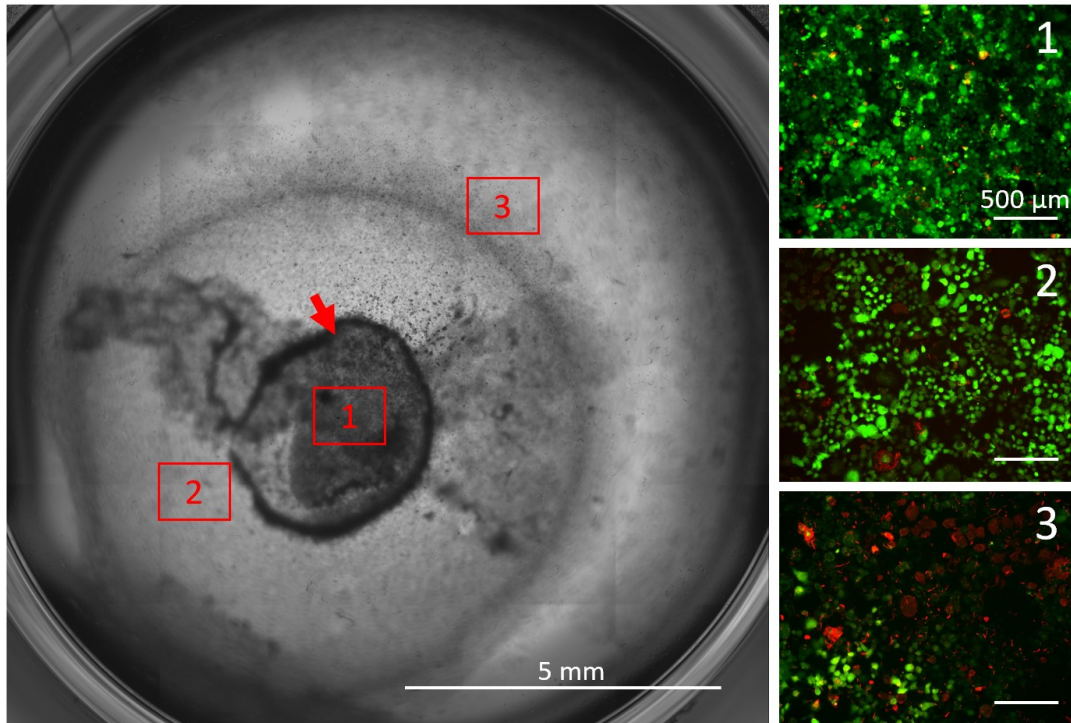
Figure 24: Representative images of regional variation in cell viability in areas protected by hydrogel coverage and exposed regions. Stitched brightfield images of whole well (24-well plate, **left panel**) containing Caco-2 cells overlaid with a 1% ALG/0.5% MUC hydrogel with S. flexneri growth (indicated by the red arrow) inoculated using a 10% PEG-DEX ATPS. (**right panel**) Live/Dead images of Caco-2 cells in the corresponding regions of the well either directly under the bacteria colony (**1**), under hydrogel and adjacent to bacterial colony (**2**), and exposed area due to hydrogel contraction (**3**).

CHAPTER 5.   DISCUSSION

The human mucus layer acts as the first line of defense against any pathogens or foreign particles that may enter the body.[134] However, some bacterial species have adapted to bypass the mucus layer, while other opportunistic bacteria will cause infection and inflammation when the mucus layer is compromised due to dysregulation.[100,135] The current gold standard for studying host-pathogen interaction is with the use of animal models.[136] It is important to consider the use of *in vitro* disease modeling as an additional tool to validate findings in the animal studies, considering that *in vivo* findings do not always align with what is observed in humans.[13,137] To model host-pathogen interactions *in vitro*, it is crucial to have controlled bacterial growth and to provide the proper microenvironment suitable for both mammalian and bacterial proliferation. Many of the current mammalian-microbial co-culture platforms have demonstrated stable growth over several days, under flow conditions,[39,138] but are complex and difficult for a general life science laboratory to adapt. Other techniques lack a sufficient mucus microenvironment for these interactions to take place.[40,47,139] Here, we demonstrate the use of a simple and robust mammalian-microbial co-culture method using a PEG-DEX ATPS with the incorporation of an alginate-mucin semi-IPN hydrogel to recapitulate the 3-D mucus microenvironment.

5.1   Varying Alginate Hydrogel Characteristics with Various Crosslinking Methods

Throughout the work of this thesis, the ALG-MUC hydrogels were assessed based on a list of design criteria, including gelation time, cytocompatibility, mammalian cell adhesiveness, diffusivity, and stability of ATPS formation. However, prior to addressing these design parameters, the hydrogel polymer was chosen according to the ease of use and fabrication method allowing for direct deposition onto a mammalian monolayer. Previous methods used to

form artificial mucus hydrogel used purified mucin, which can be crosslinked using PEG-thiol crosslinkers.[140] This method has been shown to form physiologically relevant mucin hydrogels and modifiable physical characteristics by altering the type of mucin used[140]; however, we were interested in exploring other options to broaden the types of artificial mucus suitable for mammalian-microbial co-cultures. Alginate hydrogels are known to be biologically inert, where crosslinking agents such as Ca^{2+} are commonly found in biological systems with low potential to impact cellular processes.[115,141]

When working with alginate hydrogels there are a number of crosslinking techniques using divalent cations that have been previously explored. The most commonly used method involves the use of $CaCl_2$ to form ionic crosslinks between alginate monomers, which is typically used for instantaneous gelation of alginate beads by dropwise addition of an alginate solution into a vessel containing 100 mM $CaCl_2$.[118,142] By using high concentrations of $CaCl_2$, this technique ensures the saturation of crosslink formation between G residues.[143,144] When adapting this for the application of forming a hydrogel directly on top of a mammalian monolayer, we deposited the 100 mM $CaCl_2$ crosslinking solution onto a volume of alginate in a multi-well plate containing cells. This modified technique, however, generated a heterogeneous surface topology which was undesirable for ATPS formation on top of the hydrogel. This phenomenon was likely due to the force of the $CaCl_2$ droplet dispersing the alginate solution followed by instantaneous crosslinking of the alginate, thus generating an uneven hydrogel surface.[142]

Another ionic crosslinking method used to form alginate hydrogels utilizes calcium carbonate and GDL. Calcium carbonate is poorly soluble in physiological pH solutions.[145] With the addition of GDL as a catalyst, GDL slowly acidifies the solution to solubilize Ca^{2+} for internal crosslinking of the hydrogel at a reduced gelation rate.[146,147] Studies utilizing this

technique often require molding the alginate hydrogel to a particular shape, which is granted by the slow hydrolysis of GDL and subsequent release of Ca^{2+}.[148] The characteristics of this gelation method made it a great alternative for our application. With this technique, the alginate:$CaCO_3$:GDL mixture was generated in a separate vessel prior to being deposited into the multi-well plate. Our results showed that a flat hydrogel surface was in fact formed; however, when incubated in PEG-phase media, the hydrogels were found to contract considerably. Studies have demonstrated that PEG interact with $CaCO_3$ to form PEG-$CaCO_3$ complexes.[149,150] Considering the alginic acid used in this study, containing low levels of G residues, the concentrations of $CaCO_3$ may have been in excess leading to non-utilized $CaCO_3$ within the hydrogel matrix. Assuming there were excessive amounts of $CaCO_3$, PEG-$CaCO_3$ interaction may have led to an influx of PEG and an efflux of water (or deswelling) resulting in9 contraction of the hydrogel network. An additional concern with this technique was the reduction in pH, caused by the hydrolysis of GDL to gluconic acid, during the gelation process directly on top of mammalian cells which would lead to potential cell death.[146] Air bubble formation was also observed when forming these hydrogels due to the need to vortex the alginate:$CaCO_3$:GDL mixture, which has previously been reported in Kalaf et al. (2016).[148]

Alternatively, low $CaCl_2$ concentration crosslinking is a method that has been previously performed to generate soft alginate hydrogels for 3-dimensional culture of neuronal networks as well as the production of low osmotic pressure alginate films.[89,151] This was another promising crosslinking technique for the applications in the present study due to the reduced stiffness and more pliable, yet robust, hydrogel that would allow for the formulation to be prepared in a separate vessel prior to the deposition into a multi-well plate. The rheological properties of these soft alginate hydrogels have previously been shown to be dependent on the G residue content

within the alginate polymer. Matyash et al. (2014) demonstrated the changes in storage moduli when using high G residue content and low G residue content alginates, where high G residue alginate hydrogels showed higher storage modulus and stiffness.[151] Although low crosslinking alginate hydrogels show reduced stiffness and tensile strength, they are structurally stable networks that form homogeneous surface topologies. As a result of the observed hydrogel contraction in the $CaCO_3$ crosslinked hydrogels, the generated soft alginate hydrogels were also tested for contraction in PEG-phase solutions and were found to maintain its size and shape after 24 hours of incubation. This encouraging finding allowed us to move forward with the low $CaCl_2$ crosslinking alginate hydrogels for further characterization and compatibility assessment with a PEG-DEX ATPS co-culture.

To provide the biochemical properties of natural mucus using these soft alginate hydrogels, mucin was incorporated into the crosslinked networks to form an ALG-MUC semi-IPN. Other studies have performed rheological characterization and utilized similar methods to mimic the mucus microenvironment for drug diffusion applications,[127,152] but no studies, to our knowledge, have used these hydrogels for host-microbe interaction or bacterial growth. Interestingly, the ALG-MUC hydrogels used in this study were also found to contract when incubated in PEG-phase media over time, but to a lesser extent as the $CaCO_3$ formed hydrogels. The exact cause of the ALG-MUC hydrogel contraction is unknown at this point, but we speculate that PEG oligomers may be diffusing into the hydrogel causing an efflux of water molecules due to the hydrophobic nature of PEG.[103] Moreover, the polysaccharide side chains of mucin provides a high capacity for water retention,[153] in which the loss of water by PEG repulsion can cause mucin collapse and overall hydrogel contraction. In future work, this hypothesis can be tested by using higher molecular weight PEG when forming the PEG-DEX

ATPS solutions, where larger PEG molecules with a larger hydrodynamic radius would possess a lower potential of diffusing into the hydrogel.[154]

5.2 ALG-MUC Hydrogel Compatibility with a PEG-DEX ATPS

As previously mentioned, the resulting ALG-MUC hydrogels were assessed based on specific design parameters encompassing its compatibility with a PEG-DEX ATPS mammalian-microbial co-culture. These design parameters required the hydrogels to be cytocompatible, non-cell adherent, selectively diffusive (mitigates PEG-mediated cytotoxicity), and to allow for the formation of a stable DEX droplet upon ATPS deposition. A single experiment involving overlaying mammalian cells with alginate-based hydrogels incubated with PEG-phase media was performed to verify the cytocompatibility of the hydrogel, its role in PEG-mitigation, as well as the cell adhesiveness. Our findings demonstrated that 16-HBE cells grown in RPMI media with and without a hydrogel overlay did not significantly differ in cell viability, 16-HBE monolayers remained intact after removal of the hydrogel, and that an alginate-based hydrogel overlay significantly reduced the level of cell death in PEG-phase media. Alginate hydrogels are known to be innately non-cell adhesive and have been used in a wide range of biomedical applications, where chemical modifications are required for any 3D cell culture applications.[121,122] Therefore, the observed results were not surprising. The interaction of PEG with mammalian cell plasma membranes have been reported to show both protective effects as well as detrimental effects. The role of PEG is highly dependent on the molecular weight of the oligomer, where larger PEG has shown protective effects against fluid-mechanical injury and provide barrier function to epithelial cells,[155,156] while others demonstrate cytotoxic effects of small molecular weight PEG.[114] In this study, we found that PEG 35000 significantly reduced cell viability of 16-HBE

cells. Although incubation of ALG-MUC hydrogels in PEG-phase media resulted in contracted

hydrogels, they were still able to provide sufficient protection from PEG-mediated cytotoxicity,

where regional variation of cell viability was observed between the protected and exposed cells.

The molecular weight of PEG within a PEG-DEX ATPS also influences the interfacial

tension between the two phases. When forming a polymer-polymer ATPS, one must consider the

concentration as well, where concentration ratios of polymer 1 and polymer 2 below the critical

point will result in a common phase rather than a biphasic system.[103] With higher concentrations

of polymer, the interfacial tension will be higher.[131,157] It is well established that surface

characteristics highly impact aqueous droplet formation, where hydrophobic surfaces will form

more round/dome-like droplets (higher contact angle) as opposed to hydrophilic surfaces

forming flatter droplets (lower contact angle).[158] We found that higher mucin concentrations

within the alginate-based hydrogels allowed for increased contact angle of DEX droplets,

suggesting higher interfacial tension. The mucin used in this study was a crude porcine mucin,

which contains various other proteins and lipids, suggesting that the incorporation of mucin into

the alginate-based hydrogels led to an increased hydrophobic surface characteristic and thus

increasing the DEX droplet contact angles.[158,159]

5.3   Role of Physical Characteristics in Mucus Barrier Function

Considering the protective role of the human mucus layer against opportunistic

pathogens, it is important to understand the physical characteristics and their contribution to

mucus function. The mucus layer is selectively diffusive by size exclusion and electrostatic

interaction due to the negatively charged sugar side chains of mucin glycoproteins.[52-54] Under

healthy conditions the mucus layer harbors copious amounts of bacterial species within the

airway and the gut.[57,160,161] The mucus layer can do so by the formation of dense layers of mucin to prevent bacterial penetration and maintain a reservoir of antimicrobial proteins to keep the microbiota at bay.[55,84] Here we assessed the diffusivity characteristics of antimicrobial biomolecules such as LL-37 and IgG through our alginate-based hydrogels, where effective diffusion coefficients were calculated using a MATLAB code from Hettiaratchi et al. (2018).[130] LL-37 is an antimicrobial peptide that is constantly secreted by epithelial cells lining the mucosal epithelium to maintain homeostasis of the microbiota.[71,162] Due to its cationic nature, LL-37 is known to interact with mucin and pool in the mucus layer to prevent over-proliferation of bacterial species.[71,163] Unfortunately, when assessing the diffusivity of a carboxy fluorescein labelled LL-37, we found that the fluorescence within the reservoir would diminish over time as well as fluorescent cluster formation; therefore, the D_{eff} could not be calculated. The mechanism by which LL-37 kills bacteria is by membrane disruption through interaction with the lipid headgroups. Interestingly, Wildman et al. (2003) found the interaction between LL-37 and lipid head groups to be higher at low LL-37 concentrations and reduced at high LL-37 concentrations, suggesting that at higher concentrations, LL-37 peptides cluster together and potentially precipitate out of solution.[164] Although the data did not allow for the calculation of D_{eff}, we observed fluorescent cluster formation within the ALG-MUC hydrogel, but not in the 1% ALG hydrogels, which suggest that the LL-37 are binding to the mucin contained within the alginate, likely through interaction with the negatively charged carbohydrate side chains.

Secreted immunoglobulins have also been identified to play a major role in host defense within the mucus layer, the most prevalent being IgA and IgG.[165] IgAs are secreted into the mucus layer in the form of dimers, which are connected by a peptide chain, known as the J chain, that is highly glycosylated.[83] Due to the glycosylated nature of these secretory IgA, they can

interact with mucin side chains that help maintain a high level of immunoglobulins within the mucus and higher potential to bind pathogenic bacteria as a mechanism of innate defense.[50] IgG, on the other hand, are not as prevalent in the GI mucus, but there is evidence of higher prevalence in the airway where they are secreted by immunocytes.[72,73] Because IgG are monomeric, they can easily diffuse into the mucus,[166] but have also been shown to demonstrate interaction with mucin as well as other proteins within bodily fluids. This interaction occurs specifically at the Fc portion at the constant region of the antibody, therefore exposing the variable region to bind bacterial and viral particles.[167-170] This would lead to the expectation that antibody diffusion within the mucus layer is reduced due to these interactions with mucin. However, our findings did not show any differences in the D_{eff} of IgG between ALG-MUC hydrogels and 1% ALG hydrogels. Although, it was observed that changes in cross sectional fluorescent profiles (1 mm away from the hydrogel reservoir interface) were reduced in ALG-MUC hydrogels compared to 1% ALG hydrogels, which might suggest some antibody-mucin interaction.

Mucus viscosity is another important physical characteristic in determining its protective ability. One of the main contributing factors to mucus viscosity in the airway is hydration.[171] Dysregulation of ion concentrations can result in a highly dense mucus layer and overall increased mucin concentration, which is typically associated with chronic infection.[26,27] In the GI tract, reduction of mucin density has also been associated with inflammation, where the barrier function is compromised. This phenomenon can be induced by specific pathogens as well as individuals who are genetically predisposed to altered mucus production.[96,100,172] For instance, *H. pylori* have demonstrated reduction in pH in the immediate environment which reduces the viscoelasticity of the mucus barrier, and thus they are able to bypass the mucus to infect the

epithelial cells.[100] Some CD patients are genetically predisposed to a lower viscosity mucus layer in the GI tract. These genetic mutations typically occur in the goblet cells within the GI tract where gel forming mucins are secreted with reduced glycosylation.[96] When measuring the viscosity of the hydrogels in this study, a falling ball viscometer was used where viscosity was found to be decreasing with increasing mucin concentrations. Previously mucin has been shown to interact with Ca^{2+} cations through their negatively charged side chains.[81] By increasing mucin concentrations in the alginate-based hydrogels it is likely that Ca^{2+} was sequestered by the mucin leading to reduced crosslinking in the alginate network. Other interactions between polymer and calcium ions may have been taking place as well, such as intermolecular alginate-mucin or mucin-mucin interactions resulting in reduction of alginate crosslinking as well (Figure 25). Although hydrogel viscosity was reduced with the introduction of mucin, we observed improved cell viability in both cell lines when co-culturing with pathogenic bacteria on top of an ALG-MUC hydrogel. This finding might suggest that in the presence of mucin, an improved barrier function is provided due to increased content within the hydrogel and potential interaction with bacteria. Other studies have also demonstrated that bacteria use mucin as a binding site, which in this case may reduce the rate at which bacteria migrate towards the mammalian cells.[173-175]
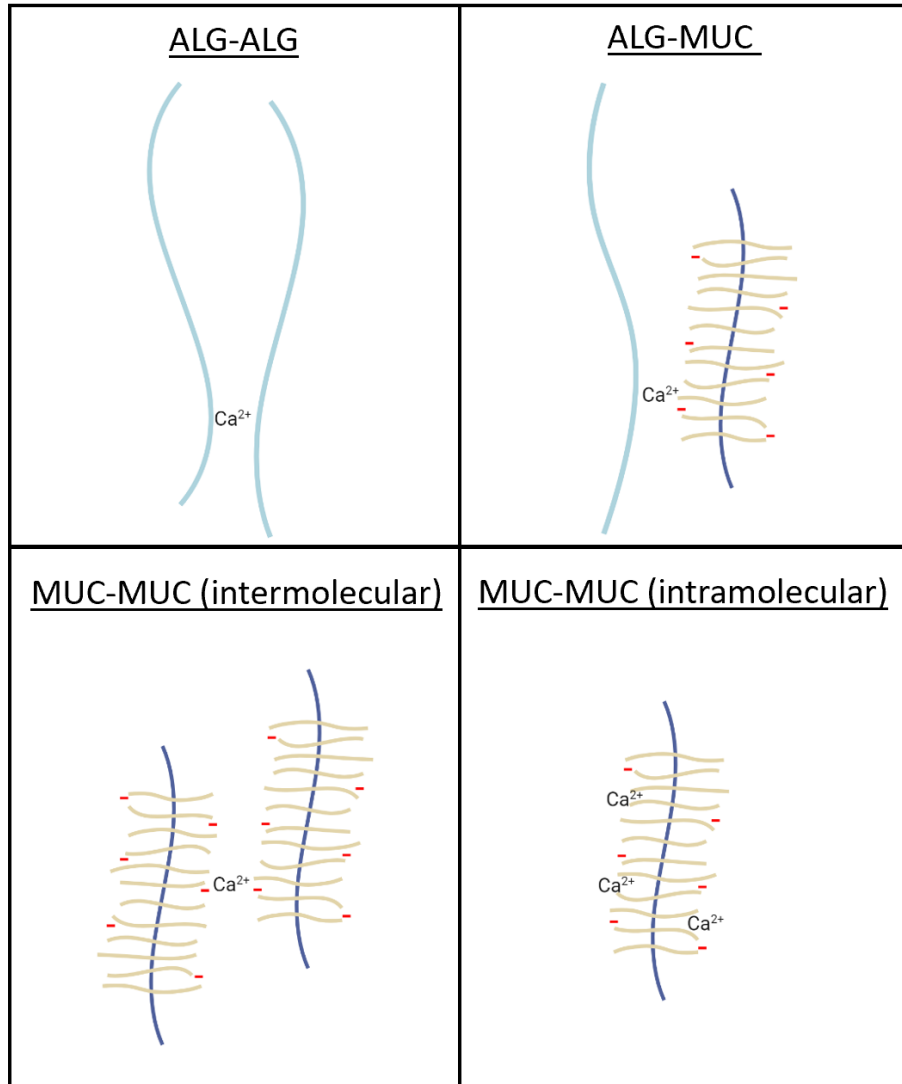
Figure 25: Illustration of potential interactions between alginate and mucin monomers within an ALG-MUC hydrogel.

5.4 Pathogenic Bacteria Behavior and Distribution within the Mucus Layer

In addition to being bacterial binding sites, mucin sugar side chains are also known to be used as a carbon source.[176] The O-linked glycan structures make up much of the entire glycoprotein weight, which provides bacteria with an abundance of oligosaccharides to thrive off. Our assessment of bacterial distribution within the ATPS containing alginate-based hydrogels demonstrate the preferential growth of *S. flexneri* within the hydrogel layer when

mucin is present. Many commensal species along with *S. flexneri* have been shown to express mucolytic enzymes to metabolize the mucin sidechains as well as a mechanism to bypass the mucus barrier.[101] *P. aeruginosa* showed higher abundance within the 1% ALG hydrogel as opposed to the ALG-MUC hydrogels. This is consistent with other i*n vitro* studies that have shown that *P. aeruginosa* form *in vivo*-like biofilms when grown in alginate hydrogels.[123] During chronic infection in the lung, *P. aeruginosa* undergo changes in genetic expression to enter a mucoid state where flagella protein expression is reduced, and alginate polysaccharide production is increased to form dense biofilms to resist antibiotics as well as the host immune cell responses.[92,177] This may explain the preferential growth in the 1% ALG hydrogels. However, the increased biopolymer content of the ALG-MUC hydrogels compared to the 1% ALG hydrogels might also contribute the reduction in bacterial permeation in ALG-MUC hydrogels.

5.5   Potential Mechanisms of Mammalian Cell Death

In our Live/Dead assessment of the mammalian cell component within the co-cultures, there seemed to be some correlation between bacterial abundance within the hydrogel layer and cell viability. As previously mentioned, we found *P. aeruginosa* abundance to be higher in the 1% ALG hydrogels compared to the ALG-MUC hydrogels. This difference in bacterial abundance was reflected in the viability of 16-HBE cells, where viability was lower in wells containing a 1% ALG overlay with increasing cell viability as mucin concentration was increased. This suggests that the ALG-MUC hydrogels provide better barrier function to *P. aeruginosa* compared to the 1% ALG hydrogels. With the ability to penetrate the 1% ALG hydrogel layer, *P. aeruginosa* in contact with the mammalian cells are capable of toxin secretion

through the type III secretion system (T3SS), where various proteases and exotoxins can be directly injected into the host cell leading to cell death.[178] Rajan et al. (2000) examine the effects of various mutant strains of *P. aeruginosa*, including a strain lacking the T3SS, on a human tracheal epithelial cell line.[179] They found that without a functioning T3SS, the number of apoptotic mammalian cells is reduced, when incubated with *P. aeruginosa*.[179] Interestingly, they also demonstrate that polarized 16-HBE cells forming tight junctions better resist apoptosis in the presence of *P. aeruginosa*, potentially as a result of NF-κB activation (confer antiapoptotic effects).[180] The 16-HBE cells used in this study were grown as monolayers, which typically contain fewer tight junctions than polarized monolayers making the cells more sensitive to *P. aeruginosa*.

Caco-2 cells in co-culture with *S. flexneri* showed consistently high cell viability between wells containing the different alginate-based hydrogels. When differentiated on semi-permeable membranes, Caco-2 cells have been shown to generate a glycocalyx, which provided some barrier function to microbial adherence.[181] However, flat Caco-2 monolayers lack a glycocalyx; therefore, the lack of cell death might suggest a strong barrier function against *S. flexneri* due to their lack of motility. While they are non-motile, *S. flexneri* are known to secrete mucolytic enzymes that allow them to efficiently bypass the mucus layer.[55] Some of the symptoms associated with *Shigella* infections include severe diarrhea (bloody and with mucus), fever and dehydration.[182] However, it is not the mucolytic activity that make *S. flexneri* cause such severe GI symptoms but rather its toxin production and virulent ability to enter host cells to evade the host immune response.[183] Studies have suggested multiple mechanisms by which *Shigella* cross the epithelium barrier either directly through translocation into specialized epithelial cells to bypass the epithelium layer[184] or through polymorphonuclear neutrophil

leukocytes (PMN) that are recruited to the epithelium by initial inflammatory response.[185] This then allows bacterial cells to proliferate and invade other epithelial cells causing destruction of the epithelium layer.[183] The destructive nature of *S. flexneri* invasion into cells is likely what was observed in our co-cultures considering the Live/Dead staining, where dead stained cells were uncountable due to the dispersed red staining.

5.6   Antibiotic Treatment and Bacterial Resistance

Chronic infection of *P. aeruginosa* is commonly associated with CF. Once established biofilms are formed within the thickened mucus layer, bacteria persist and develop resistance to antibiotic treatments.[92] Therefore, we were interested in testing ciprofloxacin treatment against established bacterial colonies within the alginate-based hydrogel layers. To perform this experiment, co-cultures were first incubated for 7 hours to establish some bacterial growth within the system, followed by a 12-hour incubation with a ciprofloxacin supplemented PEG-phase. We observed a reduction in *P. aeruginosa* abundance and near full eradication of *S. flexneri* within the PEG-phase; however, both species were found to persist within the ALG-MUC hydrogel layers. These findings demonstrate that the hydrogel layer does in fact provide the established bacterial colonies some protection from antibiotic treatment, especially in the ALG-MUC hydrogels. Cell viability of 16-HBE cells overlaid with 1% ALG showed improved viability compared to no antibiotic treatment, suggesting that the antibiotic was capable of diffusing into the hydrogel and eliminated enough bacteria for improved cell survival. However, the reduced cell viability of 16-HBE and Caco-2, overlaid with ALG-MUC hydrogels, indicates that the added incubation time (in antibiotic treatment experiments) allowed the persistent bacteria to further migrate towards the underlying epithelium to cause cell death.

CHAPTER 6.   CONCLUSIONS & FUTURE DIRECTIONS

6.1 Limitations and Future Work

Although the work discussed within this thesis demonstrates the compatibility of an ALG-MUC hydrogel with a PEG-DEX ATPS co-culture, further characterization and optimization is needed. There are various limitations/shortcomings that should be addressed in future work, regarding the validation of the proposed mammalian-microbial co-culture model.

It is likely that the fabricated hydrogels in this study have non-Newtonian rheological properties based on previous studies that have characterized similar hydrogels. The falling ball viscometer was used to assess the apparent viscosity of the partially crosslinked alginate-based hydrogels; however, to gain a full understanding of the rheological properties the viscoelasticity should be explored using alternative tools such as a plate rheometer. Our findings demonstrated an unexpected result, where hydrogel viscosity decreased with increasing mucin concentrations, which may have been the result of alternate interactions between mucin and alginate monomers or between mucin and mucin (intermolecular or intramolecular interaction), thus reducing the level of calcium crosslinking between the alginate molecules.

As a result, we speculate whether the ALG-MUC hydrogels produced are true semi-IPNs. To test this hypothesis, an alternative hydrogel polymer that can be crosslinked, independent of calcium, could be used in place of alginate, such as hyaluronic acid. If the same reduction in viscosity is not observed, this would suggest that the incorporated mucin monomers were in fact interacting with the free calcium ions and reducing the alginate-alginate interaction. The diffusivity characterization of the hydrogels was assessed using straight PDMS chips containing straight channels with reservoirs on either side containing liquid levels at equal height to reduce convective flow. However, the level of the liquid on either side may have differed

considering the height of the liquid meniscus was assessed by the naked eye during experimentation. Alternatively, fluorescent recovery after photobleaching (FRAP) can be performed to measure the diffusivity of various fluorescent molecules.

Throughout this work Live/Dead Assay was performed to assess the cell viability, which can be a crude measure of cell viability considering that the cells will either stain red or green. In our observations, several cells were found to be stained with both calcein AM (viable, green) and ethidium-homodimer (non-viable, red). However, the state of the cell's viability is more complex than this. To obtain a more accurate measure of the state of the mammalian cells, metabolic assays can be carried out such as the 3-(4,5-dimethylthiazol-2-yl)-2,5-diphenyl-2H-tetrazolium bromide (MTT) assay that can measure total cellular metabolic activity.

Furthermore, the assessment of bacterial distribution within the co-culture system was focused on the total abundance of bacteria within either the hydrogel layer or the liquid phase. To further assess the bacterial distribution within the hydrogel layer, techniques such as fluorescence in situ hybridization (FISH) staining can be used with confocal microscopy to better understand the specific location of dense bacterial colonies within the system.

Another concern with this co-culture system is its longevity. Here, we demonstrate that the co-culture of 16-HBE and Caco-2 cells with *P. aeruginosa* and *S. flexneri*, respectively, over a 12-hour incubation period without bacterial overgrowth within the system. With the introduction of ciprofloxacin at MIC, we find that bacterial colonies can be maintained over longer periods of time (19 hours) without over proliferation throughout the system. To further the use of this host-microbe interaction system for disease modelling, antibiotic supplementation can be used to maintain the bacteria colonies at inhibitory concentrations. Additionally, the mammalian cell component in the current model lacks complexity in that it does not fully

represent the columnar cell barrier found in natural mucosal epithelium. The goal of this project was to demonstrate the ability to form an ATPS co-culture on top of an artificial mucus hydrogel where monolayers were used as a crude measure to determine the cytotoxic effects of both the hydrogel and bacteria. To further improve this system, a differentiated tissue culture should be used to provide the specialized functions of the particular organ of interest.

Lastly, we did not address the immunological response of the mammalian cells to the bacterial infection. Chemokine response such as IL-8 secretion by epithelial cells is common in bacterial infections as a mechanism to recruit immunocytes to the infection site to rid the bacteria. This can be tested by performing ELISA with the co-culture media after the incubation to determine the level of chemokine secretion under the different conditions.

6.2   Conclusions

The findings presented in this study demonstrate a simple yet robust method to creating a mucus-like hydrogel for the application of mammalian-microbial co-culture using a PEG-DEX ATPS formulation. The ALG-MUC semi-IPN hydrogel can be fabricated using a simple ionic crosslinking method which allows for the deposition of the hydrogel directly on top of a mammalian cell monolayer without disruption of the underlying cells. Furthermore, we show that the ALG-MUC hydrogels are, in fact, compatible with a PEG-DEX ATPS in that it is cytocompatible over extended periods of time, non-cell adherent, protective against PEG-mediated cytotoxicity, and able to support the formation of an ATPS for bacterial deposition. These hydrogels also demonstrate selective diffusivity of biomolecules as well as barrier function in mammalian-microbial co-culture when using pathogenic bacteria.

By successfully establishing a mammalian-microbial co-culture using an ALG-MUC hydrogel within an ATPS method, this model has the potential to provide the spatial-temporal niche of the mucus microenvironment *in vitro*. With the recent rise in interest of fabricating a realistic *in vitro* host-microbe interaction model, this model uses equipment and chemicals that are available to the typically equipped life science laboratory. By addressing the limitations of this model to optimize its use in future studies, there is the potential to provide a readily available *in vitro* model for studying specific interactions between mammalian and microbial cells as well as a validation tool for preclinical drug screening.

BIBLIOGRAPHY

1   Antoni, L., Nuding, S., Wehkamp, J. & Stange, E. F. Intestinal Barrier in Inflammatory Bowel Disease. *World Journal of Gastroenterology* **20**, 1165-1179, doi:10.3748/wjg.v20.i5.1165 (2014).

2   Fahy, J. V. & Dickey, B. F. Airway Mucus Function and Dysfunction. *New England Journal of Medicine* **363**, 2233-2247, doi:10.1056/NEJMra0910061 (2010).

3   Hickman, D. L., Johnson, J., Vemulapalli, T. H., Crisler, J. R. & Shepherd, R. Commonly Used Animal Models. *Principles of Animal Research for Graduate and Undergraduate Students*, 117-175, doi:10.1016/B978-0-12-802151-4.00007-4 (2017).

4   Gupta, V. K., Paul, S. & Dutta, C. Geography, Ethnicity or Subsistence-Specific Variations in Human Microbiome Composition and Diversity. *Frontiers in Microbiology* **8**, doi:10.3389/fmicb.2017.01162 (2017).

5   Krakowka, S., Morgan, D. R., Kraft, W. G. & Leunk, R. D. Establishment of Gastric *Campylobacter pylori* Infection in the Neonatal Gnotobiotic Piglet. *Infect Immun* **55**, 2789-2796, doi:10.1128/iai.55.11.2789-2796.1987 (1987).

6   Raibaud, P. *et al.* Implantation of Bacteria from the Digestive Tract of Man and Various Animals into Gnotobiotic Mice. *The American Journal of Clinical Nutrition* **33**, 2440-2447, doi:10.1093/ajcn/33.11.2440 (1980).

7   Nagao-Kitamoto, H. *et al.* Functional Characterization of Inflammatory Bowel Disease–Associated Gut Dysbiosis in Gnotobiotic Mice. *Cellular and Molecular Gastroenterology and Hepatology* **2**, 468-481, doi:https://doi.org/10.1016/j.jcmgh.2016.02.003 (2016).

8   Escribano-Vazquez, U. *et al.* The Commensal *Escherichia coli* CEC15 Reinforces Intestinal Defences in Gnotobiotic Mice and is Protective in a Chronic Colitis Mouse Model. *Scientific Reports* **9**, 11431, doi:10.1038/s41598-019-47611-9 (2019).

9   Rath, H. C. *et al.* Different Subsets of Enteric Bacteria Induce and Perpetuate Experimental Colitis in Rats and Mice. *Infect Immun* **69**, 2277-2285, doi:10.1128/IAI.69.4.2277-2285.2001 (2001).

10   Cowley, E. A., Wang, C. G., Gosselin, D., Radzioch, D. & Eidelman, D. H. Mucociliary Clearance in Cystic Fibrosis Knockout Mice Infected with *Pseudomonas aeruginosa*. *European Respiratory Journal* **10**, 2312 (1997).

11   Sun, X. *et al.* Lung Phenotype of Juvenile and Adult Cystic Fibrosis Transmembrane Conductance Regulator-Knockout Ferrets. *American Journal of Respiratory Cell and Molecular Biology* **50**, 502-512, doi:10.1165/rcmb.2013-0261OC (2014).

12   Nguyen, T. L. A., Vieira-Silva, S., Liston, A. & Raes, J. How Informative is the Mouse for Human Gut Microbiota Research? *Disease Models & Mechanisms* **8**, 1-16, doi:10.1242/dmm.017400 (2015).

13   Semaniakou, A., Croll, R. P. & Chappe, V. Animal Models in the Pathophysiology of Cystic Fibrosis. *Front Pharmacol* **9**, 1475-1475, doi:10.3389/fphar.2018.01475 (2019).

14   Kühn, R., Löhler, J., Rennick, D., Rajewsky, K. & Müller, W. Interleukin-10-Deficient Mice Develop Chronic Enterocolitis. *Cell* **75**, 263-274, doi:https://doi.org/10.1016/0092-8674(93)80068-P (1993).

15   Okayasu, I. *et al.* A Novel Method in the Induction of Reliable Experimental Acute and Chronic Ulcerative Colitis in Mice. *Gastroenterology* **98**, 694-702, doi:https://doi.org/10.1016/0016-5085(90)90290-H (1990).

16   Ostanin, D. V. *et al.* T Cell Transfer Model of Chronic Colitis: Concepts, Considerations, and Tricks of the Trade. *American Journal of Physiology. Gastrointestinal and Liver Physiology* **296**, G135-G146, doi:10.1152/ajpgi.90462.2008 (2009).

17   Fiorentino, D. F. *et al.* IL-10 Acts on the Antigen-Presenting Cell to Inhibit Cytokine Production by Th1 Cells. *The Journal of Immunology* **146**, 3444 (1991).

18   Seregin, S. S. *et al.* NLRP6 Protects Il10−/− Mice from Colitis by Limiting Colonization of *Akkermansia muciniphila*. *Cell Reports* **19**, 733-745, doi:https://doi.org/10.1016/j.celrep.2017.03.080 (2017).

19   Kitajima, S., Takuma, S. & Morimoto, M. Tissue Distribution of Dextran Sulfate Sodium (DSS) in the Acute Phase of Murine DSS-Induced Colitis. *Journal of Veterinary Medical Science* **61**, 67-70, doi:10.1292/jvms.61.67 (1999).

20   Ohkusa, T., Okayasu, I., Tokoi, S., Araki, A. & Ozaki, Y. Changes in Bacterial Phagocytosis of Macrophages in Experimental Ulcerative Colitis. *Digestion* **56**, 159-164, doi:10.1159/000201236 (1995).

21   Ostanin, D. V. *et al.* T Cell-Induced Inflammation of the Small and Large Intestine in Immunodeficient Mice. *American Journal of Physiology-Gastrointestinal and Liver Physiology* **290**, G109-G119, doi:10.1152/ajpgi.00214.2005 (2006).

22   Chiaranunt, P., Tometich, J. T., Ji, J. & Hand, T. W. T Cell Proliferation and Colitis Are Initiated by Defined Intestinal Microbes. *The Journal of Immunology* **201**, 243, doi:10.4049/jimmunol.1800236 (2018).

23   Zhang, Z. & Liu, Z. Paneth Cells: the Hub for Sensing and Regulating Intestinal Flora. *Science China Life Sciences* **59**, 463-467, doi:10.1007/s11427-016-5018-5 (2016).

24   Gassler, N. Paneth Cells in Intestinal Physiology and Pathophysiology. *World J Gastrointest Pathophysiol* **8**, 150-160, doi:10.4291/wjgp.v8.i4.150 (2017).

25   Matsui, H. *et al.* Evidence for Periciliary Liquid Layer Depletion, Not Abnormal Ion Composition, in the Pathogenesis of Cystic Fibrosis Airways Disease. *Cell* **95**, 1005-1015, doi:https://doi.org/10.1016/S0092-8674(00)81724-9 (1998).

26   Ulrich, M. *et al.* Localization of Staphylococcus aureus in Infected Airways of Patients with Cystic Fibrosis and in a Cell Culture Model of S. aureus Adherence. *American Journal of Respiratory Cell and Molecular Biology* **19**, 83-91, doi:10.1165/ajrcmb.19.1.3137 (1998).

27   Lam, J., Chan, R., Lam, K. & Costerton, J. W. Production of Mucoid Microcolonies by *Pseudomonas aeruginosa* within Infected Lungs in Cystic Fibrosis. *Infect Immun* **28**, 546-556, doi:doi:10.1128/iai.28.2.546-556.1980 (1980).

28   Haq, I. J., Gray, M. A., Garnett, J. P., Ward, C. & Brodlie, M. Airway Surface Liquid Homeostasis in Cystic Fibrosis: Pathophysiology and Therapeutic Targets. *Thorax* **71**, 284, doi:10.1136/thoraxjnl-2015-207588 (2016).

29   Zahm, J. M. *et al.* Early Alterations in Airway Mucociliary Clearance and Inflammation of the Lamina Propria in CF Mice. *American Journal of Physiology-Cell Physiology* **272**, C853-C859, doi:10.1152/ajpcell.1997.272.3.C853 (1997).

30   Clarke, L. L. *et al.* Relationship of a Non-Cystic Fibrosis Transmembrane Conductance Regulator-Mediated Chloride Conductance to Organ-Level Disease in Cftr(-/-) Mice. *Proceedings of the National Academy of Sciences* **91**, 479, doi:10.1073/pnas.91.2.479 (1994).

31   Grubb, B. R., Paradiso, A. M. & Boucher, R. C. Anomalies in Ion Transport in CF Mouse Tracheal Epithelium. *American Journal of Physiology-Cell Physiology* **267**, C293-C300, doi:10.1152/ajpcell.1994.267.1.C293 (1994).

32   Zhou, Z. *et al.* The ENaC-Overexpressing Mouse as a Model of Cystic Fibrosis Lung Disease. *Journal of Cystic Fibrosis : Official Journal of the European Cystic Fibrosis Society* **10 Suppl 2**, S172-182, doi:10.1016/s1569-1993(11)60021-0 (2011).

33   McCray, P. B., Jr., Zabner, J., Jia, H. P., Welsh, M. J. & Thorne, P. S. Efficient Killing of Inhaled Bacteria in ΔF508 Mice: Role of Airway Surface Liquid Composition. *American Journal of Physiology-Lung Cellular and Molecular Physiology* **277**, L183-L190, doi:10.1152/ajplung.1999.277.1.L183 (1999).

34   Hoffmann, N. *et al.* Novel Mouse Model of Chronic *Pseudomonas aeruginosa* Lung Infection Mimicking Cystic Fibrosis. *Infect Immun* **73**, 2504-2514, doi:10.1128/IAI.73.4.2504-2514.2005 (2005).

35   Moser, C. *et al.* Novel Experimental *Pseudomonas aeruginosa* Lung Infection Model Mimicking Long-Term Host-Pathogen Interactions in Cystic Fibrosis. *APMIS* **117**, 95-107, doi:https://doi.org/10.1111/j.1600-0463.2008.00018.x (2009).

36   Guilbault, C. *et al.* Cystic Fibrosis Lung Disease Following Infection with *Pseudomonas aeruginosa* in Cftr Knockout Mice using Novel Non-Invasive Direct Pulmonary Infection Technique. *Lab Anim* **39**, 336-352, doi:10.1258/0023677054306944 (2005).

37   Stoltz, D. A. *et al.* Cystic Fibrosis Pigs Develop Lung Disease and Exhibit Defective Bacterial Eradication at Birth. *Science Translational Medicine* **2**, 29ra31-29ra31, doi:10.1126/scitranslmed.3000928 (2010).

38   Meyerholz, D. K., Stoltz, D. A., Pezzulo, A. A. & Welsh, M. J. Pathology of Gastrointestinal Organs in a Porcine Model of Cystic Fibrosis. *The American Journal of Pathology* **176**, 1377-1389, doi:10.2353/ajpath.2010.090849 (2010).

39   Jalili-Firoozinezhad, S. *et al.* A Complex Human Gut Microbiome Cultured in an Anaerobic Intestine-On-a-Chip. *Nature Biomedical Engineering* **3**, 520-531, doi:10.1038/s41551-019-0397-0 (2019).

40   Yonker, L. M. *et al.* Development of a Primary Human Co-Culture Model of Inflamed Airway Mucosa. *Sci Rep* **7**, 8182, doi:10.1038/s41598-017-08567-w (2017).

41   Trapecar, M., Goropevsek, A., Gorenjak, M., Gradisnik, L. & Slak Rupnik, M. A Co-Culture Model of the Developing Small Intestine Offers New Insight in the Early Immunomodulation of Enterocytes and Macrophages by *Lactobacillus* spp. through STAT1 and NF-kB p65 Translocation. *PLOS ONE* **9**, e86297, doi:10.1371/journal.pone.0086297 (2014).

42   Huh, D. *et al.* Microfabrication of Human Organs-On-Chips. *Nature Protocols* **8**, 2135-2157, doi:10.1038/nprot.2013.137 (2013).

43   Barkal, L. J. *et al.* Microbial Volatile Communication in Human Organotypic Lung Models. *Nature Communications* **8**, 1770, doi:10.1038/s41467-017-01985-4 (2017).

44   Parlesak, A., Haller, D., Brinz, S., Baeuerlein, A. & Bode, C. Modulation of Cytokine Release by Differentiated CACO-2 Cells in a Compartmentalized Coculture Model with Mononuclear Leucocytes and Nonpathogenic Bacteria. *Scandinavian Journal of Immunology* **60**, 477-485, doi:https://doi.org/10.1111/j.0300-9475.2004.01495.x (2004).

45   Alemka, A. *et al.* Probiotic Colonization of the Adherent Mucus Layer of HT29MTXE12 Cells Attenuates *Campylobacter jejuni* Virulence Properties. *Infect Immun* **78**, 2812-2822, doi:10.1128/IAI.01249-09 (2010).

46   Navabi, N., McGuckin, M. A. & Lindén, S. K. Gastrointestinal Cell Lines Form Polarized Epithelia with an Adherent Mucus Layer when Cultured in Semi-Wet Interfaces with Mechanical Stimulation. *PLOS ONE* **8**, e68761, doi:10.1371/journal.pone.0068761 (2013).

47   Dwidar, M., Leung, B. M., Yaguchi, T., Takayama, S. & Mitchell, R. J. Patterning Bacterial Communities on Epithelial Cells. *PLOS ONE* **8**, e67165, doi:10.1371/journal.pone.0067165 (2013).

48   Johansson, M. E. V., Sjövall, H. & Hansson, G. C. The Gastrointestinal Mucus System in Health and Disease. *Nat Rev Gastroenterol Hepatol* **10**, 352-361, doi:10.1038/nrgastro.2013.35 (2013).

49   Kommineni, S. *et al.* Bacteriocin Production Augments Niche Competition by *Enterococci* in the Mammalian Gastrointestinal Tract. *Nature* **526**, 719-722, doi:10.1038/nature15524 (2015).

50   Rogier, E. W., Frantz, A. L., Bruno, M. E. C. & Kaetzel, C. S. Secretory IgA is Concentrated in the Outer Layer of Colonic Mucus along with Gut Bacteria. *Pathogens* **3**, 390-403 (2014).

51   Meyer-Hoffert, U. *et al.* Secreted Enteric Antimicrobial Activity Localises to the Mucus Surface Layer. *Gut* **57**, 764, doi:10.1136/gut.2007.141481 (2008).

52   Lai, S. K., Wang, Y.-Y., Hida, K., Cone, R. & Hanes, J. Nanoparticles Reveal that Human Cervicovaginal Mucus is Riddled with Pores Larger than Viruses. *Proceedings of the National Academy of Sciences of the United States of America* **107**, 598-603, doi:10.1073/pnas.0911748107 (2010).

53   Lai, S. K. *et al.* Drug Carrier Nanoparticles that Penetrate Human Chronic Rhinosinusitis Mucus. *Biomaterials* **32**, 6285-6290, doi:https://doi.org/10.1016/j.biomaterials.2011.05.008 (2011).

54   Huang, J. X. *et al.* Mucin Binding Reduces Colistin Antimicrobial Activity. *Antimicrob Agents Chemother* **59**, 5925-5931, doi:10.1128/AAC.00808-15 (2015).

55   Johansson, M. E. V. *et al.* Bacteria Penetrate the Normally Impenetrable Inner Colon Mucus Layer in both Murine Colitis Models and Patients with Ulcerative Colitis. *Gut* **63**, 281, doi:10.1136/gutjnl-2012-303207 (2014).

56   Kamphuis, J. B. J., Mercier-Bonin, M., Eutamène, H. & Theodorou, V. Mucus Organisation is Shaped by Colonic Content; a New View. *Scientific Reports* **7**, 8527, doi:10.1038/s41598-017-08938-3 (2017).

57   Li, H. *et al.* The Outer Mucus Layer Hosts a Distinct Intestinal Microbial Niche. *Nature Communications* **6**, 8292, doi:10.1038/ncomms9292 (2015).

58   Martens, E. C., Chiang, H. C. & Gordon, J. I. Mucosal Glycan Foraging Enhances Fitness and Transmission of a Saccharolytic Human Gut Bacterial Symbiont. *Cell Host Microbe* **4**, 447-457, doi:10.1016/j.chom.2008.09.007 (2008).

59   Al-Saedi, F., Vaz, D. P., Stones, D. H. & Krachler, A. M. 3-Sulfogalactosyl-Dependent Adhesion of *Escherichia coli* HS Multivalent Adhesion Molecule is Attenuated by Sulfatase Activity. *The Journal of Biological Chemistry* **292**, 19792-19803, doi:10.1074/jbc.M117.817908 (2017).

60   Kamada, N., Chen, G. Y., Inohara, N. & Núñez, G. Control of Pathogens and Pathobionts by the Gut Microbiota. *Nat Immunol* **14**, 685-690, doi:10.1038/ni.2608 (2013).

61   Corr, S. C. *et al.* Bacteriocin Production as a Mechanism for the Antiinfective Activity of *Lactobacillus salivarius* UCC118. *Proceedings of the National Academy of Sciences of the United States of America* **104**, 7617-7621, doi:10.1073/pnas.0700440104 (2007).

62   Kesimer, M. *et al.* Molecular Organization of the Mucins and Glycocalyx Underlying Mucus Transport Over Mucosal Surfaces of the Airways. *Mucosal Immunol* **6**, 379-392, doi:10.1038/mi.2012.81 (2013).

63   Fahy, J. V. & Dickey, B. F. Airway Mucus Function and Dysfunction. *The New England Journal of Medicine* **363**, 2233-2247, doi:10.1056/NEJMra0910061 (2010).

64   Atuma, C., Strugala, V., Allen, A. & Holm, L. The Adherent Gastrointestinal Mucus Gel Layer: Thickness and Physical State In Vivo. *American Journal of Physiology-Gastrointestinal and Liver Physiology* **280**, G922-G929, doi:10.1152/ajpgi.2001.280.5.G922 (2001).

65   Hofmann, W. & Asgharian, B. The Effect of Lung Structure on Mucociliary Clearance and Particle Retention in Human and Rat Lungs. *Toxicological Sciences* **73**, 448-456, doi:10.1093/toxsci/kfg075 (2003).

66   Rokicki, W., Rokicki, M., Wojtacha, J. & Dżeljijli, A. The Role and Importance of Club Cells (Clara cells) in the Pathogenesis of some Respiratory Diseases. *Kardiochir Torakochirurgia Pol* **13**, 26-30, doi:10.5114/kitp.2016.58961 (2016).

67   Vieira, A. T. *et al.* Control of *Klebsiella pneumoniae* Pulmonary Infection and Immunomodulation by Oral Treatment with the Commensal Probiotic *Bifidobacterium longum* 51A. *Microbes and Infection* **18**, 180-189, doi:https://doi.org/10.1016/j.micinf.2015.10.008 (2016).

68   Toure, R., Kheadr, E., Lacroix, C., Moroni, O. & Fliss, I. Production of Antibacterial Substances by Bifidobacterial Isolates from Infant Stool Active Against *Listeria monocytogenes*. *J Appl Microbiol* **95**, 1058-1069, doi:10.1046/j.1365-2672.2003.02085.x (2003).

69   Flynn, S. *et al.* Characterization of the Genetic Locus Responsible for the Production of ABP-118, a Novel Bacteriocin Produced by the Probiotic Bacterium *Lactobacillus salivarius* subsp. *salivarius* UCC118 The GenBank Accession Number for the Sequence Reported in this Paper is AF408405. *Microbiology* **148**, 973-984, doi:https://doi.org/10.1099/00221287-148-4-973 (2002).

70   Kandel, P. P., Baltrus, D. A. & Hockett, K. L. *Pseudomonas* Can Survive Tailocin Killing via Persistence-Like and Heterogenous Resistance Mechanisms. *J Bacteriol* **202**, doi:10.1128/jb.00142-20 (2020).

71   Antoni, L. *et al.* Human Colonic Mucus is a Reservoir for Antimicrobial Peptides. *Journal of Crohn's and Colitis* **7**, e652-e664, doi:10.1016/j.crohns.2013.05.006 (2013).

72   Hill, S. L., Mitchell, J. L., Burnett, D. & Stockley, R. A. IgG Subclasses in the Serum and Sputum from Patients with Bronchiectasis. *Thorax* **53**, 463-468, doi:10.1136/thx.53.6.463 (1998).

73   Bell, D. Y., Haseman, J. A., Spock, A., McLennan, G. & Hook, G. E. R. Plasma Proteins of the Bronchoalveolar Surface of the Lungs of Smokers and Nonsmokers. *American Review of Respiratory Disease* **124**, 72-79, doi:10.1164/arrd.1981.124.1.72 (1981).

74   Sellers, L. A., Allen, A., Morris, E. R. & Ross-Murphy, S. B. Mucus Glycoprotein Gels. Role of Glycoprotein Polymeric Structure and Carbohydrate Side-Chains in Gel-Formation. *Carbohydrate Research* **178**, 93-110, doi:https://doi.org/10.1016/0008-6215(88)80104-6 (1988).

75   Bansil, R. & Turner, B. S. Mucin Structure, Aggregation, Physiological Functions and Biomedical Applications. *Current Opinion in Colloid & Interface Science* **11**, 164-170, doi:https://doi.org/10.1016/j.cocis.2005.11.001 (2006).

76   Wagner, C. E., Wheeler, K. M. & Ribbeck, K. Mucins and Their Role in Shaping the Functions of Mucus Barriers. *Annual Review of Cell and Developmental Biology* **34**, 189-215, doi:10.1146/annurev-cellbio-100617-062818 (2018).

77   Desseyn, J.-L. *et al.* Evolutionary History of the 11p15 Human Mucin Gene Family. *Journal of Molecular Evolution* **46**, 102-106, doi:10.1007/PL00006276 (1998).

78   Ambort, D. *et al.* Calcium and pH-Dependent Packing and Release of the Gel-Forming MUC2 Mucin. *Proceedings of the National Academy of Sciences* **109**, 5645, doi:10.1073/pnas.1120269109 (2012).

79   Verdugo, P. Mucin Exocytosis. *American Review of Respiratory Disease* **144**, S33-S37, doi:10.1164/ajrccm/144.3_pt_2.S33 (1991).

80   Kesimer, M. & Sheehan, J. K. Mass Spectrometric Analysis of Mucin Core Proteins. *Methods in Molecular Biology (Clifton, N.J.)* **842**, 67-79, doi:10.1007/978-1-61779-513-8_4 (2012).

81   Chen, E. Y. T., Yang, N., Quinton, P. M. & Chin, W.-C. A New Role for Bicarbonate in Mucus Formation. *Am J Physiol Lung Cell Mol Physiol* **299**, L542-L549, doi:10.1152/ajplung.00180.2010 (2010).

82   Holmén Larsson, J. M., Karlsson, H., Sjövall, H. & Hansson, G. C. A Complex, but Uniform O-Glycosylation of the Human MUC2 Mucin from Colonic Biopsies Analyzed by nanoLC/MSn. *Glycobiology* **19**, 756-766, doi:10.1093/glycob/cwp048 (2009).

83   Royle, L. *et al.* Secretory IgA N- and O-Glycans Provide a Link between the Innate and Adaptive Immune Systems. *Journal of Biological Chemistry* **278**, 20140-20153, doi:https://doi.org/10.1074/jbc.M301436200 (2003).

84   Ganz, T. Antimicrobial Polypeptides in Host Defense of the Respiratory Tract. *The Journal of Clinical Investigation* **109**, 693-697, doi:10.1172/JCI15218 (2002).

85   Hansson, G. C. Mucus and Mucins in Diseases of the Intestinal and Respiratory Tracts. *J Intern Med* **285**, 479-490, doi:10.1111/joim.12910 (2019).

86   Okumura, R. & Takeda, K. Maintenance of Intestinal Homeostasis by Mucosal Barriers. *Inflammation and Regeneration* **38**, 5, doi:10.1186/s41232-018-0063-z (2018).

87   De Rose, V., Molloy, K., Gohy, S., Pilette, C. & Greene, C. M. Airway Epithelium Dysfunction in Cystic Fibrosis and COPD. *Mediators Inflamm* **2018**, 1309746, doi:10.1155/2018/1309746 (2018).

88   Kanner, R. E., Anthonisen, N. R. & Connett, J. E. Lower Respiratory Illnesses Promote FEV1 Decline in Current Smokers but not Ex-Smokers with Mild Chronic Obstructive Pulmonary Disease. *American Journal of Respiratory and Critical Care Medicine* **164**, 358-364, doi:10.1164/ajrccm.164.3.2010017 (2001).

89   Li, J. *et al.* Major Air Pollutants and Risk of COPD Exacerbations: A Systematic Review and Meta-Analysis. *Int J Chron Obstruct Pulmon Dis* **11**, 3079-3091, doi:10.2147/COPD.S122282 (2016).

90   Kohri, K., Ueki, I. F. & Nadel, J. A. Neutrophil Elastase Induces Mucin Production by Ligand-Dependent Epidermal Growth Factor Receptor Activation. *American Journal of Physiology-Lung Cellular and Molecular Physiology* **283**, L531-L540, doi:10.1152/ajplung.00455.2001 (2002).

91   Boucher, R. C. Airway Surface Dehydration in Cystic Fibrosis: Pathogenesis and Therapy. *Annual Review of Medicine* **58**, 157-170, doi:10.1146/annurev.med.58.071905.105316 (2007).

92   Mathee, K. *et al.* Mucoid Conversion of *Pseudomonas aeruginosa* by Hydrogen Peroxide: A Mechanism for Virulence Activation in the Cystic Fibrosis Lung. *Microbiology* **145**, 1349-1357, doi:https://doi.org/10.1099/13500872-145-6-1349 (1999).

93   Ghafoor, A., Hay, I. D. & Rehm, B. H. A. Role of Exopolysaccharides in *Pseudomonas aeruginosa* Biofilm Formation and Architecture. *Applied and Environmental Microbiology* **77**, 5238-5246, doi:10.1128/AEM.00637-11 (2011).

94   Alam, M. T. *et al.* Microbial Imbalance in Inflammatory Bowel Disease Patients at Different Taxonomic Levels. *Gut Pathogens* **12**, 1, doi:10.1186/s13099-019-0341-6 (2020).

95   Fu, J. *et al.* Loss of Intestinal Core 1-Derived O-Glycans Causes Spontaneous Colitis in Mice. *The Journal of Clinical Investigation* **121**, 1657-1666, doi:10.1172/JCI45538 (2011).

96   Raouf, A. H. *et al.* Sulphation of Colonic and Rectal Mucin in Inflammatory Bowel Disease: Reduced Sulphation of Rectal Mucus in Ulcerative Colitis. *Clinical Science* **83**, 623-626, doi:10.1042/cs0830623 (1992).

97   Seishima, J. *et al.* Gut-Derived *Enterococcus faecium* from Ulcerative Colitis Patients Promotes Colitis in a Genetically Susceptible Mouse Host. *Genome Biology* **20**, 252, doi:10.1186/s13059-019-1879-9 (2019).

98   Zhou, F. *et al.* Mice with Inflammatory Bowel Disease are Susceptible to *Clostridium difficile* Infection with Severe Disease Outcomes. *Inflammatory Bowel Diseases* **24**, 573-582, doi:10.1093/ibd/izx059 (2018).

99   Tamboli, C. P., Neut, C., Desreumaux, P. & Colombel, J. F. Dysbiosis in Inflammatory Bowel Disease. *Gut* **53**, 1, doi:10.1136/gut.53.1.1 (2004).

100   Celli, J. P. *et al. Helicobacter pylori* moves through Mucus by Reducing Mucin Viscoelasticity. *Proceedings of the National Academy of Sciences of the United States of America* **106**, 14321-14326, doi:10.1073/pnas.0903438106 (2009).

101   Henderson, I. R., Czeczulin, J., Eslava, C., Noriega, F. & Nataro, J. P. Characterization of pic, a Secreted Protease of *Shigella flexneri* and Enteroaggregative *Escherichia coli*. *Infect Immun* **67**, 5587-5596, doi:10.1128/IAI.67.11.5587-5596.1999 (1999).

102   Iqbal, M. *et al.* Aqueous Two-Phase System (ATPS): An Overview and Advances in its Applications. *Biological Procedures Online* **18**, 18, doi:10.1186/s12575-016-0048-8 (2016).

103   Albertsson, P.-Å. in *Advances in Protein Chemistry* Vol. 24 (eds C. B. Anfinsen, John T. Edsall, & Frederic M. Richards) 309-341 (Academic Press, 1970).

104   Hachem, F., Andrews, B. A. & Asenjo, J. A. Hydrophobic Partitioning of Proteins in Aqueous Two-Phase Systems. *Enzyme and Microbial Technology* **19**, 507-517, doi:https://doi.org/10.1016/S0141-0229(96)80002-D (1996).

105   Yano, K., Hasegawa, T., Kuboi, R., Komasawa, I. & Tsuchido, T. Characterization of Surface Properties of Heat Shock Proteins for the Separation using Aqueous Two-Phase Systems. *Journal of Chemical Engineering of Japan* **27**, 808-814, doi:10.1252/jcej.27.808 (1994).

106   Rosa, P. A. J. *et al.* Application of Aqueous Two-Phase Systems to Antibody Purification: A Multi-Stage Approach. *Journal of Biotechnology* **139**, 306-313, doi:https://doi.org/10.1016/j.jbiotec.2009.01.001 (2009).

107   Rosa, P. A. J. *et al.* Downstream Processing of Antibodies: Single-Atage versus Multi-Stage Aqueous Two-Phase Extraction. *Journal of Chromatography A* **1216**, 8741-8749, doi:https://doi.org/10.1016/j.chroma.2009.02.024 (2009).

108   Kim, J., Shin, H., Kim, J., Kim, J. & Park, J. Isolation of High-Purity Extracellular Vesicles by Extracting Proteins Using Aqueous Two-Phase System. *PlOS ONE* **10**, e0129760-e0129760, doi:10.1371/journal.pone.0129760 (2015).

109   Atefi, E., Joshi, R., Mann, J. A. & Tavana, H. Interfacial Tension Effect on Cell Partition in Aqueous Two-Phase Systems. *ACS Applied Materials & Interfaces* **7**, 21305-21314, doi:10.1021/acsami.5b05757 (2015).

110   Frampton, J. P., White, J. B., Abraham, A. T. & Takayama, S. Cell Co-Culture Patterning using Aqueous Two-Phase Systems. *Journal of Visualized Experiments : JoVE*, 50304, doi:10.3791/50304 (2013).

111   Frampton, J. P. *et al.* Aqueous Two-Phase System Patterning of Detection Antibody Solutions for Cross-Reaction-Free Multiplex ELISA. *Scientific Reports* **4**, 4878, doi:10.1038/srep04878 (2014).

112   Yaguchi, T. *et al.* Aqueous Two-Phase System-Derived Biofilms for Bacterial Interaction Studies. *Biomacromolecules* **13**, 2655-2661, doi:10.1021/bm300500y (2012).

113   Munchow, G., Schonfeld, F., Hardt, S. & Graf, K. Protein Diffusion Across the Interface in Aqueous Two-Phase Systems. *Langmuir* **24**, 8547-8553, doi:10.1021/la800956j (2008).

114   Liu, G. *et al.* Cytotoxicity Study of Polyethylene Glycol Derivatives. *RSC Advances* **7**, 18252-18259, doi:10.1039/C7RA00861A (2017).

115   Genes, N. G., Rowley, J. A., Mooney, D. J. & Bonassar, L. J. Effect of Substrate Mechanics on Chondrocyte Adhesion to Modified Alginate Surfaces. *Archives of Biochemistry and Biophysics* **422**, 161-167, doi:https://doi.org/10.1016/j.abb.2003.11.023 (2004).

116   Maiti, S., Singha, K., Ray, S., Dey, P. & Sa, B. Adipic Acid Dihydrazide Treated Partially Oxidized Alginate Beads for Sustained Oral Delivery of Flurbiprofen. *Pharmaceutical Development and Technology* **14**, 461-470, doi:10.1080/10837450802712658 (2009).

117   Balakrishnan, B., Mohanty, M., Fernandez, A. C., Mohanan, P. V. & Jayakrishnan, A. Evaluation of the Effect of Incorporation of Dibutyryl Cyclic Adenosine Monophosphate in an In Situ-Forming Hydrogel Wound Dressing Based on Oxidized Alginate and Gelatin. *Biomaterials* **27**, 1355-1361, doi:https://doi.org/10.1016/j.biomaterials.2005.08.021 (2006).

118   Lee, K. Y. & Mooney, D. J. Alginate: Properties and Biomedical Applications. *Prog Polym Sci* **37**, 106-126, doi:10.1016/j.progpolymsci.2011.06.003 (2012).

119   Moxon, S. R. *et al.* Blended Alginate/Collagen Hydrogels Promote Neurogenesis and Neuronal Maturation. *Materials Science and Engineering: C* **104**, 109904, doi:https://doi.org/10.1016/j.msec.2019.109904 (2019).

120   Yao, R., Zhang, R., Luan, J. & Lin, F. Alginate and Alginate/Gelatin Microspheres for Human Adipose-Derived Stem Cell Encapsulation and Differentiation. *Biofabrication* **4**, 025007, doi:10.1088/1758-5082/4/2/025007 (2012).

121   Kang, S.-W. *et al.* The Effect of Conjugating RGD into 3D Alginate Hydrogels on Adipogenic Differentiation of Human Adipose-Derived Stromal Cells. *Macromolecular Bioscience* **11**, 673-679, doi:https://doi.org/10.1002/mabi.201000479 (2011).

122   Alsberg, E., Anderson, K. W., Albeiruti, A., Franceschi, R. T. & Mooney, D. J. Cell-Interactive Alginate Hydrogels for Bone Tissue Engineering. *Journal of Dental Research* **80**, 2025-2029, doi:10.1177/00220345010800111501 (2001).

123   Sønderholm, M. *et al. Pseudomonas aeruginosa* Aggregate Formation in an Alginate Bead Model System Exhibits in Vivo-Like Characteristics. *Applied and environmental microbiology* **83**, e00113-00117, doi:10.1128/AEM.00113-17 (2017).

124   Bouhadir, K. H., Alsberg, E. & Mooney, D. J. Hydrogels for Combination Delivery of Antineoplastic Agents. *Biomaterials* **22**, 2625-2633, doi:https://doi.org/10.1016/S0142-9612(01)00003-5 (2001).

125   Boateng, J. S., Matthews, K. H., Stevens, H. N. & Eccleston, G. M. Wound Healing Dressings and Drug Delivery Systems: A Review. *J Pharm Sci* **97**, 2892-2923, doi:10.1002/jps.21210 (2008).

126   Rabbany, S. Y. *et al.* Continuous Delivery of Stromal Cell-Derived Factor-1 from Alginate Scaffolds Accelerates Wound Healing. *Cell Transplantation* **19**, 399-408, doi:10.3727/096368909x481782 (2010).

127   Pacheco, D. P. *et al.* Disassembling the Complexity of Mucus Barriers to Develop a Fast Screening Tool for Early Drug Discovery. *J Mater Chem B* **7**, 4940-4952, doi:10.1039/c9tb00957d (2019).

128   Taylor, C., Pearson, J. P., Draget, K. I., Dettmar, P. W. & Smidsrød, O. Rheological Characterisation of Mixed Gels of Mucin and Alginate. *Carbohydrate Polymers* **59**, 189-195, doi:https://doi.org/10.1016/j.carbpol.2004.09.009 (2005).

129   Gupta, D., Tator, C. H. & Shoichet, M. S. Fast-Gelling Injectable Blend of Hyaluronan and Methylcellulose for Intrathecal, Localized Delivery to the Injured Spinal Cord. *Biomaterials* **27**, 2370-2379, doi:https://doi.org/10.1016/j.biomaterials.2005.11.015 (2006).

130   Hettiaratchi, M. H. *et al.* A Rapid Method for Determining Protein Diffusion through Hydrogels for Regenerative Medicine Applications. *APL Bioengineering* **2**, 026110, doi:10.1063/1.4999925 (2018).

131   Atefi, E., Mann, J. A. & Tavana, H. Ultralow Interfacial Tensions of Aqueous Two-Phase Systems Measured using Drop Shape. *Langmuir* **30**, 9691-9699, doi:10.1021/la500930x (2014).

132   Thomas, P., Sekhar, A. C., Upreti, R., Mujawar, M. M. & Pasha, S. S. Optimization of Single Plate-Serial Dilution Spotting (SP-SDS) with Sample Anchoring as an Assured Method for Bacterial and Yeast CFU Enumeration and Single Colony Isolation from Diverse Samples. *Biotechnology Reports* **8**, 45-55, doi:https://doi.org/10.1016/j.btre.2015.08.003 (2015).

133   LeBel, M. Ciprofloxacin: Chemistry, Mechanism of Action, Resistance, Antimicrobial Spectrum, Pharmacokinetics, Clinical Trials, and Adverse Reactions. *Pharmacotherapy: The Journal of Human Pharmacology and Drug Therapy* **8**, 3-30, doi:https://doi.org/10.1002/j.1875-9114.1988.tb04058.x (1988).

134   Abt, M. C. & Pamer, E. G. Commensal Bacteria Mediated Defenses Against Pathogens. *Current Opinion in Immunology* **29**, 16-22, doi:https://doi.org/10.1016/j.coi.2014.03.003 (2014).

135   Flynn, J. M., Niccum, D., Dunitz, J. M. & Hunter, R. C. Evidence and Role for Bacterial Mucin Degradation in Cystic Fibrosis Airway Disease. *PLOS Pathogens* **12**, e1005846, doi:10.1371/journal.ppat.1005846 (2016).

136   Elzinga, J., van der Oost, J., de Vos, W. M. & Smidt, H. The use of Defined Microbial Communities to Model Host-Microbe Interactions in the Human Gut. *Microbiol Mol Biol Rev* **83**, e00054-00018, doi:10.1128/MMBR.00054-18 (2019).

137   Wall, R. J. & Shani, M. Are Animal Models as Good as we Think? *Theriogenology* **69**, 2-9, doi:https://doi.org/10.1016/j.theriogenology.2007.09.030 (2008).

138   Yu, J., Carrier, R. L., March, J. C. & Griffith, L. G. Three Dimensional Human Small Intestine Models for ADME-Tox Studies. *Drug Discovery Today* **19**, 1587-1594, doi:https://doi.org/10.1016/j.drudis.2014.05.003 (2014).

139   Detzel, C. J. *et al.* Bovine Immunoglobulin/Protein Isolate Binds Pro-Inflammatory Bacterial Compounds and Prevents Immune Activation in an Intestinal Co-Culture Model. *PLOS ONE* **10**, e0120278, doi:10.1371/journal.pone.0120278 (2015).

140   Joyner, K., Song, D., Hawkins, R. F., Silcott, R. D. & Duncan, G. A. A Rational Approach to Form Disulfide Linked Mucin Hydrogels. *Soft Matter* **15**, 9632-9639, doi:10.1039/C9SM01715A (2019).

141   Yu, J. *et al.* The Effect of Injected RGD Modified Alginate on Angiogenesis and Left Ventricular Function in a Chronic Rat Infarct Model. *Biomaterials* **30**, 751-756, doi:https://doi.org/10.1016/j.biomaterials.2008.09.059 (2009).

142   Kim, H.-S. A Kinetic Study on Calcium Alginate Bead Formation. *Korean Journal of Chemical Engineering* **7**, 1-6, doi:10.1007/BF02697334 (1990).

143   Stokke, B. T. *et al.* Small-Angle X-Ray Scattering and Rheological Characterization of Alginate Gels. 1. Ca−Alginate Gels. *Macromolecules* **33**, 1853-1863, doi:10.1021/ma991559q (2000).

144   Yuguchi, Y., Hasegawa, A., Padoł, A. M., Draget, K. I. & Stokke, B. T. Local Structure of Ca2+ Induced Hydrogels of Alginate–Oligoguluronate Blends Determined by Small-Angle-X-Ray Scattering. *Carbohydrate Polymers* **152**, 532-540, doi:https://doi.org/10.1016/j.carbpol.2016.07.020 (2016).

145   Coto, B., Martos, C., Peña, J. L., Rodríguez, R. & Pastor, G. Effects in the Solubility of CaCO3: Experimental Study and Model Description. *Fluid Phase Equilibria* **324**, 1-7, doi:https://doi.org/10.1016/j.fluid.2012.03.020 (2012).

146   Ingar Draget, K., Østgaard, K. & Smidsrød, O. Homogeneous Alginate Gels: A Technical Approach. *Carbohydrate Polymers* **14**, 159-178, doi:https://doi.org/10.1016/0144-8617(90)90028-Q (1990).

147   Fernández Farrés, I. & Norton, I. T. Formation Kinetics and Rheology of Alginate Fluid Gels Produced by In-Situ Calcium Release. *Food Hydrocolloids* **40**, 76-84, doi:https://doi.org/10.1016/j.foodhyd.2014.02.005 (2014).

148   Growney Kalaf, E. A., Flores, R., Bledsoe, J. G. & Sell, S. A. Characterization of Slow-Gelling Alginate Hydrogels for Intervertebral Disc Tissue-Engineering Applications. *Materials Science and Engineering: C* **63**, 198-210, doi:https://doi.org/10.1016/j.msec.2016.02.067 (2016).

149   Siva, T., Muralidharan, S., Sathiyanarayanan, S., Manikandan, E. & Jayachandran, M. Enhanced Polymer Induced Precipitation of Polymorphous in Calcium Carbonate: Calcite Aragonite Vaterite Phases. *Journal of Inorganic and Organometallic Polymers and Materials* **27**, 770-778, doi:10.1007/s10904-017-0520-1 (2017).

150   Xu, X., Zhao, Y., Lai, Q. & Hao, Y. Effect of Polyethylene Glycol on Phase and Morphology of Calcium Carbonate. *Journal of Applied Polymer Science* **119**, 319-324, doi:https://doi.org/10.1002/app.32559 (2011).

151   Matyash, M., Despang, F., Ikonomidou, C. & Gelinsky, M. Swelling and Mechanical Properties of Alginate Hydrogels with Respect to Promotion of Neural Growth. *Tissue Eng Part C Methods* **20**, 401-411, doi:10.1089/ten.TEC.2013.0252 (2014).

152   Fuongfuchat, A., Jamieson, A. M., Blackwell, J. & Gerken, T. A. Rheological Studies of the Interaction of Mucins with Alginate and Polyacrylate. *Carbohydrate Research* **284**, 85-99, doi:https://doi.org/10.1016/0008-6215(95)00396-7 (1996).

153   R Bansil, E Stanley, a. & Lamont, J. T. Mucin Biophysics. *Annual Review of Physiology* **57**, 635-657, doi:10.1146/annurev.ph.57.030195.003223 (1995).

154   Lee, H., Venable, R. M., Mackerell, A. D., Jr. & Pastor, R. W. Molecular Dynamics Studies of Polyethylene Oxide and Polyethylene Glycol: Hydrodynamic Radius and Shape Anisotropy. *Biophys J* **95**, 1590-1599, doi:10.1529/biophysj.108.133025 (2008).

155   Michaels, J. D. & Papoutsakis, E. T. Polyvinyl Alcohol and Polyethylene Glycol as Protectants Against Fluid-Mechanical Injury of Freely-Suspended Animal Cells (CRL 8018). *Journal of Biotechnology* **19**, 241-257, doi:https://doi.org/10.1016/0168-1656(91)90062-Z (1991).

156   Chiang, E. T. *et al.* Protective Effects of High-Molecular Weight Polyethylene Glycol (PEG) in Human Lung Endothelial Cell Barrier Regulation: Role of Actin Cytoskeletal Rearrangement. *Microvasc Res* **77**, 174-186, doi:10.1016/j.mvr.2008.11.007 (2009).

157   Tavana, H. *et al.* Contact Angle Measurements with Liquids Consisting of Bulky Molecules. *Journal of Colloid and Interface Science* **279**, 493-502, doi:https://doi.org/10.1016/j.jcis.2004.06.090 (2004).

158   Abraham, M., Claudio, D. V., Stefano, S., Alidad, A. & W., D. J. Contact Angles and Wettability: Towards Common and Accurate Terminology. *Surface Innovations* **5**, 3-8, doi:10.1680/jsuin.17.00002 (2017).

159   Schömig, V. J. *et al.* An Optimized Purification Process for Porcine Gastric Mucin with Preservation of its Native Functional Properties. *RSC Advances* **6**, 44932-44943, doi:10.1039/C6RA07424C (2016).

160   Biesbroek, G. *et al.* Early Respiratory Microbiota Composition Determines Bacterial Succession Patterns and Respiratory Health in Children. *American Journal of Respiratory and Critical Care Medicine* **190**, 1283-1292, doi:10.1164/rccm.201407-1240OC (2014).

161   Pettigrew, M. M. *et al.* Upper Respiratory Tract Microbial Communities, Acute Otitis Media Pathogens, and Antibiotic use in Healthy and Sick Children. *Applied and Environmental Microbiology* **78**, 6262-6270, doi:10.1128/AEM.01051-12 (2012).

162   Bals, R., Weiner, D. J., Moscioni, A. D., Meegalla, R. L. & Wilson, J. M. Augmentation of Innate Host Defense by Expression of a Cathelicidin Antimicrobial Peptide. *Infect Immun* **67**, 6084-6089, doi:10.1128/IAI.67.11.6084-6089.1999 (1999).

163   Bergsson, G. *et al.* LL-37 Complexation with Glycosaminoglycans in Cystic Fibrosis Lungs Inhibits Antimicrobial Activity, which can be Restored by Hypertonic Saline. *The Journal of Immunology* **183**, 543, doi:10.4049/jimmunol.0803959 (2009).

164   Henzler Wildman, K. A., Lee, D.-K. & Ramamoorthy, A. Mechanism of Lipid Bilayer Disruption by the Human Antimicrobial Peptide, LL-37. *Biochemistry* **42**, 6545-6558, doi:10.1021/bi0273563 (2003).

165   Reynolds, H. Y., Kazmierowski, J. A. & Newball, H. H. Specificity of Opsonic Antibodies to Enhance Phagocytosis of *Pseudomonas aeruginosa* by Human Alveolar Macrophages. *J Clin Invest* **56**, 376-385, doi:10.1172/JCI108102 (1975).

166   Saltzman, W. M., Radomsky, M. L., Whaley, K. J. & Cone, R. A. Antibody Diffusion in Human Cervical Mucus. *Biophysical Journal* **66**, 508-515, doi:https://doi.org/10.1016/S0006-3495(94)80802-1 (1994).

167   Kobayashi, K. *et al.* Distribution and Partial Characterisation of IgG Fc Binding Protein in Various Mucin Producing Cells and Body Fluids. *Gut* **51**, 169, doi:10.1136/gut.51.2.169 (2002).

168   Gunn, B. M. *et al.* Enhanced Binding of Antibodies Generated during Chronic HIV Infection to Mucus Component MUC16. *Mucosal Immunol* **9**, 1549-1558, doi:10.1038/mi.2016.8 (2016).

169   Yamamoto-Furusho, J. K., Ascaño-Gutiérrez, I., Furuzawa-Carballeda, J. & Fonseca-Camarillo, G. Differential Expression of MUC12, MUC16, and MUC20 in Patients with Active and Remission Ulcerative Colitis. *Mediators Inflamm* **2015**, 659018-659018, doi:10.1155/2015/659018 (2015).

170   Schroeder, H. A. *et al.* LPS-Binding IgG Arrests Actively Motile *Salmonella typhimurium* in Gastrointestinal Mucus. *Mucosal Immunol* **13**, 814-823, doi:10.1038/s41385-020-0267-9 (2020).

171   Lin, V. Y. *et al.* Excess Mucus Viscosity and Airway Dehydration Impact COPD Airway Clearance. *Eur Respir J* **55**, 1900419, doi:10.1183/13993003.00419-2019 (2020).

172   Moehle, C. *et al.* Aberrant Intestinal Expression and Allelic Variants of Mucin Genes Associated with Inflammatory Bowel Disease. *Journal of Molecular Medicine* **84**, 1055-1066, doi:10.1007/s00109-006-0100-2 (2006).

173   Huang, J. Y., Lee, S. M. & Mazmanian, S. K. The Human Commensal *Bacteroides fragilis* Binds Intestinal Mucin. *Anaerobe* **17**, 137-141, doi:https://doi.org/10.1016/j.anaerobe.2011.05.017 (2011).

174   Kankainen, M. *et al.* Comparative Genomic Analysis of *Lactobacillus rhamnosus* GG Reveals Pili Containing a Human- Mucus Binding Protein. *Proc Natl Acad Sci U S A* **106**, 17193-17198, doi:10.1073/pnas.0908876106 (2009).

175   González-Rodríguez, I. *et al.* Role of Extracellular Transaldolase from *Bifidobacterium bifidum* in Mucin Adhesion and Aggregation. *Applied and Environmental Microbiology* **78**, 3992-3998, doi:10.1128/AEM.08024-11 (2012).

176   Marcobal, A., Southwick, A. M., Earle, K. A. & Sonnenburg, J. L. A Refined Palate: Bacterial Consumption of Host Glycans in the Gut. *Glycobiology* **23**, 1038-1046, doi:10.1093/glycob/cwt040 (2013).

177   Kharazmi, A. Mechanisms Involved in the Evasion of the Host Defence by *Pseudomonas aeruginosa*. *Immunology Letters* **30**, 201-205, doi:https://doi.org/10.1016/0165-2478(91)90026-7 (1991).

178   Wareham, D. W., Papakonstantinopoulou, A. & Curtis, M. A. The *Pseudomonas aeruginosa* PA14 Type III Secretion System is Expressed but not Essential to Virulence in the *Caenorhabditis elegans–P. aeruginosa* Pathogenicity Model. *FEMS Microbiology Letters* **242**, 209-216, doi:10.1016/j.femsle.2004.11.018 (2005).

179   Rajan, S. *et al. Pseudomonas aeruginosa* Induction of Apoptosis in Respiratory Epithelial Cells. *American Journal of Respiratory Cell and Molecular Biology* **23**, 304-312, doi:10.1165/ajrcmb.23.3.4098 (2000).

180   Clifton, D. R. *et al.* NF-κB-Dependent Inhibition of Apoptosis is Essential for Host Cell Survival during *Rickettsia rickettsii* Infection. *Proceedings of the National Academy of Sciences* **95**, 4646-4651, doi:10.1073/pnas.95.8.4646 (1998).

181   Frey, A. *et al.* Role of the Glycocalyx in Regulating Access of Microparticles to Apical Plasma Membranes of Intestinal Epithelial Cells: Implications for Microbial Attachment and Oral Vaccine Targeting. *J Exp Med* **184**, 1045-1059, doi:10.1084/jem.184.3.1045 (1996).

182   Niyogi, S. K. Shigellosis. *Journal of Microbiology (Seoul, Korea)* **43**, 133-143 (2005).

183   Jennison, A. V. & Verma, N. K. *Shigella flexneri* Infection: Pathogenesis and Vaccine Development. *FEMS Microbiology Reviews* **28**, 43-58, doi:10.1016/j.femsre.2003.07.002 (2004).

184   Sakaguchi, T., Köhler, H., Gu, X., McCormick, B. A. & Reinecker, H.-C. *Shigella flexneri* Regulates Tight Junction-Associated Proteins in Human Intestinal Epithelial Cells. *Cellular Microbiology* **4**, 367-381, doi:https://doi.org/10.1046/j.1462-5822.2002.00197.x (2002).

185   Beatty, W. L. & Sansonetti, P. J. Role of Lipopolysaccharide in Signaling to Subepithelial Polymorphonuclear Leukocytes. *Infect Immun* **65**, 4395-4404, doi:10.1128/iai.65.11.4395-4404.1997 (1997).

Main Code

```
% Specify the bounds for the diffusion coefficient in cm^2/s
lowbound = 10e-15;
upbound = 10e-4;
% Set options for running the fmincon
% Enable plotting of the results
options =
optimset('PlotFcns',{@optimplotfval,@optimplotstepsize});
% options.StepTolerance = 1e-10;
pmin = 3.5*10e-7;

% pmin = 10^-6;
[pminf,Smin,exitflag,output]=fmincon(@Data_ToMinimize,...
    pmin,[],[],[],[],lowbound,upbound,[],options);

% Data_ToMinimize(pmin);
```

Function to Minimize

```
function S = Data_ToMinimize(p)
load('fluorescence_1')
% distance = distance(2:end);
% matrix = matrix(:,2:end);

% matrix = matrix([1 2 15 30],:);
% time = time([1 2 15 30]);

distance(1,1) = eps;
for i = 1:length(time)
    for j = 1:length(distance)
        if matrix(i,j) == 0
            matrix(i,j) = eps;
        end
    end
end

% matrix = matrix./100;

% Parameter to solve for: diffusion of protein
D_eff = p; % cm^2/s
% Time in seconds for each image
t = 60*time; % s
% Convert distance to centimeters
```

```matlab
x = 10*(distance); %cm
% Calculate the value to plug into our erfc, defined in Clauss,
et al. 1990
% First, create empty vectors
y = zeros(length(t),length(x)); % Value to plug into the
equation
C = zeros(length(t),length(x)); % Calculated concentration, as
fcn of time and position
% Step through each time point to calculate the input variable,
y
% And the resulting concentration, C
for i = 1:length(t)
y(i,:) = x./(2*sqrt(D_eff.*t(i)));
C(i,:) = erfc(y(i,:));
end
% C = 0.1*C;

% Create plots
subplot(2,1,1)
plot(x*10000,matrix,'LineWidth',2)
xlabel('Distance, µm')
ylabel('Normalized Fluorescence')
ax = gca;
ax.LineWidth = 1;
ax.FontSize = 14;

subplot(2,1,2)
plot(x*10000,C,'LineWidth',2)
xlabel('Distance, µm')
ylabel('Normalized Fluorescence')
ax = gca;
ax.LineWidth = 1;
ax.FontSize = 14;

% Error Function
S = 0;
for i = 1:length(x)
S = S + sum(((C(:,i) - matrix(:,i))./matrix(:,i)).^2);
end

end
```
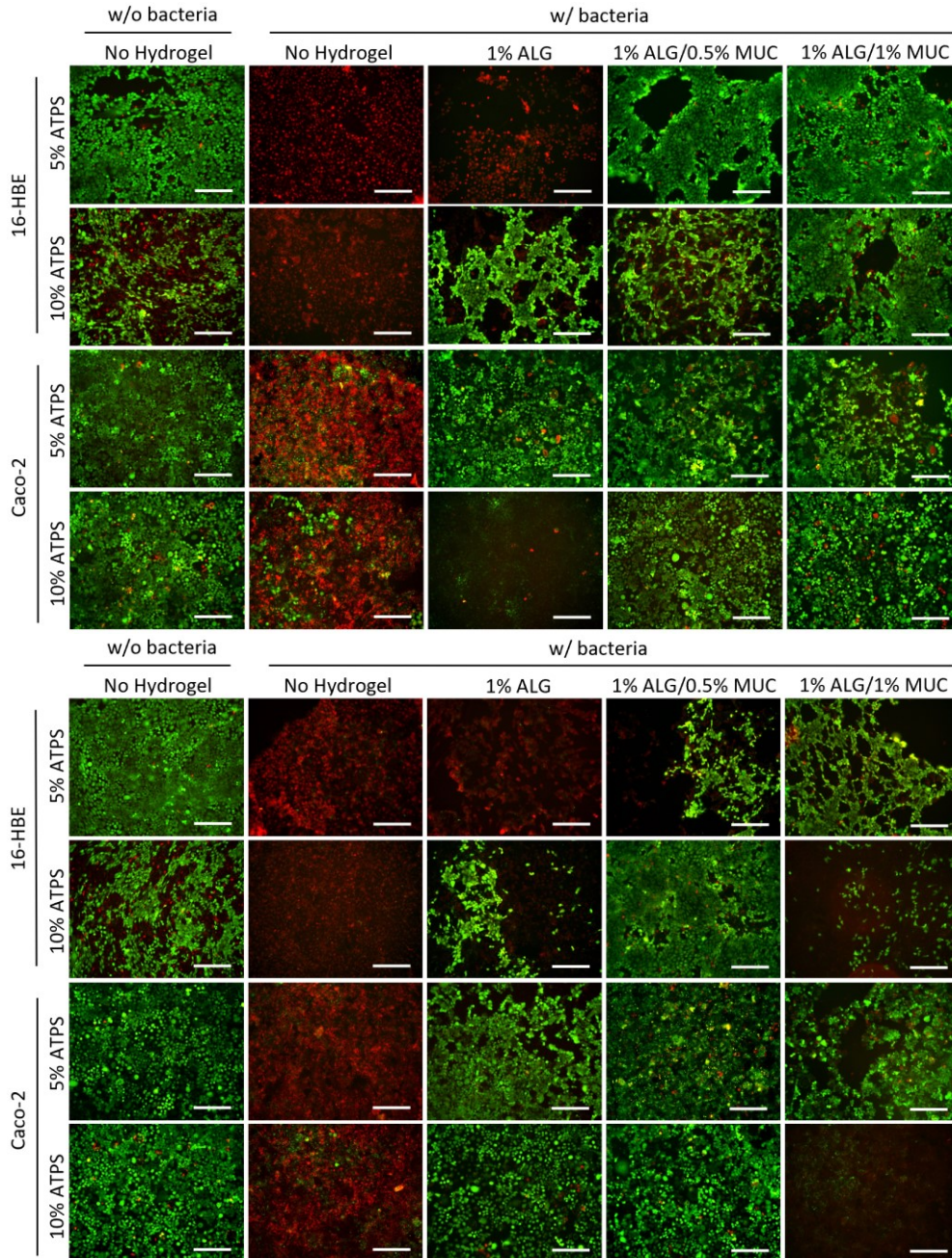
Figure 26: Live/Dead staining images of 16-HBE and Caco-2 monolayers after a 12-hour co-culture incubation with *P. aeruginosa* or *S. flexneri*, respectively, either with or without alginate-based hydrogels between monolayer and ATPS (Trial 2, top; Trial 3, bottom). Bacteria were deposited using a 5% PEG/5% DEX ATPS or 10% PEG/10% DEX ATPS onto monolayers with or without an alginate-based hydrogel overlay, where a DEX droplet without bacteria was deposited directly onto a monolayer as a control (Scale bars = 500 μm).
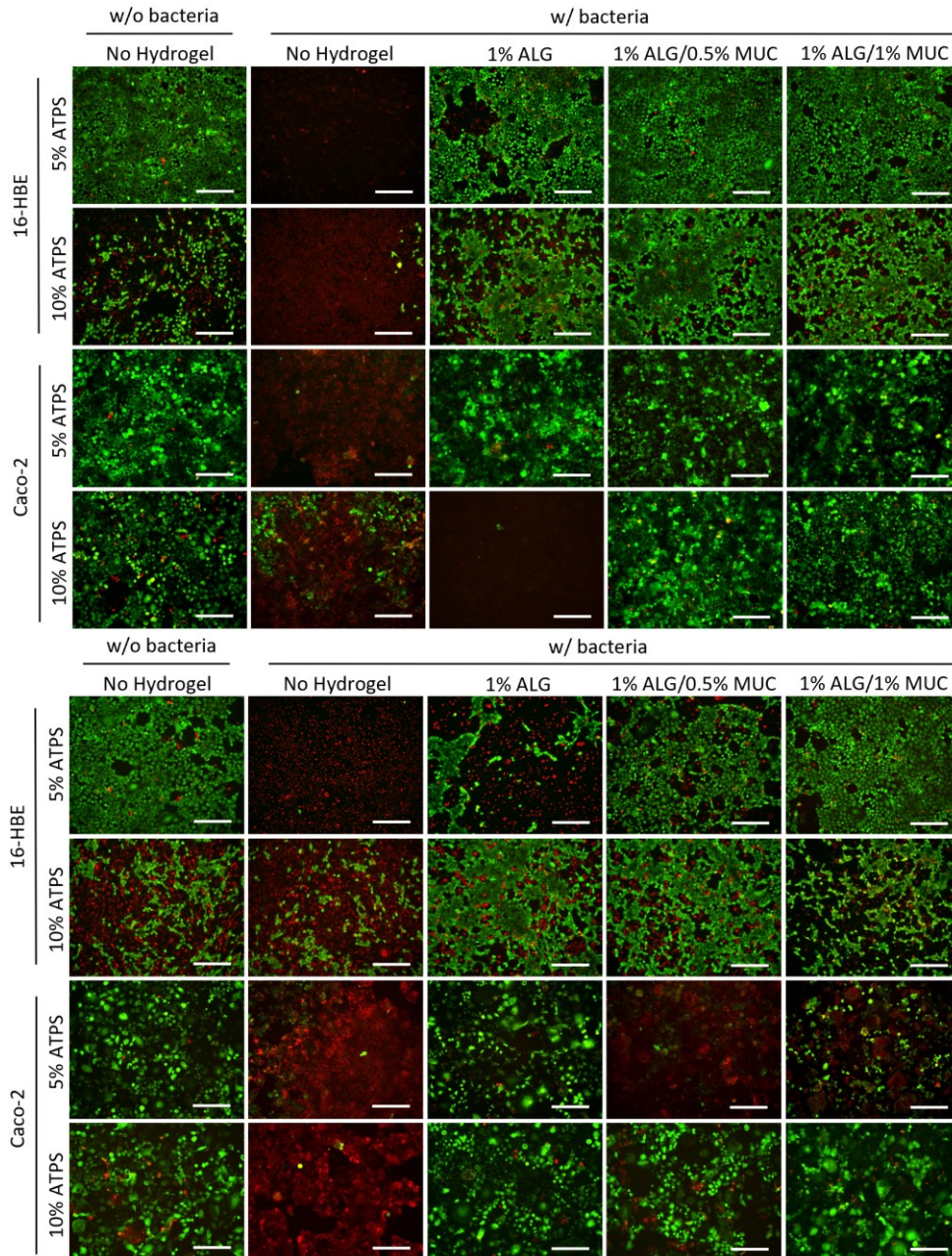
Figure 27: Live/Dead staining images of 16-HBE and Caco-2 monolayers after a 19-hour (cipro added at 7 hr) co-culture incubation with *P. aeruginosa* or *S. flexneri*, respectively, either with or without an alginate-based hydrogel between monolayer and ATPS (Trial 2, top; Trial 3, bottom). Bacteria were deposited using a 5% PEG/5% DEX ATPS or 10% PEG/10% DEX ATPS onto monolayers with or without an alginate-based hydrogel overlay, where a DEX droplet without bacteria was deposited directly onto a monolayer as a control (Scale bars = 500 μm).